THÈSE

En vue de l'obtention du

DOCTORAT DE L'UNIVERSITÉ DE TOULOUSE

Délivré par :

Université Toulouse 3 Paul Sabatier (UT3 Paul Sabatier)

Présentée et soutenue par :
Yves Angel DAVILA MONTAÑO

le mardi 27 janvier 2015

Titre :

Etude multi-échelle du couplage matériau-procédé pour l'identification et la modélisation des variabilités au sein d'une structure composite

---

École doctorale et discipline ou spécialité :
ED MEGEP : Génie mécanique, mécanique des matériaux

Unité de recherche :
Institut Clément Ader

Directeur/trice(s) de Thèse :
Francis COLLOMBET, Professeur des Universités, ICA, Directeur
Bernard DOUCHIN, Maître de Conférences, ICA, Co-directeur
Laurent CROUZEIX, Maître de Conférences, ICA, Co-directeur

Jury :
Alaa CHATEAUNEUF, Professeur des Universités, Univ. Blaise Pascal, Clermont-F., Rapporteur
Jacques RENARD, Directeur de Recherche, Mines Paris Tech, Rapporteur
Peter DAVIES, Ingénieur de Recherche (HdR), Ifremer Brest, Examinateur
Yves-Henri GRUNEVALD, Senior Expert, Composites, Expertise & Solutions, Invité

Remerciements

Résumé des travaux en français

Introduction

Ce travail porte sur l'étude des variabilités au sein de plaques composites carbone/epoxy en M10.1/38%/UD300/CHS avec une stratification quasi-isotrope de 16 plis. Un spectre large de variabilités est adressé, depuis le pli non polymérisé jusqu'à la pièce polymérisée, en passant par la phase de drapage et de polymérisation.

L'objectif de l'ensemble des identifications de variabilités est de permettre d'introduire l'effet de ces variabilités dans des modèles de calcul du comportement de la pièce composite, et d'en évaluer l'influence sur le comportement mécanique.

Chapitre 1 : étude bibliographique

Dans ce chapitre 1, on montre que l'étude des variabilités sur des pièces composites reste un problème ouvert qui peut être abordé de plusieurs manières. En effet, il n'existe pas une méthodologie générale applicable pour chaque étape associée à l'établissement de la solution composite. La définition même de la variabilité reste l'interprétation des chercheurs ou des concepteurs.

Sur l'analyse et la conception des structures composites, il existe une quantité importante de méthodes permettant l'introduction des variabilités dans le calcul des propriétés structurelles. La méthode Monte-Carlo est la plus utilisée pour alimenter ce type d'analyse. Elle sert ainsi comme une sorte de benchmark des autres types de méthodes. Malgré la quantité importante de méthodes dédiées à l'étude des problèmes composites, la prise en compte les variations continues des propriétés au sein d'une pièce composite ou la présence d'un défaut localisé sont

peu ou pas réalisées. Les propriétés mécaniques sont variables à chaque itération mais en utilisant la même valeur pour tous les éléments finis.

De plus, une grande quantité de méthodes pour l'introduction des variabilités est obtenue à partir d'éprouvettes normalisées. Celles-ci n'ont pas la même stratification que la structure finale et elles ne sont pas fabriquées dans des conditions identiques. Il est bien établi que les propriétés de la structure composite dépendent des matières premières et du procédé de fabrication car les interactions entre la matrice et le renfort ont une nature très complexe. Les variabilités au sein des matériaux composites sont souvent regardées comme des défauts, mais elles sont en réalité le résultat de l'interaction d'un nombre non déterminé de paramètres.

Chapitre 2 : Vers une modélisation de la variabilité répartie sur une structure CFRP

Le chapitre 2 explique le parti pris initial de ce travail. Il s'agit de la volonté d'inclure dans des modèles de calcul des variations locales de géométrie et de propriétés matériaux, tout en retenant comme idée principale que ces variations ne devaient pas être distribuées aléatoirement au sein de la structure composite, mais présenter des lois d'évolution spatiale qui soient en accord avec la réalité du matériau. Cette volonté d'injecter des lois d'évolution spatiale contrôlées constitue le fil conducteur des analyses, identifications et modélisation au cœur de ce travail. De plus, l'objectif affiché n'est pas de recréer à l'identique une unique pièce composite en « injectant » des lois d'évolution figées. Il s'agit de proposer une stratégie de modélisation qui respecte la réalité du matériau tout en contenant des grandeurs déterminées aléatoirement afin d'être capable de mener des études variabilistes. On souhaite ainsi restituer le fait que deux pièces a priori semblables ne se ressemblent pas tout à fait. Ainsi pour chaque paramètre étudié, il est proposé une loi mathématique retranscrivant de façon représentative ces variations, et à laquelle on adjoint une étude probabiliste effectuée sur les paramètres pilotant ces lois.

Chapitre 3 : Etude des variabilités sur une structure CFRP polymérisée en autoclave

Dans ce chapitre, la fabrication de plaques composites est décrite ainsi que les mesures de certaines propriétés qui sont prises à chaque étape du processus de fabrication.

Le premier paramètre étudié est, suivant l'ordre chronologique de fabrication de la structure composite, les variations de masse surfacique du pli de préimprégné. Une procédure, inspirée d'approches normatives, est proposée pour obtenir une mesure précise de cette grandeur, notamment via la numérisation de l'échantillon afin d'en déterminer l'étendue sans être influencée par les défauts géométriques des bords de l'échantillon. Une variabilité est identifiée sur cette grandeur avec un coefficient de variation de moins de 2 % au sein de chacun des lots de matériaux étudiés. Une forte variation de la masse surfacique entre deux rouleaux différents est mise en évidence. Cependant, aucune corrélation à ce stade n'a pu être identifiée entre la masse surfacique mesurée et la position de l'échantillon au sein du rouleau de pré-imprégné. De ce fait pour ce paramètre, aucune modélisation mathématique de son évolution spatiale n'a été effectuée.

Une fois les structures composites polymérisées, les plaques ainsi créées ont été caractérisées au moyen d'une machine à mesurer tridimensionnelle. On met en évidence des variations conséquentes d'épaisseurs existant entre des plaques de différents lots de pré-imprégné pour un même matériau et une même stratification. Ces différences ont un lien probable avec le flot de résine se produisant au cours de la polymérisation, lui-même étant directement impacté par le choix et la place des produits d'environnement utilisés. De plus, les mesures démontrent que si l'ensemble des plaques ne possède pas une épaisseur constante, elles présentent une épaisseur maximale en leur centre. Une modélisation mathématique de l'évolution spatiale globale de l'épaisseur de la plaque est proposée comme la somme d'une valeur moyenne et de la valeur d'une sinusoïde de longueur d'onde de l'ordre de la longueur de la plaque avec un déphasage de manière à présenter un maximum au centre de la plaque. L'amplitude des écarts

d'épaisseur entre le centre et les bords d'une plaque est estimée dans cette étude comme supérieure à la valeur de l'épaisseur d'un pli. Il s'agit donc d'un facteur majeur d'écart des propriétés mécaniques entre une représentation géométriquement parfaite de la pièce et la réalité.

Des analyses physico-chimiques sont réalisées sur des échantillons découpés au sein des plaques ainsi polymérisées. De par la nature de ces analyses, ces mesures n'ont pu être faites qu'à l'échelle de la plaque, et non du pli. L'objectif de ces analyses est de relier l'évolution des propriétés volumiques matériau avec les épaisseurs. Il est montré que le taux de porosité semble augmenter avec l'épaisseur de la plaque, malgré une importante dispersion des résultats. En partant de cette constatation, une loi d'évolution de la porosité en fonction de l'épaisseur est proposée. Cette loi contient un paramètre qui suit une évolution linéaire directement liée à l'épaisseur de la plaque, mais elle est bornée de manière à obtenir une porosité nulle en dessous d'un seuil identifié par les mesures. A ce paramètre dépendant uniquement de l'épaisseur, on ajoute un terme déterminé par un tirage aléatoire basé sur les dispersions identifiées grâce aux mesures expérimentales.

Chapitre 4 : Détermination et modélisation des désalignements de fibres dans le plan apparus pendant le drapage manuel d'un stratifié CFRP

Dans ce chapitre, le paramètre étudié est l'orientation des fibres de chacun des plis. Un système optique est utilisé pour obtenir une image numérique de l'ensemble pli juste après son drapage et avant le drapage du pli suivant. Une analyse des photographies permet de remonter, via l'analyse d'images, aux orientations des mèches de fibres. Ainsi un écart ou une erreur d'orientation moyenne de chaque pli est aisément obtenue. La valeur de cet écart d'orientation semble faible, moins de 2° au maximum, et plus dépendante de l'habilité et de la fatigue de l'opérateur que de la valeur de l'orientation du pli. Une procédure est mise en place pour remonter à un champ d'orientations des mèches au sein du pli. De par la qualité des images et la résolution de l'appareil de mesure comparée à la

largeur de la pièce fabriquée, la procédure ne permet pas de remonter à des désorientations sur une zone de petite taille. Malgré cela, la procédure est suffisante pour identifier des évolutions locales d'orientation des mèches de fibres. L'analyse de ces évolutions démontre que toutes les fibres d'un pli ne présentent pas une orientation identique, mais que des zones de plusieurs cm² présentent des écarts par rapport à une valeur moyenne. Ces zones peuvent être par exemple le résultat de la manipulation du pli non polymérisé par l'opérateur. Cependant, on relève que ces zones, dont l'amplitude maximale ne dépasse pas 1°, ne présentent pas de régularité quant à leur position au sein du pli, ni de dépendance suivant l'orientation théorique du pli.

Suite à ces constatations, les lois mathématiques d'évolution de l'orientation à travers un pli proposées contiennent un écart moyen une ondulation systématique dont la valeur est issue de la littérature de travaux anglo-saxons (mais qui n'est pas identifiée dans ces travaux parce que correspondant à des zones trop petites pour être atteignables par la stratégie de mesure), et enfin une somme de perturbations locales correspondant aux écarts identifiés par rapport à la valeur moyenne. Ces perturbations sont modélisées comme des surfaces gaussiennes, et une analyse probabiliste est faite sur l'amplitude et l'étendue de ces surfaces gaussiennes pour en définir des bornes qui soient basées sur la physique du matériau. Il est démontré qu'une somme d'une douzaine de surfaces gaussiennes est suffisante pour représenter fidèlement les évolutions d'orientation au sein de plis de 600 x 300 mm dans le plan. Pour l'exploitation numérique de ces résultats, on fera l'hypothèse que le placement des fibres n'est pas affecté par la polymérisation de la pièce.

Chapitre 5 : Evolution spatiale de la variabilité de l'épaisseur de pli répartie sur une structure CFRP

D'une part, l'étude des variations d'épaisseur des plis dans une section montre que les valeurs pour un même pli peuvent varier, le long de quelques millimètres dans le plan, d'une valeur supérieure à 30 % de sa valeur moyenne.

D'autre part, les variations d'épaisseur des plis dans une direction donnée semblent présenter des régularités, avec notamment l'existence de longueurs d'onde privilégiées. Cette constatation est confortée par une analyse fréquentielle sur les variations d'épaisseur dans une direction de plaque donnée. Elle démontre que les ondulations de chaque pli pris indépendamment peuvent être décrites sous la forme de sommes de sinusoïde, et peuvent être retranscrites fidèlement avec moins d'une dizaine de sinusoïdes. Cependant, la comparaison des résultats entre les différents plis d'une même section reste difficile à effectuer. Si certaines plages de longueurs d'onde semblent présentes dans tous les plis, d'autres ne le sont pas de façon systématique. De plus, aucun lien n'a pu être démontré pour l'instant entre les amplitudes, les longueurs d'onde de ces variations et l'orientation des plis. Néanmoins, on peut retenir d'une manière générale pour l'ensemble des plis que leurs épaisseurs varient via des répétitions périodiques allant de 50 mm à moins d'un millimètre.

Ces variations périodiques d'épaisseur peuvent être « injectées » dans les modèles de calcul, en identifiant les lois mathématiques d'évolution spatiale, basées sur les résultats d'analyse fréquentielle. Ces lois mathématiques reposent sur la somme de fonctions sinusoïdales, dans lesquelles les amplitudes et longueurs d'onde sont tirées de manière aléatoire, tout en étant bornées dans des espaces de recherche basés sur les résultats des grandeurs expérimentales. Les déphasages des fonctions sinusoïdales sont également soumis à un tirage aléatoire, mais avec un contrôle permettant d'assurer le couplage entre les variations d'épaisseur de chaque pli et de la plaque.

Chapitre 6 : Proposition d'un modèle éléments finis avec prise en compte des variabilités locales avec gradient contrôlé

L'ensemble des modélisations mathématiques, proposées pour la représentation de l'évolution spatiale au sein d'une pièce respectivement de l'épaisseur des plis, de l'épaisseur de la pièce, du taux de porosité et de l'orientation réelle des plis, est utilisé pour la création de modèle par Eléments

Finis prenant en compte des variations locales de propriétés. La modélisation proposée est basée sur une modélisation en éléments coques 2D, de manière à être capable de mener un grand nombre de simulations en changeant les paramètres variables au sein des modélisations mathématiques proposées. Dans cette proposition de modèle, les valeurs des paramètres matériaux et géométriques changent non seulement d'une maille à l'autre, mais également pour une même maille, entre chacun des 16 plis constituant l'élément coque composite.

Le premier paramètre déterminé l'est, pour chaque maille et en utilisant les formulations identifiées par les mesures (l'épaisseur de chaque pli) pour lequel on tient compte non seulement de ses variations propres mais également de l'évolution de l'épaisseur de la plaque. Ensuite, le taux de porosité par pli et par maille est déterminé en fonction de l'épaisseur du pli et d'un tirage aléatoire. En utilisant une hypothèse de volume constant de fibres, le taux de porosité et l'épaisseur du pli sont utilisés pour calculer les taux volumiques de fibres et matrice, et ainsi les propriétés mécaniques du pli orthotrope dans le repère lié à la direction des fibres. Enfin, l'orientation des fibres est déterminée et « injectée » dans le modèle comme un paramètre indépendant.

L'utilisabilité de ce type de modélisation fine des variations locales des propriétés géométriques et matériaux d'un composite est illustrée par trois cas. Dans un premier temps, le modèle ainsi créé est confronté à des résultats expérimentaux et une analyse numérique faisant varier toutes les grandeurs de manière homogène dans le cas d'un essai de flexion 4 points, sur un échantillon de taille plus réduite que la pièce finale. L'étude démontre que la modélisation proposée permet d'obtenir des variations de propriétés en flexion qui sont cohérentes avec les variations identifiées via le dispositif expérimental, malgré un écart moyen qui est probablement dû plus à la stratégie de modélisation numérique plus qu'à la stratégie de prise en compte des variabilités. Afin de démontrer la faisabilité de cette stratégie d'introduction des variabilités dans des cas de structures de plus grandes dimensions, un calcul de déformations résiduelles dues aux contraintes internes de cuisson est effectué, sur une structure

de 600 x 300 mm. Ces calculs démontrent qu'à cette échelle, il apparaît, uniquement, du fait des variabilités identifiées, des variations de déformations non négligeables au sein d'une même pièce (de l'ordre de 10^{-4}). Enfin, la stratégie est utilisée pour l'analyse d'un essai multi-axial pour un trajet de chargement complexe sur un évaluateur technologique. Elle requiert une simulation non linéaire géométrique car on se place dans le cas du flambage d'une structure composite sous une sollicitation de compression/flexion. Les premières applications de la stratégie font en particulier apparaître des dissymétries et hétérogénéités du champ des déformations liées aux variabilités, et pourraient ainsi permettre de mieux comprendre les résultats expérimentaux quand des couplages responsables de voilement ou de gauchissement des pièces se mettent en place au sortir de la polymérisation.

Conclusions

L'ensemble des travaux de ce document prétend d'une part illustrer l'existence des variabilités dans les structures composites, phénomène connu de tous mais souvent non considéré dans la phase de conception. De plus, on propose une démarche de prise en compte numérique de ces variabilités, basée de façon prioritaire sur l'observation du matériau. Si dans ce document, n'est présenté uniquement que le cas d'une plaque plane et théoriquement homogène, il sert à démontrer la faisabilité de l'approche et des modèles associés. Il serait nécessaire d'explorer à terme des géométries et matériaux différents, et notamment toutes les zones proches des zones singulières, dont on sait qu'elles sont sources de fortes variabilités. De la même manière, si une seule stratification et un seul matériau ont été utilisés durant cette étude, la démarche proposée se veut applicable à un grand nombre de cas, mais nécessitera pour chaque application une mesure des différentes grandeurs sur des pièces témoins si possibles représentatives des structures finales, afin d'identifier les grandeurs caractéristiques des lois mathématiques proposées, voire proposer de nouvelles lois mathématiques de variations adaptées aux cas traités.

- xi -

Table of contents

List of figures

List of tables

General introduction

The employment of composite structures in transport and civil applications has shown an exponential growth during the last decade. Today, the aeronautical industry relies heavily on the use of these advanced materials to decrease the structural weight and maintenance costs associated to corrosion and fatigue. However, polymer matrix composite materials present a higher variability of their mechanical properties compared to the classic engineering materials, such as metals. The origins of the material variability can be traced from the elementary material variability, the manufacturing conditions and chosen geometries of the composite structure, thus the notion of variability cannot be dissociated from the finished product. From the point of view of a finite element model, the input parameters that modify the structural behaviour include, but are not limited to the volume fractions of the fibres, resin, and porosity; the fibre orientation, both in-plane and out-of-plane, characteristics of the type of material of the reinforcement and resin system employed, etc. In fact, the list of parameters and its couplings at the different material scales can be considered infinite, adding an unknown complexity to the composite solution. A first step to address the problem is through the geometric description of the composite structure at the mesoscopic and structural scales. This geometric description is driven by the evolution of the thicknesses of the plies and the structure itself.

For design purposes, the structure thickness is given by the sum of the ply thicknesses that form the laminate, or alternatively the thicknesses of the plies are obtained by dividing the total structure thickness by the number of plies of the given stratification. The thickness of the structure is thus considered as constant and equal for all plies, provided that there is not change of the geometry of the

cross section and stratification. In reality, each ply in the stratification does not present a constant thickness (cf. Figure 1).
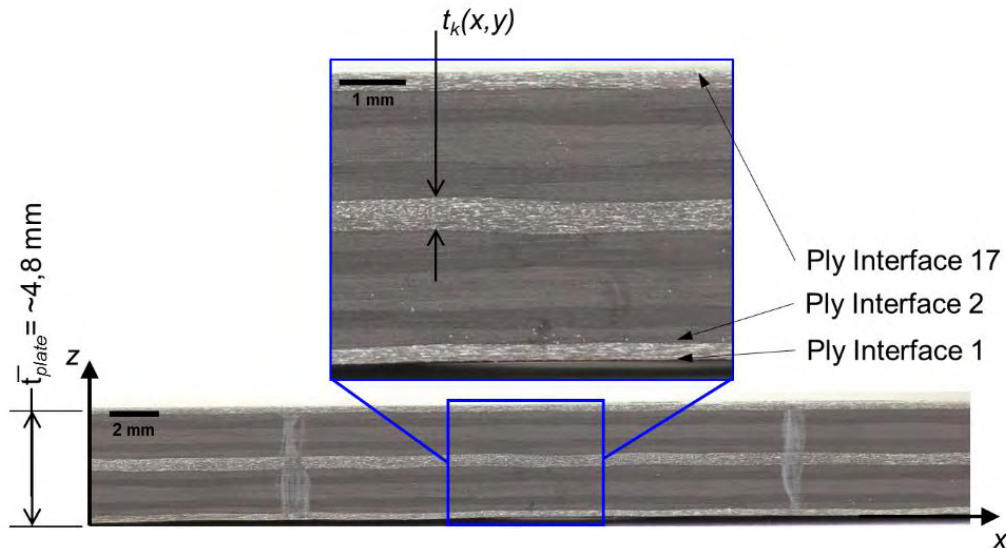
Figure 1. Micrograph showing the ply thickness variations spread over a layered composite plate.

The main goal of our approach is to propose a finite element model that takes account of the geometric and material variability present in a composite structure. This model is based on the assumption that the property variation shows a continuous evolution through the composite dimensions that cannot be reproduced by only randomly assigning a set property to each element of the model.

This dissertation is composed by six chapters.

The Chapter 1 is dedicated to a literature review where the variability parameters are shown to be tightly linked to the manufacturing process of the composite plate, as well as the raw materials.

In Chapter 2, an overall solution for the variability introduction into a FE model is proposed.

In Chapter 3, the general process of fabrication and measurement of the sources of variability are described for a chosen composite plate, with a particular focus on the measurement of the following parameters.

The mass per unit area of the composite prepreg is a parameter associated with the variability of volume fractions of the elementary constituents. The influence of resin flow during the polymerisation by weighing the plates before and after the cure cycle is considered. The plate thickness variation through the composite plate and the differences that are due to the sequence of the used vacuum products in different autoclave batches are taken into account. It deals with the determination of the volume fractions of the constituent materials of the cured plates.

In Chapter 4, the reinforcement misalignments are quantified during the lay-up procedure of the prepreg plies. A more in-depth analysis on the evolution of the ply thickness variations and the fibre orientations, describing the methods to obtain the geometric properties and as well the mathematical laws for their modelling is described. In a first step, the difference between the actual orientation and theoretical orientation of the plies is obtained. Then by the implementation of an in-house program, the values of local misalignments are determined.

In Chapter 5, the evolutions of both the ply and the plate thicknesses are quantified. Using images of the cross-section of the composite, the variations in the thicknesses are modelled. It is demonstrated that the profile of the ply thickness exhibits a periodic variation. The amplitude spectrum, obtained by a discrete Fourier transform of the thickness profile, is then used to determine the representative pairs of frequencies and amplitudes. These representative peaks are used to model a digital ply that has variability of the same order of magnitude as the measured thickness profiles.

Finally, in Chapter 6 three cases of FE model are considered using the methodology proposed in Chapter 2 and the mathematical laws proposed in Chapters 3 through 5.

Chapter 1: Literature review

1.1 Introduction

Variability in composite materials is referred to the dispersion of the properties that these materials exhibit, and such are much more significant than for classic engineering materials, like the metals. The Military Handbook 17 [1] states that the variability of the composites property data may originate from different sources, like batch to batch variability in raw materials, variability in the fabrication process of the composite part, variability during the testing and the intrinsic variability of the material. However, in the literature, the definitions of variability and uncertainty are often used indifferently, as they are included within the boundaries of the lack of knowledge of the system [2].

1.2 Definition of variability

Thunnisen [3] made a recompilation of different definitions of uncertainty grouped by areas of knowledge. In this recompilation, he states that there is no agreement in the different terms that are understood under the term uncertainty, the variability being one of these definitions. Likewise, he found that different areas of knowledge assign a different classification and term definitions for the same words. For the mechanical engineering domain, one of the most suitable taxonomy of the systems uncertainty is offered by Oberkampf [4], in which the variability is defined as the inherent variation associated to the physical system under consideration. Meanwhile, the uncertainty is the potential deficiency in any

phase or activity of the modelling process due to a lack of knowledge or incomplete information. Finally, an error is a recognisable deficiency in any phase or activity that is not due to the lack of knowledge. As can be seen, it is extremely difficult to draw the line between each definition, especially when dealing with multilevel systems with complex interactions such as the composite materials.

Therefore, the material variability can be defined as the dispersion of properties that are due to the spatial and consistency variations of the material itself, and due to variations in its processing. The components of the material variability can be the combination of fixed effects and random effects and as well as errors. The fixed effects are produced by the controlled variables which are a systematic shift in a measured quantity due a particular level change or a treatment or condition, which is often under the control of the experimenter. The random effects are produced by uncontrolled variables that produce a particular change in the measured properties. This random effect is never under the control of the experimenter. The shift in the measured quantities is viewed as a random variable with a zero mean and a non-zero variance. The errors are the part of the data that varies due to unknown or uncontrolled external factors that affect the observation independently and unpredictably. A random error is a special case of a random effect where the errors vary independently from measurement to measurement. To further classify the errors, they can be divided into acknowledged and unacknowledged errors. An acknowledged error is for example the approximations or assumptions to simplify the modelling of a physical process, meanwhile an unacknowledged error can be referred as a simple mistake [3]. Defect is another term that is usually found in the literature linked to experimental work. A defect can be defined as an involuntary split, or flaw, from the theoretical properties produced by a physical imperfection of the material or caused by an error during the composite part processing.

In order to successfully design a composite structure, the reliability of the system must be demonstrated. This exercise consists in the evaluation of the probabilities for the various structural responses to satisfy the specified design

criteria and quantify the uncertainty ranges for each response. The scatter in the structural behaviour cannot be simulated by the traditional deterministic methods that use a safety factor to account for uncertain structural behaviour. A probabilistic method is thus needed to accurately determine the structural reliability of a composite structure [5, 6].

Effectively, the vast quantity of variabilities and the infinite possible effects make difficult the calculation and analysis of composite structures. There are multiple methods and approaches that can be used. The acknowledgement of variability is therefore limited to the fields of study and the expected results. This implies that there is no global framework to introduce the variability in composite structure design.

The properties of composite materials are cure and process dependent. In most of the cases, the composite structures are the product of complex multi-step procedures, and with each step, additional variability is introduced [7]. One important point to take into consideration is that most of the work done to design a composite structures is based on the test pyramid [1]. Thus, the design properties of composite material are derived from small laboratory scale coupons. It has been thought that when increasing the size of the composite its strength decreases. This is based on the assumption that the probability of encountering a flaw large enough to initiate the structural failure increases with the size of the specimen. However, this is not necessarily true since the processing techniques to fabricate a test coupon are not the same as those used to fabricate as full scale structure [8].

As is often the case, there is a strong dichotomy on the calculation aspects of the composite structures and the compilation of data in a real composite structure. This literature review intends to cover, on one side, the general aspects on how the variabilities in composite materials are studied during the design and analysis phases, and on the other side the lack of actual properties of the composites materials. The first part of this review is dedicated to the analysis and design of composite structures; starting from the most used methods to the required data

that is introduced into the models. The second part of this review focuses on the sources of variability of the real composite material and the techniques used to measure the material properties.

1.3 Variability calculation of the composite materials

1.3.1 Introduction to a stochastic design of composite materials

The analysis of composite materials is performed usually at three different scales of the material: at the level of the elementary materials (fibre and matrix), known also as micromechanical level; at level of the homogenised ply or meso-scale, and at the structural scale, also known as macromechanical scale. Sriramula and Chryssanthopoulos [9] considered a significant number of studies and classified them into these three major groups regarding the scale at which the material is observed. The class A is set at micromechanical level, and it is further divided into two subgroups:

The class A1 deals with the analysis of the composite from the determination of the material properties by the use of the micromechanical structure of the composite. In this class, the identified probabilistic models for the random variables can be introduced into composite micro-mechanics theory, leading to effective property estimation at lamina level, which can be later combined with the laminate theory and finite element (FE) analysis [10].

The class A2 builds the micromechanical properties from the morphology of the composite microstructure by the use of sophisticated numerical modelling of microstructural randomness in conjunction with spatial variability modelling of the studied variables. These methods consider of a representative volume element (RVE) of the composite structure linked to an appropriate micro-mechanical model to evaluate the response behaviour (cf. Figure 1-1). An example of a class A2 methodology is given by Guillaumat and Dau [11,12] where, using a micrograph of a composite cross-section, a RVE of the composite is determined.

Then, by varying the diameter of the fibres and the elastic moduli of the fibres and matrix, as well as the Poisson's ratio for each variable, the compliance matrix of the composite lamina is determined. To reduce the impact of uncertainties at this stage, a material database is stablished to show the admissible and non-admissible values for each property at any given scale [13].
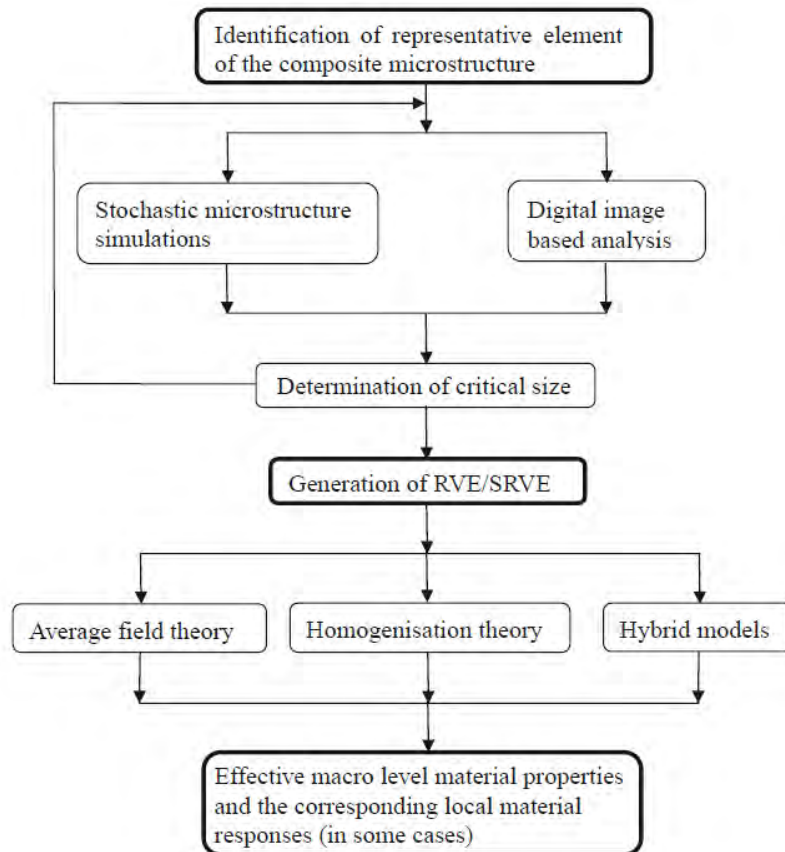
Figure 1-1. Uncertainty modelling and propagation in Class A2 approach [9].

Class B problems are studied at a component level (composite beam or panel). In this case, the models are based on random variables based on experimental evidence and engineering judgment. Typically the probability distributions for random variables representing stiffness or strength properties are specified. Finally, the meso-scale modelling, or Class AB, which is an intermediate stage of modelling, is suggested when the ply characteristics significantly influence the composite properties. This class is also used to verify the propagation of uncertainties across the length scales.

The rational treatment of the great number of variables considered in a composite system can be achieved by means of probability theory and statistics, and cannot be addressed by the traditional deterministic approach. Stochastic methods provide a way to represent a wide range of structural loading and strength scenarios. A stochastic field is defined as:

$$F(x) = \overline{F}\left[1 + \xi(x)\right] \tag{1-1}$$

where the stochastic response of a variable $F(x)$ is described by the mean value of said variable $\overline{F}$ and a zero mean stochastic field $\xi(x)$. There are two major approaches to assess a composite structure through a stochastic framework: reliability based methods and stochastic finite element methods (SFEM). For both approaches, the Monte Carlo simulation (MCS) is the most used method to solve stochastic problems and serves as well as a benchmark to qualify the results obtained by other types of methods [14].

As an example of a stochastic method to analyse composite structures presenting variability, Venini [15] used the Rayleigh-Ritz method to study an out-of-plane vibration of a cantilever composite beam. In this problem, five zero-mean random fields are introduced at a macromechanical level (E_1, E_2, v_{12}, G_{12}, and the material density ρ). The properties were modelled as homogeneous random fields to be averaged into random variables by means of the stochastic Rayleigh-Ritz method, where each random variable results from a spatial average over the whole domain of the structure and therefore is representative of the entire structural system.

1.3.2 *Reliability based methods*

The reliability is defined as the probability that the system performs its intended functions for a specific period of time under a given set of conditions. In other words, the reliability is the probability that unsatisfactory performance or failure will not occur.

The probability of failure P_f is:

$$P_f = P[G(x) \leq 0] = \int_{G(x) \leq 0} f_X(x) dx \qquad (1\text{-}2)$$

where $f_X(x)$ is the joint probability density function (PDF) of the random variables X, whose realisations are x, and $G(x) \leq 0$ denotes the failure domain. The reliability index β is the shortest distance between the origin of the space and the failure domain in the normalised space (cf. Figure 1-2).
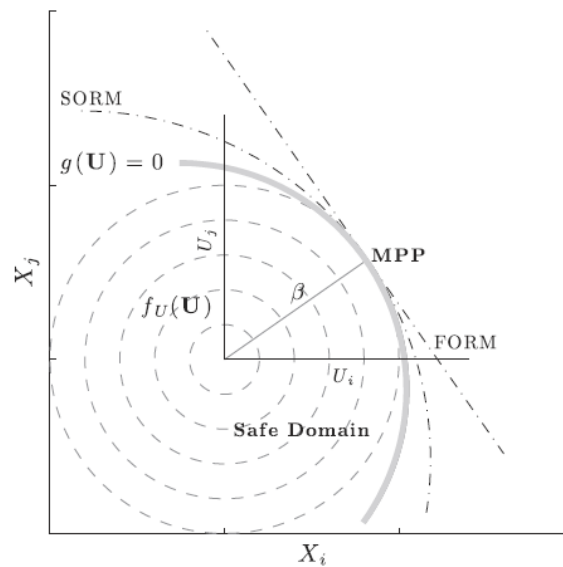
Figure 1-2. Schematic representation of FORM/SORM approximations [16].

A first order reliability method (FORM) is used to approximate the boundary of the failure domain $G(x)$ into a linear function, by means of a first order Taylor series approximation of $G(x)$ in the vicinity of the design point to evaluate the β index. A second order reliability method approximates the failure domain using the second order derivatives of $G(x)$.

The strength of a fibre reinforced in a composite material can be adequately described by probabilistic methods. Soares [17] introduced the different probabilistic approaches to represent the strength of fibre reinforced composite materials and to assess the reliability of laminated components. Di Sciuva [14] compared the mechanical properties of a composite beam obtained by MCS and several algorithms. In this study, the deformation of a cantilever composite beam

is calculated using stochastic variables which are the moment of inertia J, the Young's modulus E, the length of the beam L and the transverse load applied to the beam q. Using a convergence criterion pre-established, they determined both the maximum deflection of the beam and the reliability. It is evident that FORM algorithms offer quick convergence and low computational costs.

A probabilistic approach can be used to construct the macroscopic properties of a composite plate from the constituent materials to obtain a stochastic response of the macroscopic properties. Shaw et al. [18] used 14 random properties of the elementary constituents of a composite plate obtained from the literature to determine the macroscopic properties of the studied plate. By using MCS the macroscopic properties of the composite plate were then obtained. The properties include the longitudinal and transversal moduli in the principal directions, E_1 and E_2, the shear modulus G_{12} and the Poisson's ratio ν_{12}, as well as the ultimate longitudinal and transversal stresses, X_T and Y_T. The derived macromechanical properties were compared against three probability distributions to determine the most suitable distribution for each property using a Kolmogorov-Smirnov (K-S) goodness-of-fit test. The tested probabilistic laws were the Normal law, the 2-parameters Weibull distribution and the lognormal (L-N) distribution. The failure probability estimates were then calculated by a combination of MCS and FORM/SORM using the Tsai-Hill failure criterion. Although this study compares the macroscopic properties derived from the micromechanical analysis to the values obtained by experimental setups found in the literature, it does not takes into account neither the details of the used material system, other than being a carbon/epoxy, nor the fabrication process. In comparison, Lekou and Philippidis [19,20] created a material database obtained from the tensile test coupons. The E-glass/polyester coupons were fabricated by hand lay-up. Nine macroscopic properties were obtained by experimental means. Each property was compared against 6 probability laws using the K-S test and the Tsai-Hahn criterion is used as a limit state function.

The reliability methods are used also to obtain the sensitivity factors of certain variables and how they affect the global behaviour of the system. Antonio [21] used MCS in a global sensitivity analysis to determine the reliability of a composite plate. The parameters used to assess the reliability were the maximum displacement and the critical Tsai number covering four stochastic variables: the ply angle, the elastic strength, the lamina thickness and the loading of the composite. The study assesses the effect of each property at different ply angles, ranging from 0 to 90°. The material properties are obtained from the literature and the coefficients of variation of each property are assigned.

1.3.3 Optimisation methods

The variability of the composite material does not only impact the reliability of the structure, but also it must be taken into account in the optimisation phase of the composite structure.

Walker [22] developed a technique for optimally designing fibre-reinforced symmetric laminated plates under buckling loads for minimum mass accounting for manufacturing uncertainties in the fibre layup orientation. The constraint implemented is a minimum buckling load carrying capacity constraint, and the objective is to determine the value of the fibre orientation that corresponds to a minimum plate thickness, with the uncertainty included.

Correspondingly, the optimisation techniques can be coupled with reliability analysis. This is the case of cylinders subject to pressure. Boyer and Béakou [23,24] obtained the optimal winding angle which reduces the mass of the composite structure by maximising the distance between the operating point and the failure domain. The failure mode used in this study is the Tsai-Wu criterion. The mechanical properties of the composite are built from the micromechanics of the elementary materials, using 9 properties with values obtained from the literature. Bouhafs et al. [25,26] expanded on the study of pipes to the sensitivity analysis of the design parameters, within a macromechanical study. This time the

variable parameter was the thickness variation of the container. Khiat et al. [27] continued with the micromechanical level by studying the fibre arrangement and analysed the sensitivity against the failure criterion, that in this case is the ineffective length of the broken fibres. A sensitivity analysis is performed to see how the probability distribution of the behaviour response changes when adding the stochastic parameters. The mean response remains the same, but the tails of the distribution function are more spread, indicating a higher value of uncertainty (cf. Figure 1-3).
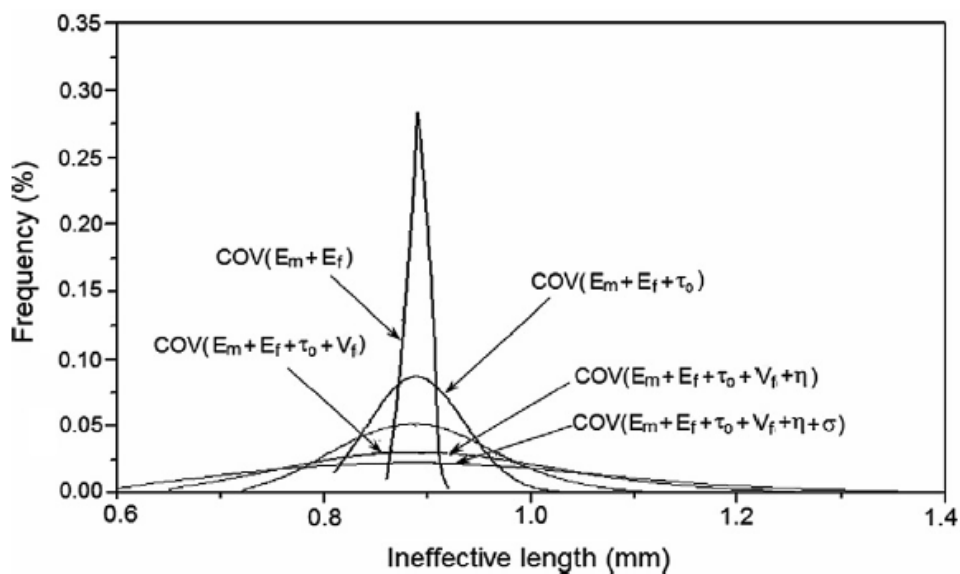
Figure 1-3. Probability distributions of the ineffective length for various combinations of random variables [27].

Composite materials show a wide variety of failure mechanisms as a result of their complex structure and manufacturing process. The accuracy of the reliability analysis is critically dependent on the appropriate criterion for the study conditions. Moreover, the reliability methods can be used to provide a reliability-based calibration to define the safety factors in the composite structure [16].

1.3.4 Stochastic finite element methods

Previous works are oriented into obtaining an analytical solution to the reliability calculation of composite structures. Therefore, they have their limitations on the size and the shape of the structure to be analysed. The FE analysis is a powerful tool to study the behaviour of complex structural systems. A stochastic finite element modelling (SFEM) implies that the values at each element are stochastic in nature, leading to random properties [28]. Computer power has grown at an increasing pace during the last few years permitting the SFEM to resolve large scale problems.

Mendoza-Jasso [29] studied the open hole off-axis test of a unidirectional IM7/8552 carbon epoxy composite. In this case, the macromechanical properties E_1, E_2, v_{12} and G_{12} were treated as stochastic variables, with their values varying for the entire coupon. A local variability of the fibre volume fraction V_f is introduced in bands aligned with the fibre axis. V_f of 0.556 with 2 different standard deviations of 0.03 and 0.09 are evaluated. The value of standard deviation was obtained from experimental data. Their results show that the dispersion in the fibre volume fraction is one of the causes of the probabilistic distribution of the failure initiation location in the coupons tested experimentally. The SFEM analysis of complex structures can be coupled with a first-order reliability approach [30]. This approach is applicable to any limit-state criterion that is prescribed in terms of random variables. Measurements of reliability sensitivity with respect to any set of parameters can be easier computed than with MC Simulation.

SFEM is a particularly powerful tool to assign at each element a different property, as shown by Spanos [31]. In this study that deals with single-walled carbon nano tubes, a methodology to assign a different element property to composite plate is introduced. The most used method to deal with the response variability calculation is the Monte Carlo simulation [28]. The mechanical properties are derived from MCS of the volume fraction of the reinforcement at each element. The MCS is the easiest method since it does not require a reformulation of the deterministic formulation of the FE analysis in order to take

account the random field. Thus, the homogenised properties can be used to determine the local Young modulus and the local Poisson's ratio. The volume fractions of the reinforcement were obtained from the micrographic observations. Thus, the values obtained are representative of the reality of the composite plate.

Regardless of the type of analysis to be performed, whether analytical or SFEM, in the majority of cases, the statistical data used as model input assumes that the mechanical properties are independent from the manufacturing process. Indeed, many of the structural performance calculations are based on the data obtained from elementary coupons. When changing the scale and the size of the tested element, the mechanical properties do not correlate with the model prediction. This is often linked to the increased probability of finding a material defect that initiates the failure. However, as Sutherland [32] suggested, the conditions of manufacturing of test specimens having larger dimensions are different from those employed to produce elementary coupons. Thus, the scale of the composite, as well as the fabrication process, must be taken into account when building a material database in order to feed stochastic models.

In order to better understand how the different sources of variability affect the composite structure, another literature survey is performed. This time, the focus is put on the actual manufacturing and how the measuring techniques affect the material properties.

1.4 Identification and quantification of the variability during the manufacturing of composite structures

1.4.1 Interdependencies of the sources of variability of composite materials

As stated, composite materials are the product of multiple complex processing stages to form the composite structure. Each stage adds its own variables that affect the material in various forms. This makes the problem even

more complex, as a unique solution cannot be obtained. As important as it would seem, the study of variability englobing all the composite life cycle sources of variability, starting from the manufacturing process up to the completion of the final part is not a problem widely studied on the open literature. The research is more interested into knowing how a particular variable affects the composite structure for a particular set of manufacturing process and application. This is most probably due to the great number of variables that are involved during the processing of composite components.

In a great effort to understand the sources of variability in composites processing in order to generate more robust design and manufacturing process, Potter [33] identified more than 60 sources of variability and more than 130 defect types. His work is centred on aeronautic structures manufactured by autoclave process and resin transfer moulding (RTM). This work covers the variability sources having origins in the composite prepregs, the shape of the structure, and the effects that are due to thermal stresses and strains resulting from the curing process. One of the most important points to be considered is that the defects in composite materials do not necessarily come from poorly controlled manufacturing processes, but mostly form the complex interactions between the structure geometry and the manufacturing process.

For the autoclave process, which is still a key process in manufacturing composite components principally in the aeronautic industry, the uncertainties that affect the final characteristics of the composite part are dependent of the fibre, matrix and processing. The uncertainties due to reinforcement are the fibre architecture variations which are generated during production, handling or storage of prepregs, dry textiles and preforms. For the matrix, the uncertainties are caused by variations in storage conditions, and by the resin composition and formulations. Finally variations in environmental parameters and processing conditions also affect the properties of the final part. One of the difficulties to deal with the problem during the manufacturing process itself is the interdependencies in each stage of the process [34] (cf. Figure 1-4).
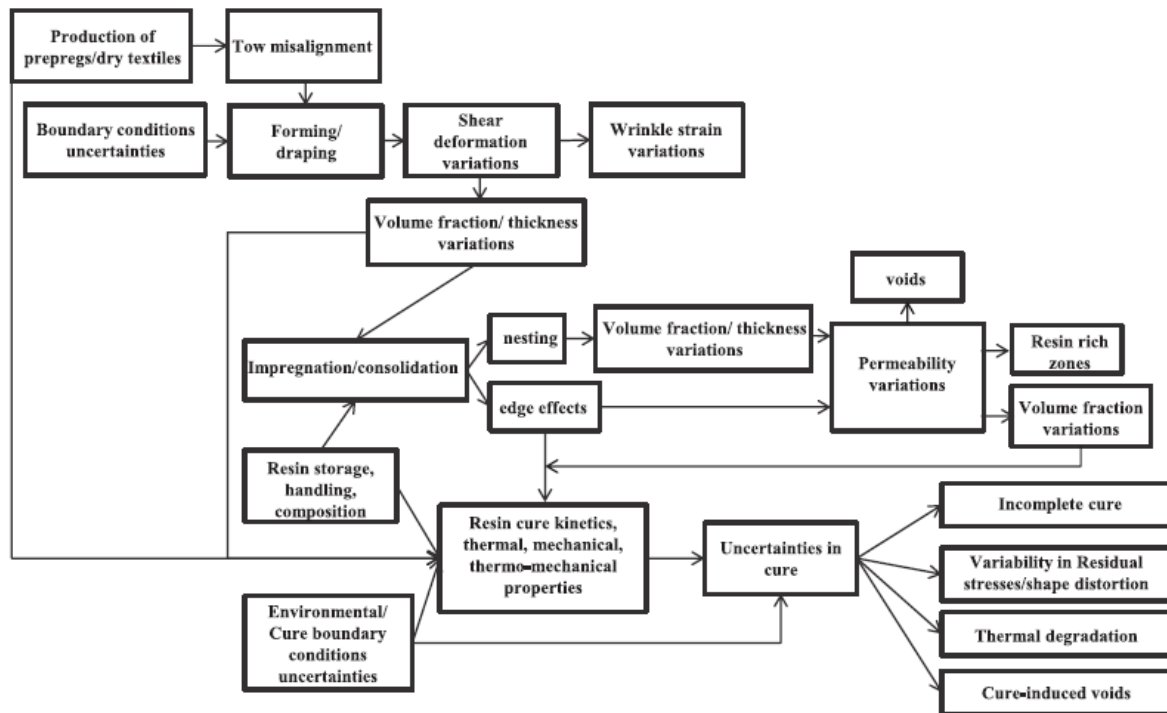
Figure 1-4. Schematic representation of interdependencies in composites manufacturing [34]**.**

1.4.2 Sources of variability in uncured unidirectional prepreg systems

The variability in composite materials can be traced from the prepreg that are used to generate the laminate that conform the structure. For unidirectional (UD) prepregs, they present variations in the mass per unit area. This property is directly linked to the density and thus the volume fractions of the elementary materials in the prepreg. A coefficient of variation (CV) of 1.04 % has been measured for an undisclosed aerospace grade prepreg system [35], with a mean value of 406.54 g m^{-2}. In this study, samples taken from 14 different prepreg batches have been controlled by a standard acceptance test. The fibre content and the resin weight fraction have been also controlled. It is found that the mass per unit area of the controlled prepreg rolls has a mean value of 267.19 g m^{-2} with a CV of 0.74 %. The resin content of the system, evaluated as the resin weight fraction, is 34.27 % with a CV of 1.67 %. As can be seen, the prepreg material presents variations in its constitutive properties; these variations can be

transferred to the cured part, especially on thinner laminates that are more dependent on point-to-point variability.

The composite prepreg can also be a source of porosity, both by the presence of entrapped voids and by the surface roughness of the prepreg, which shows a preferential orientation transverse to the fibre direction [36].

1.4.3 Fibre misalignments

Variations in fibre orientation have an important impact on the composite structure performance. These variations are the result of several factors present during the different stages of the structure manufacturing. Fibre misalignment is one of the few sources of variability, that is well studied in the literature due to its importance to the mechanical strength of the composite, especially during buckling [22,36,37].

The fibre misalignment can be determined in two different stages of the composite material. The first one is a direct measure on the prepreg or reinforcement preform. The second one is the determination of the fibre shape of the cross-section of the composite material.

A direct measurement on the prepreg to determine a maximum misalignment angle and a mean wavelength of the undulations is presented by Potter [39]. The UD prepregs are wound onto a drum for transportation and storage. This process causes undulations of the inner part of the ply to eliminate the path difference that is due to the ply thickness, which is between 0.250 to 0.350 mm, thus creating a sinusoidal in-plane waviness. The measured undulations present a wavelength of 3 mm with an amplitude of 0.03 mm. These values correspond to a prepreg stored on a 300 mm diameter drum. This effect causes that the variability in the fibre orientation is already a pre-existing condition of the otherwise considered UD prepregs. Although the global response will not be greatly influenced by the inevitable fibre misalignments, it is not true to say that the misalignments will not have effects on local responses.

Autocorrelation methods can be coupled with image analysis to obtain a statistical representation of the fibre misalignments in a woven textile [40]. It was found that the mean warp direction was -0.1° with a standard deviation of 0.36°, and for the weft direction the orientation is 86.68° with a SD of 0.95°. The same methodology was also applied for a ± 45 non-crimp fabric (NCF) with results yielding a zero deviation from the mean orientation with a standard deviation of 1.22° for both directions [41].

The majority of the works that deal with fibre misalignments is done by observing the cross section of cured specimens by measuring the fibre diameter. Yurgartis [42] was the first to propose a method in which the actual fibre misalignment can be calculated from the ellipsoidal form of the fibres. He measured a carbon/APC-2 composite obtaining a mean angle of 3.71° with a standard deviation of 0.794°. Even though this method is sensible to the assumed fibre diameter, it is however powerful in the sense that it can be used to determine the in-plane and out-of-plane misalignments of the fibre bundles and it is widely used to estimate the porosity fractions in cured composites [43].

The limitation of this method is the careful treatment that must be given to the surface of the composite cross-section for microscopic analysis. The use of a fast Fourier transform (FFT) on lower resolution images of the cross-sections coupled with autocorrelation function allows the mean fibre orientation to be obtained on a specific zone [43–45]. The FFT coupled with filtering techniques means that the quality of the images of the cross-section can be lower and thus being taken by other means than optic microscopy, like X-rays. New technologies, like the use of a 3D tomography, allow the determination of the 3D behaviour of a fibre by means of a micro tomography technique [47]. This last technique can be used to determine the local volume fractions and fibre orientations in the three major axes of the specimens.

1.4.4 Ply thickness

The ply thickness of a composite structure is usually considered as constant and equal for all plies, provided that there is no change of the geometry of the cross-section and stratification. In reality, each ply in the stratification can have different mean thicknesses that are dependent on the ply orientation and their position in the stratification [48]. As seen in the literature, the study in changes on the ply thickness is related to sudden changes in the geometry of the composite part (singularities) like the sections in the vicinity of bended sections leading to ply wrinkling [48,49] (cf. Figure 1-5). Regardless its major importance on the strength of a composite structure [10], the variation of this property is not well documented in the open literature, and the ply thicknesses are derived from the plate thickness measurements and their values are assumed constant over all the plate [47,50].
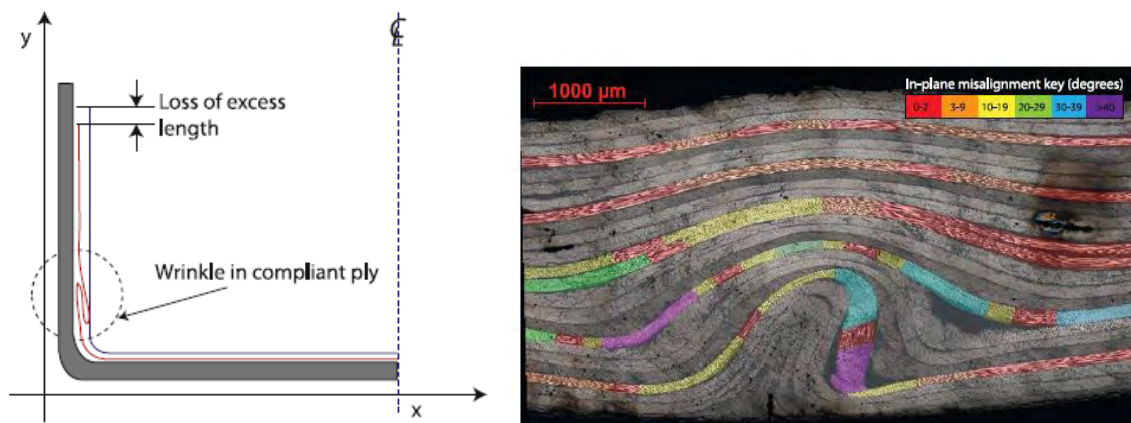
Figure 1-5. On the left hand side the shear slip representation resulting in the formation of an S-shaped wrinkle and on the right hand side the of 0° plies showing severe out-of-plane misalignment in a micrograph of a ([90/45/0/-45]₃)ₛ stratification with intermediate debulks, showing an in-plane misalignment of greater than 20° in three of the six 0° plies in the vicinity of the S-shaped wrinkle [49].

1.4.5 Composite properties affected during autoclave curing

The polymerisation cycle of a composite part plays a major role in the determination of the properties of the composite structure. The interactions

between all the factors involved in the cure cycle, such as the visco-elastic properties of the resin system, resin flow, resin shrinkage, cure degree, arrangement of the reinforcements, temperature and pressure cycles, make the correlation between the entry parameters and the composite properties a challenging task [34].

The principal parameters that control the material properties are the applied pressure and temperature cycles, and thus are the ones subjected to optimisation in order to extract the best material properties of the structure [52,53]. When dealing with thick laminates, a substantial amount of temperature lag and overshoot at the centre of a laminate is usually experienced due to the large thickness and low thermal conductivity of the composites. Furthermore, it requires a longer time for the resin to bleed out of the laminate. In some cases, consolidation is not completed before the resin viscosity rises beyond the processable range, which results in a poor consolidation region at the core area [54]. When compared to thin laminates, the properties of a thick laminate exhibit an evolution through the thickness of the core of the structure, showing an increasing fibre volume fraction through the top of the laminate [55].

Nonetheless, the parameter that has a greater impact on the properties of the composite material is the void content. Voids can develop inside laminates if the pressure conditions of the cure cycle are not correctly controlled. There are several causes of void formation, but the most commonly studied are the entrapment of gases (mostly wet air) during impregnation of the fibres with resin or during the lay-up process; and the volatiles arising from the resin system itself [55–58]. In the process, resin flow is the primary mechanism to remove the excess resin and voids entrapped in the laminate to obtain a uniform composite plate. The data shows that there is a large resin pressure drop at the laminate bleeder interface when the resin flow in the bleeder was considered, which leads to a variation of the resin pressure, fibre compaction and fibre rearrangement [60]. The permeability of the bleeder has control over the resin absorbing capacity. A bad selection of the bleeder material results in resin rich and resin starved regions

within the laminate, thus affecting the laminate quality. The fibre volume fraction of the laminate is a function of the resin pressure distribution [61], the number and the sequence of the employed vacuum bagging products, the nature of the resin and reinforcements, the part thickness, and the lay-up sequence. The outputs of the system are the volume fractions of the elementary materials, the volume fraction and size of the voids in the structure, the resin flow, the degree of polymerisation of the resin and the presence of exothermal peaks during curing that are traduced into matrix cracking.

Another effect that impacts the properties of a composite structure is the interaction between the composite and the tool, since a mismatch of the coefficient of thermal expansion generates warpage of the composite piece caused by the residual strains and stresses in the cured part.

Furthermore, the internal stresses generated during the cure process are one of the subjects studied with great interest in the open literature. The presence of internal stresses are due to different material and manufacturing conditions such as the mismatch between the thermo-elastic properties of fibres and resin, resin shrinkage, and the interaction between the composite part and the tool [62]. Figure 1-6 [62] shows, on the left hand side, the 'input' variables such as material, geometry and process. On the right hand side the 'output' variables are the residual stress and shape distortions. The two branches indicate the origin of stress factors which are present during the forming of the composite products.
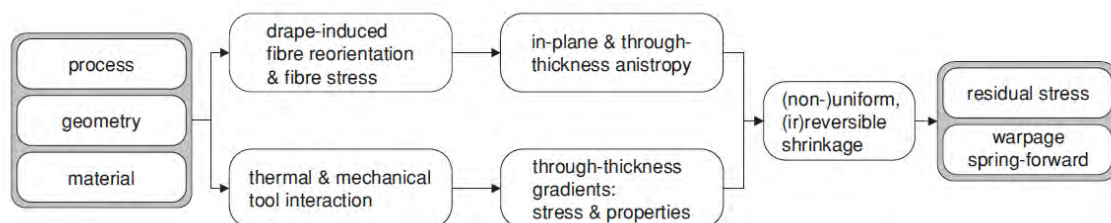
Figure 1-6. Diagram showing the origin of residual stress and shape distortions in CFRP composite processing [62]**.**

The residual stresses and strains can generate matrix cracking and de-bonding in the interface of the fibre and matrix, and generate geometric distortions on the composite part. The variation of angled parts due to resin shrinkage and anisotropic thermo-elastic properties is known as spring-in, whereas the global deformation of originally flat parts, caused by tool-part interaction, is described as warpage [63].

Using optical fibre Bragg grating (FBG) sensors, Mulle et al. [64,65] assessed the residual strains of a composite plate cured in autoclave. First, the residual strains were evaluated in an elementary specimen consisting of 8 unidirectional plies of the HexPly® M21/T700 carbon-epoxy system. One FBG was placed between the ply #2 and #3, while the second FBG was placed between the ply #7 and #8. This arrangement was chosen in order to determine a gradient in the residual strains. The thin unidirectional specimen does not exhibit a gradient of residual stains between the layers closer to the mould-side and the layers on top of the composite. Subsequently, using a technological specimen consisting in a 28 plies in a thick zone and 20 plies in a thin zone with an optimized stratification, the FBG were placed in 4 different layers to assess the strain distribution generated during the cooling phase during the cure process in the autoclave. A clear distribution of the residual strains through the thickness was found. These differences were attributed to the possible influence of environmental effects and the variability of the thought-the-thickness thermal properties. The use of FBG to determine the internal state of the material during the curing process can be complemented with ultrasonic measurements to follow the different stages of the cycles in order to measure at what stage the composite consolidates [66].

1.4.6 Variability attributed to an inclusion of a structural feature

The added variability, which is a structural feature (or singularity) of a composite structure, represents a great challenge for the designers and manufacturers. The sudden change in the material properties, which are mostly

due to material discontinuities and added materials, leads to a new level of complexity in the study of structures. However, the majority of the structures have material singularities that accomplish a very precise function within the composite structure. Among the singularities that are most commonly present in composite structures are ply drop-offs [67,68], inclusion of stiffeners [69], drillings [70,71], and structural repairs [72].

In the following paragraph, a structural repair is used as an example of how a singularity in the composite structure can increase the variability of such structure. Unfortunately the scope of this work does not foresee the study in details of this kind of structural singularity. However, it can serve as statement of the open problems that still exist for the design and analysis of composite structures.

Few studies have been made concerning the repair of composite parts. One of the major problems, that affect the composite structures after the removal of the damaged material and the adding of a repair patch, is the loss of structural integrity and the complete transfer of loads from the parent structure to the repair patch. As shown by Whittingham [72] there exist several mismatches between the parent part and the patch in a bonded scarf joint. Using either a hard patch cured before being installed in the structure or a soft patch cured in-situ, several problems have been observed. The principal problem is the warping of the most exterior plies of the patch. This effect is more significant for the soft patches. This warpage creates a mismatch in the continuity of the repaired plies and the original plies, which can create an improper transmission of loads (cf. Figure 1-7). Another effect that is necessary to consider is the size and the form of the bond line. In an ideal repair situation, the bond line is constant between the parent structure and the repair patch. However, depending on the type of used patch, a difference in the thickness of the bond line, resin pockets, porosity and adhesive voids may appear (cf. Figure 1-8).
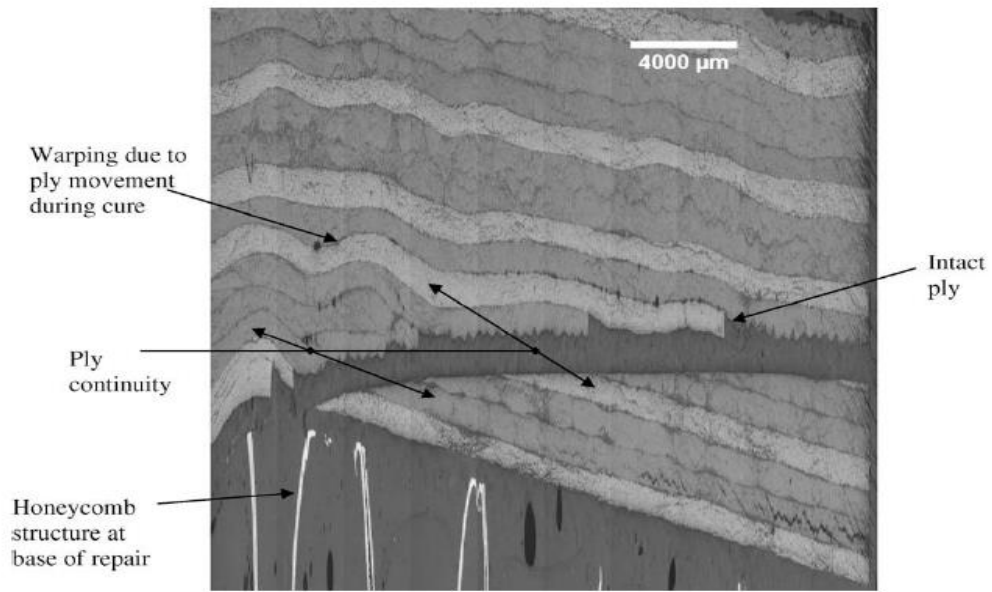
Figure 1-7. Soft-patch detail at base of repair, curvature in end of scarf cavity probably caused by hand machining error [72].
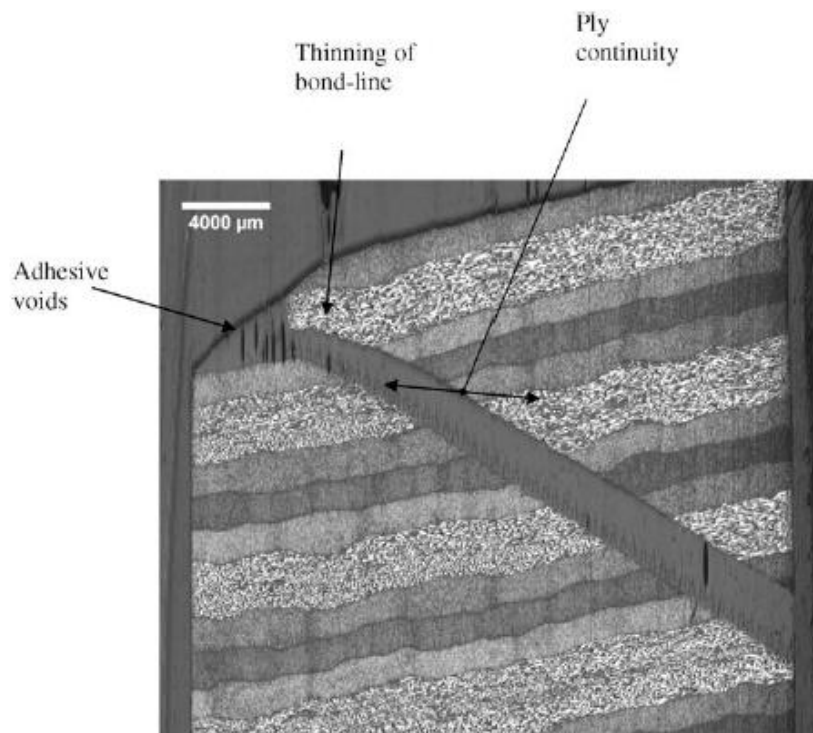
Figure 1-8. Moulded patch, detail of outer edge of repair [72].

1.5 Conclusions

As shown in the above literature review, the variability in composite materials is an open topic that is considered in many different manners. Regardless, the fact that there is no common framework applied at each stage of the composite solution, starting from the definition of variability which is open to interpretation from the researcher or designer.

Regarding the process of analysis and design of composite structures, there are many approaches to take into account the variability in the mechanical properties. The Monte Carlo simulation is the reference to which other types of methods are compared. Despite the various approaches and methods applied to study the composite problems, the majority does not account for the continuous variations of a property within a single part, other than the study of localised defects. The mechanical properties are varied for all elements at each iteration, with the same value for all elements.

Additionally, many approaches use the mechanical properties obtained from standard test coupons that do not have the same geometry (stratification) of the designed structure and are not made with the same manufacturing process. As shown, the material properties are highly dependent on the raw materials and manufacturing process, since the interaction between the matrix and reinforcement are very complex. The study of the material variability cannot be detached from the manufacturing process, fibre architecture, resin system, tooling and structure geometry. Therefore, many of otherwise regarded as defects are, in fact, the direct result of the interaction of these parameters.

In this review, a major importance is given to the autoclave processing and unidirectional reinforcements, since this process will be employed in further stages of this document. However, it is important to acknowledge that processes like resin transfer moulding (RTM), filament winding, pultrusion, have their own sources of variability and, thus, must be studied accordingly.

1.6 References

[1]   US Department of Defense, "MIL-HDBK-17-1F: Composite Materials Handbook. Polymer matrix composites: guidelines for characterization of structural materials." 2002.

[2]   Y. Rollet, "Vers une maitrise des incertitudes en calculs des structures composites," ONERA, 2007.

[3]   D. P. Thunnissen, "Propagating and Mitigating Uncertainty in the Design of Complex Multidisciplinary Systems," California Institute of Technology, 2005.

[4]   W. L. Oberkampf, S. M. DeLand, B. M. Rutherford, K. V. Diegert, and K. F. Alvin, "Error and uncertainty in modeling and simulation," Reliab. Eng. Syst. Saf., vol. 75, no. 3, pp. 333–357, Mar. 2002.

[5]   C. C. Chamis, "Probabilistic Composite Design," Compos. Mater. Test. Des., vol. 13, pp. 23–42, 1997.

[6]   C. C. Chamis, "Probabilistic Design of Composite Structures," Int. Conf. Comput. Exp. Eng. Siences, 2007.

[7]   US Department of Defense, "MIL-HDBK-17-3F: Composite Materials Handbook. Polymer matrix composites: materials usage, design, and analysis." US Department of Defense, 2002.

[8]   L. S. Sutherland, R. A. Shenoi, and S. M. Lewis, "Size and scale effects in composites : I. Literature review," Compos. Sci. Technol., no. 59, pp. 209–220, 1999.

[9]   S. Sriramula and M. K. Chryssanthopoulos, "Quantification of uncertainty modelling in stochastic analysis of FRP composites," Compos. Part A Appl. Sci. Manuf., vol. 40, no. 11, pp. 1673–1684, Nov. 2009.

[10]   M. C. Shiao and C. C. Chamis, "Probabilistic evaluation of fuselage-type composite structures," Probabilistic Eng. Mech., vol. 14, no. 1–2, pp. 179–187, Jan. 1999.

[11]   A. Alzina, F. Dau, and L. Guillaumat, "Approche multiéchelle du transport d'incertitudes pour les matériaux composites," in 5ème Journées Fiabilité des Matériaux et des Structures, 2008, pp. 195–204.

[12]   R. Chermaneanu, L. Guillaumat, and F. Dau, "Transport de la variabilité dans les matériaux composites," in JNC 16, 2009.

[13]   Y. Rollet, M. Bonnet, N. Carrère, F.-H. Leroy, and J.-F. Maire, "Improving the reliability of material databases using multiscale approaches," Compos. Sci. Technol., vol. 69, no. 1, pp. 73–80, Jan. 2009.

[14]   M. Di Sciuva and D. Lomario, "A comparison between Monte Carlo and FORMs in calculating the reliability of a composite structure," Compos. Struct., vol. 59, no. 1, pp. 155–162, Jan. 2003.

[15]   P. Venini and C. Mariani, "Free vibrations of uncertain composite plates via stochastic Rayleigh-Ritz approach," Comput. Struct., vol. 64, no. 1–4, pp. 407–423, Jul. 1997.

[16]   M. Chiachio, J. Chiachio, and G. Rus, "Reliability in composites – A selective review and survey of current development," Compos. Part B Eng., vol. 43, no. 3, pp. 902–913, Apr. 2012.

[17]   C. G. Soares, "Reliability of components in composite materials," Reliab. Eng. Syst. Saf., no. 55, pp. 171–177, 1997.

[18]   A. Shaw, S. Sriramula, P. D. Gosling, and M. K. Chryssanthopoulos, "A critical reliability evaluation of fibre reinforced composite materials based on probabilistic micro and macro-mechanical analysis," Compos. Part B Eng., vol. 41, no. 6, pp. 446–453, Sep. 2010.

[19]   T. P. Philippidis, D. J. Lekou, and D. G. Aggelis, "Mechanical property distribution of CFRP filament wound composites," Compos. Struct., vol. 45, pp. 41–50, 1999.

[20]   D. J. Lekou and T. P. Philippidis, "Mechanical property variability in FRP laminates and its effect on failure prediction," Compos. Part B Eng., vol. 39, no. 7–8, pp. 1247–1256, Oct. 2008.

[21]   C. C. António and L. N. Hoffbauer, "From local to global importance measures of uncertainty propagation in composite structures," Compos. Struct., vol. 85, no. 3, pp. 213–225, Oct. 2008.

[22]   M. Walker and R. Hamilton, "A technique for optimally designing fibre-reinforced laminated plates under in-plane loads for minimum weight with manufacturing uncertainties accounted for," Eng. Comput., vol. 21, no. 4, pp. 282–288, May 2006.

[23]   C. Boyer, A. Béakou, and M. M. Lemaire, "Design of a composite structure to achieve a specified reliability level," Reliab. Eng. Syst. Saf., vol. 56, no. 3, pp. 273–283, Jun. 1997.

[24]   A. Béakou and A. Mohamed, "Influence of variable scattering on the optimum winding angle of cylindrical laminated composites," Compos. Struct., vol. 53, pp. 287–293, 2001.

[25]   M. Bouhafs, Z. Sereir, and A. Chateauneuf, "Effet des incertitudes mécaniques et géométriques sur la conception des pipelines en composite," in JNC 17, 2011, pp. 1–9.

[26]   M. Bouhafs, Z. Sereir, and A. Chateauneuf, "Probabilistic analysis of the mechanical response of thick composite pipes under internal pressure," Int. J. Press. Vessel. Pip., vol. 95, pp. 7–15, Jul. 2012.

[27]   M. A. Khiat, Z. Sereir, and A. Chateauneuf, "Uncertainties of unidirectional composite strength under tensile loading and variation of environmental condition," Theor. Appl. Fract. Mech., vol. 56, no. 3, pp. 169–179, Dec. 2011.

[28]   G. Stefanou, "The stochastic finite element method: Past, present and future," Comput. Methods Appl. Mech. Eng., vol. 198, no. 9–12, pp. 1031–1051, Feb. 2009.

[29]   A. J. Mendoza Jasso, J. E. Goodsell, A. J. Ritchey, R. Byron Pipes, and M. Koslowski, "A parametric study of fiber volume fraction distribution on the failure initiation location in open hole off-axis tensile specimen," Compos. Sci. Technol., vol. 71, no. 16, pp. 1819–1825, Nov. 2011.

[30]   A. Der Kiureghian and J.-B. Ke, "The stochastic finite element method in structural reliability," Probabilistic Eng. Mech., vol. 3, no. 2, pp. 83–91, Jun. 1988.

[31]   P. D. Spanos and a. Kontsos, "A multiscale Monte Carlo finite element method for determining mechanical properties of polymer nanocomposites," Probabilistic Eng. Mech., vol. 23, no. 4, pp. 456–470, Oct. 2008.

[32]   L. S. Sutherland, R. A. Shenoi, and S. M. Lewis, "Size and scale effects in composites: II. Unidirectional laminates," Compos. Sci. Technol., vol. 59, no. 59, pp. 221–233, 1999.

[33]   K. D. Potter, "Understanding the origins of defects and variability in composites manufacture," in ECCM 14, 2009.

[34]   T. S. Mesogitis, A. A. Skordos, and A. C. Long, "Uncertainty in the manufacturing of fibrous thermosetting composites: A review," Compos. Part A Appl. Sci. Manuf., vol. 57, pp. 67–75, Feb. 2014.

[35]   K. D. Potter, C. Langer, B. Hodgkiss, and S. Lamb, "Sources of variability in uncured aerospace grade unidirectional carbon fibre epoxy preimpregnate," Compos. Part A Appl. Sci. Manuf., vol. 38, no. 3, pp. 905–916, Mar. 2007.

[36]   D. H.-J. a. Lukaszewicz and K. D. Potter, "The internal structure and conformation of prepreg with respect to reliable automated processing," Compos. Part A Appl. Sci. Manuf., vol. 42, no. 3, pp. 283–292, Mar. 2011.

[37]   H. M. Hsiao and I. M. Daniel, "Effect of fiber waviness on stiffness and strength reduction of unidirectional composites under compressive loading," Compos. Sci. Technol., vol. 56, no. 5, pp. 581–593, Jan. 1996.

[38]   P. Berbinau, C. Soutis, P. Goutas, and P. T. Curtis, "Effect of off-axis ply orientation on $0°$ -fibre microbuckling," Compos. Part A Appl. Sci. Manuf., vol. 30, pp. 1197–1207, 1999.

[39]   K. D. Potter, B. Khan, M. R. Wisnom, T. Bell, and J. Stevens, "Variability, fibre waviness and misalignment in the determination of the properties of composite materials and structures," Compos. Part A Appl. Sci. Manuf., vol. 39, no. 9, pp. 1343–1354, Sep. 2008.

[40] A. A. Skordos and M. P. F. Sutcliffe, "Stochastic simulation of woven composites forming," Compos. Sci. Technol., vol. 68, no. 1, pp. 283–296, Jan. 2008.

[41] T. S. Mesogitis, A. A. Skordos, and A. C. Long, "Non-crip fabrics geometrical variability and its influence on composite cure," in ECCM 16, 2014.

[42] S. W. Yurgartis, "Measurement of small angle fiber misalignments in continuous fiber composites," Compos. Sci. Technol., vol. 30, no. 4, pp. 279–293, Jan. 1987.

[43] A. F. Avila and D. T. S. Morais, "A multiscale investigation based on variance analysis for hand lay-up composite manufacturing," Compos. Sci. Technol., vol. 65, no. 6, pp. 827–838, May 2005.

[44] C. J. Creighton, M. P. F. Sutcliffe, and T. . Clyne, "A multiple field image analysis procedure for characterisation of fibre alignment in composites," Compos. Part A Appl. Sci. Manuf., vol. 32, no. 2, pp. 221–229, Feb. 2001.

[45] K. Kratmann, M. P. F. Sutcliffe, L. Lilleheden, R. Pyrz, and O. Thomsen, "A novel image analysis procedure for measuring fibre misalignment in unidirectional fibre composites," Compos. Sci. Technol., vol. 69, no. 2, pp. 228–238, Feb. 2009.

[46] M. P. F. Sutcliffe, S. L. Lemanski, and A. E. Scott, "Measurement of fibre waviness in industrial composite components," Compos. Sci. Technol., vol. 72, no. 16, pp. 2016–2023, Nov. 2012.

[47] G. Requena, G. Fiedler, B. Seiser, P. Degischer, M. Di Michiel, and T. Buslaps, "3D-Quantification of the distribution of continuous fibres in unidirectionally reinforced composites," Compos. Part A Appl. Sci. Manuf., vol. 40, no. 2, pp. 152–163, Feb. 2009.

[48] F. Collombet, M. Mulle, Y.-H. Grunevald, and R. Zitoune, "Contribution of Embedded Optical Fiber with Bragg Grating in Composite Structures for Tests-Simulations Dialogue," Mech. Adv. Mater. Struct., vol. 13, no. 5, pp. 429–439, Aug. 2006.

[49] J. S. Lightfoot, M. R. Wisnom, and K. Potter, "A new mechanism for the formation of ply wrinkles due to shear between plies," Compos. Part A Appl. Sci. Manuf., vol. 49, pp. 139–147, Jun. 2013.

[50] P. Hallander, M. Akermo, C. Mattei, M. Petersson, and T. Nyman, "An experimental study of mechanisms behind wrinkle development during forming of composite laminates," Compos. Part A Appl. Sci. Manuf., vol. 50, pp. 54–64, Jul. 2013.

[51] D. Stefaniak, E. Kappel, T. Spröwitz, and C. Hühne, "Experimental identification of process parameters inducing warpage of autoclave-processed CFRP parts," Compos. Part A Appl. Sci. Manuf., vol. 43, no. 7, pp. 1081–1091, Jul. 2012.

[52]   A. V. Lombardi, "Technological optimisation of a smart thermosetting aeronautical composite subject to fatigue bending loads," Prog. Aerosp. Sci., vol. 39, no. 5, pp. 385–404, Jul. 2003.

[53]   N. Ersoy, T. Garstka, K. D. Potter, M. R. Wisnom, D. Porter, M. Clegg, and G. Stringer, "Development of the properties of a carbon fibre reinforced thermosetting composite through cure," Compos. Part A Appl. Sci. Manuf., vol. 41, no. 3, pp. 401–409, Mar. 2010.

[54]   W.-B. Young, "Compacting pressure and cure cycle for processing of thick composite laminates," Compos. Sci. Technol., vol. 54, no. 3, pp. 299–306, Jan. 1995.

[55]   P. Olivier and M. Cavarero, "Comparison between longitudinal tensile characteristics of thin and thick thermoset composite laminates : influence of curing conditions," Comput. Struct., vol. 76, pp. 125–137, 2000.

[56]   P. Olivier, J. P. Cottu, and B. Ferret, "Effects of cure cycle pressure and voids on some mechanical properties of carbon / epoxy laminates," Composites, vol. 26, no. 7, pp. 509–515, 1995.

[57]   S. Hernandez, F. Sket, J. M. Molina-Aldareguia, C. González, and J. LLorca, "Effect of curing cycle on void distribution and interlaminar shear strength in polymer-matrix composites," Compos. Sci. Technol., vol. 71, no. 10, pp. 1331–1341, Jul. 2011.

[58]   L. Liu, B.-M. Zhang, D.-F. Wang, and Z.-J. Wu, "Effects of cure cycles on void content and mechanical properties of composite laminates," Compos. Struct., vol. 73, no. 3, pp. 303–309, Jun. 2006.

[59]   L. K. Grunenfelder and S. R. Nutt, "Void formation in composite prepregs – Effect of dissolved moisture," Compos. Sci. Technol., vol. 70, no. 16, pp. 2304–2309, Dec. 2010.

[60]   Y. Li, M. Li, Y. Gu, and Z. Zhang, "Numerical and Experimental Study of the Bleeder Flow in Autoclave Process," Appl. Compos. Mater., vol. 18, no. 4, pp. 327–336, Sep. 2010.

[61]   A. S. Ganapathi, S. C. Joshi, and Z. Chen, "Simulation of bleeder flow and curing of thick composites with pressure and temperature dependent properties," Simul. Model. Pract. Theory, vol. 32, pp. 64–82, Mar. 2013.

[62]   K. Tarsha-Kurdi and P. Olivier, "Thermoviscoelastic analysis of residual curing stresses and the influence of autoclave pressure on these stresses in carbon/epoxy laminates," Compos. Sci. Technol., vol. 62, no. 4, pp. 559–565, Mar. 2002.

[63]   S. Wijskamp, "Shape distortions in composites forming," University of Twente, 2005.

[64]   C. Albert and G. Fernlund, "Spring-in and warpage of angled composite laminates," Compos. Sci. Technol., vol. 62, no. 14, pp. 1895–1912, Nov. 2002.

[65]   M. Mulle, F. Collombet, P. Olivier, and Y.-H. Grunevald, "Assessment of cure residual strains through the thickness of carbon–epoxy laminates using FBGs, Part I: Elementary specimen," Compos. Part A Appl. Sci. Manuf., vol. 40, no. 1, pp. 94–104, Jan. 2009.

[66]   M. Mulle, F. Collombet, P. Olivier, R. Zitoune, C. Huchette, F. Laurin, and Y. Grunevald, "Assessment of cure-residual strains through the thickness of carbon–epoxy laminates using FBGs Part II: Technological specimen," Compos. Part A Appl. Sci. Manuf., vol. 40, no. 10, pp. 1534–1544, Oct. 2009.

[67]   F. Collombet, G. Luyckx, C. Sonnenfeld, Y.-H. Grunevald, Y. Davila, M. Torres Arellano, X. Jacob, K.-T. Wu, B. Douchin, L. Crouzeix, R. Bazer-Bachi, T. Geernaert, J. Degrieck, and F. Berghmans, "Industrial part cure monitoring in autoclave: added value of complementary instrumentation," in 19th ICCM, 2013, pp. 1178–1187.

[68]   G. Meirinhos, J. Rocker, J. Cabanac, and J.-J. Barrau, "Tapered laminates under static and fatigue tension loading," Compos. Sci. Technol., vol. 62, no. 4, pp. 597–603, Mar. 2002.

[69]   A. Weiss, W. Trabelsi, L. Michel, J.-J. Barrau, and S. Mahdi, "Influence of ply-drop location on the fatigue behaviour of tapered composites laminates," Procedia Eng., vol. 2, no. 1, pp. 1105–1114, Apr. 2010.

[70]   C. K. Huang, "Study on co-cured composite panels with blade-shaped stiffeners," Compos. Part A Appl. Sci. Manuf., vol. 34, no. 5, pp. 403–410, May 2003.

[71]   L. Guillaumat and Z. Hamdoun, "Reliability model of drilled composite materials," Compos. Struct., vol. 74, no. 4, pp. 467–474, Aug. 2006.

[72]   R. Zitoune, L. Crouzeix, F. Collombet, T. Tamine, and Y. Grunevald, "Behaviour of composite plates with drilled and moulded hole under tensile load," Compos. Struct., vol. 93, no. 9, pp. 2384–2391, Aug. 2011.

[73]   B. Whittingham, A. Baker, A. Harman, and D. Bitton, "Micrographic studies on adhesively bonded scarf repairs to thick composite aircraft structure," Compos. Part A Appl. Sci. Manuf., vol. 40, no. 9, pp. 1419–1432, Sep. 2009.

Chapter 2: Towards the modelling of the variability spread over a CFRP structure

2.1 Problem statement

One of the main challenges linked to the use of composite materials in structural applications is the difficulty to determine the effects on the mechanical performance that are due to the inherent variability of these type of materials [1]. Such variabilities do not only make the properties of two composite parts to be different to each other, but, they can also cause significant differences between two points in the same structure.

In recent years, both designers and researchers are interested to integrate probability-based approaches in the analysis of composite structures like reliability and optimisation based methods [2–5]. Regardless of the type of approach employed, the Monte Carlo simulation (MCS) is still the most used method for solving problems with variable parameters, even though it is costly in terms of calculation time and resources [6]. For these probability-based approaches, the input values vary according to the probability distribution functions (PDF) of the composite mechanical properties, which are based on the statistical analysis of experimental data [7]. Furthermore, a proper process of identification and quantification of the input values and their variability must be performed in order to introduce realistic inputs to accurately predict the structural behaviour.

It is also important to note that, in all the studies found in the open literature that deal with composite structures having continuous reinforcements at the meso and macro scales, the variation of the material properties is done for all

elements at each simulation. Indeed, the models do not take into consideration the property variations from one point to another within the same part.

2.2 Proposal of a finite element analysis framework to take into account the variability of the composite material

The principal aim of this work is the proposition of a framework for the finite element (FE) analysis of composite structures in which the element properties vary within the same composite structure. The gradients in the property changes within the FE model are controlled at the different composite scales by means of mathematical functions. This means that the element properties are not assigned in a purely random manner in order to avoid a maximal difference in the property value between two or more neighbouring elements. The mathematical functions that control the gradient of element values are based on physical measurements. This will ensure that the set of inputs of the FE model will be in agreement with the reality of the material.

2.3 Inclusion of variability in finite element analysis of composite structures

2.3.1 Description of the modelling proposal

As an example to illustrate the concept of including and controlling a continuous variation of the properties within a single part, a composite plate consisting of a single ply divided into 40 x 20 elements is hereby presented. In this example the chosen property is the normalized stiffness in the x-direction NE_x which is obtained by the relationship $E_x / \bar{E}_x$. The mean normalised Young's modulus is 1 (GPa/GPa) with a coefficient of variation of 10 %. As explained, it is possible to assign to each element a different stiffness drawn from a known, or assumed, probability distribution. In this example, a normal distribution is used.

The distribution of the stiffness for each element is illustrated in Figure 2-1. As shown in the figure, some of the elements with a maximum normalised Young's modulus are beside elements with minimum stiffness. Indeed, the distribution of stiffness has spatial discontinuities that do not have a physical meaning other than a localised defect in the material. In contrast, the goal of this approach, in this stage, is not the characterisation of local defects, but the determination of the distribution of the material properties.
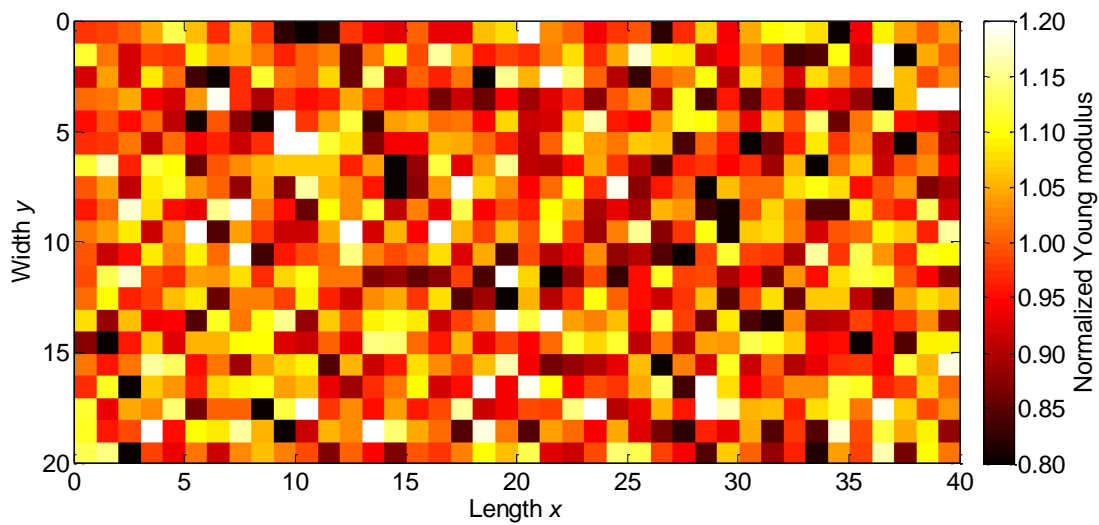
Figure 2-1. Map of a randomly distributed normalised Young's modulus over a composite lamina with a mean of 1 (MPa/MPa) and standard deviation of 0.1.

To control the variation of the stiffness over two different points of the composite lamina, the value assignation to each element can be done by means of known mathematical function. Thus, the change in the properties from one element to another maintains a spatial continuity without having significant changes between neighbouring elements. An example of a known function to introduce the values to the elements is a sine wave (cf. equation 2-1), where the parameters of each sinusoid can be controlled to maintain a specified mean and standard deviation. The resulting distribution does not contain discontinuities between neighbouring elements (cf. Figure 2-2).

$$NE_x = 0.1(\sin 2\pi x + \sin 2\pi y) \tag{2-1}$$
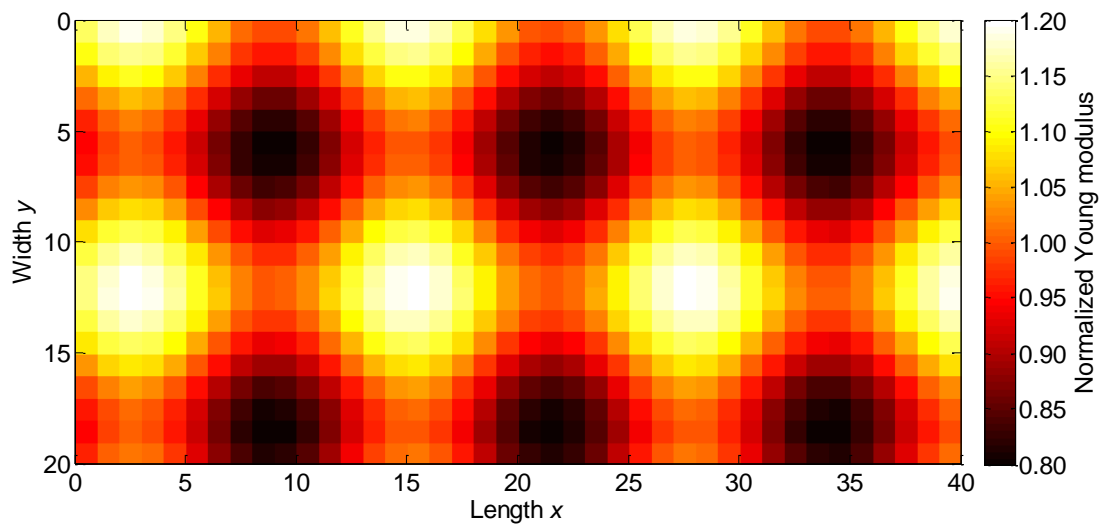
Figure 2-2. Map of the distribution of the normalised Young's modulus spread over a composite lamina with a known distribution where the mean NE_x still equal to 1 with a standard deviation of 0.1.

The introduction of random phase shifts φ_1 and φ_2 to equation 2-1 that vary with each simulation (cf. equation 2-2) can be used to obtain a distribution of stiffness that is not as structured as the previous distribution, but still maintains a spatial continuity in the assigned values (cf. Figure 2-3). The resulting distribution still has a mean normalised Young's modulus of 1 (GPa/GPa) and a standard deviation of 0.1, and since the phase shifts are variable, a different set of properties is assured at each simulation.

$$NE_x = 0.1\left[\sin\left(2\pi x + \varphi_1\right) + \sin\left(2\pi y + \varphi_2\right)\right] \tag{2-2}$$
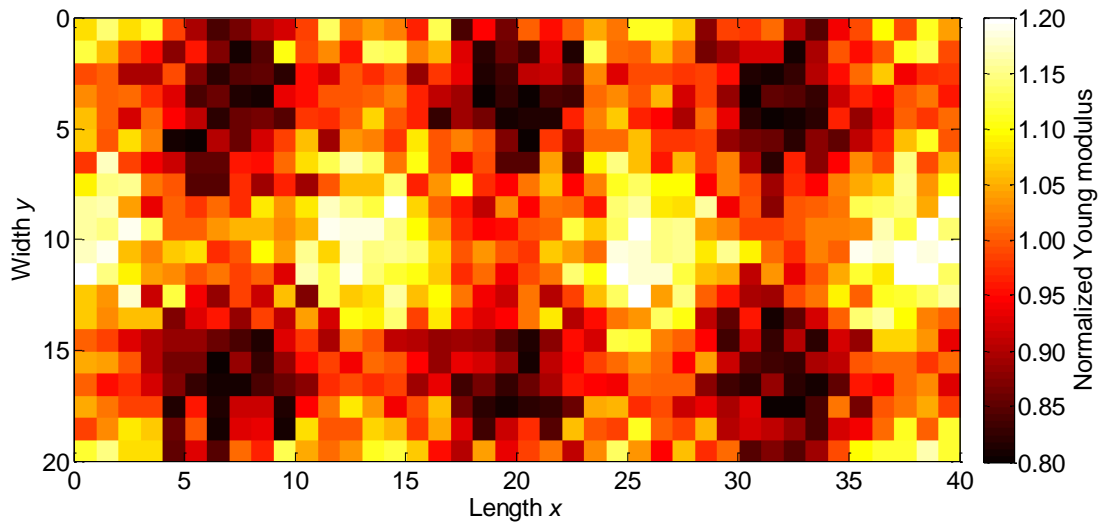
Figure 2-3. Map of the distribution of the Young's modulus spread over a composite lamina with a known distribution with random phase shifts.

Equations 2-1 and 2-2 are only meant to be examples on how the gradient of the element properties can be controlled whilst still maintaining the probability of generating randomly certain parameters so as to generate an infinity of different pieces at each simulation. It is not the goal of this work to introduce directly the material property values, such as Young's moduli and Poisson's ratios, to each element since the local values of these properties are not known. These material properties, however, can be derived from geometrical parameters that can be measured in the actual composite structure. Among the countless physical variables that affect the structure, the ply thickness and the reinforcement orientation are two parameters that can be quantified directly on the composite.

It is important to notice, that the mathematical models hereby proposed do not try to reconstruct the original variables 'as is'. The aim is to generate a property variation that exhibits the same order of magnitude as the real physical quantity. The introduction of random parameters within each model is to promote the variation at each simulation. These random parameters are also in agreement with the physical observations of the composite material.

2.3.2 *Obtaining the material properties from the geometrical variations*

The input values for the FE model are the engineering constants such the Young's and shear moduli, the Poisson's ratios, and the coefficient of thermal expansion in the principal directions of the lay-up. The FE modelling will be performed in SAMCEF® software using composite shell elements. In this program, it is possible to introduce the ply thickness and the ply orientation per element. In a first phase, the material properties of the element can be derived from the local ply thickness and the engineering constants of the constituent materials by means of the law of mixtures. The modelling strategy is presented in Figure 2-4. Starting from the evolution of the ply thickness t, the porosity of the ply V_p and the mass per unit area of the reinforcement ρ_{Af}, the volume fractions of the reinforcement V_f and matrix V_m are calculated. Using these values, the elastic constants in the principal directions of each element are calculated. The ply orientation θ remains as an independent variable that is introduced directly in the lay-up attribute file for each element.

To ensure a quality of data that can be used in a broad family of plates, we have chosen the generation of a material database that does not only draw data from probabilistic functions of the input variables, but generates continuous variations according with simple mathematical models to represent the spatial variation of certain properties.
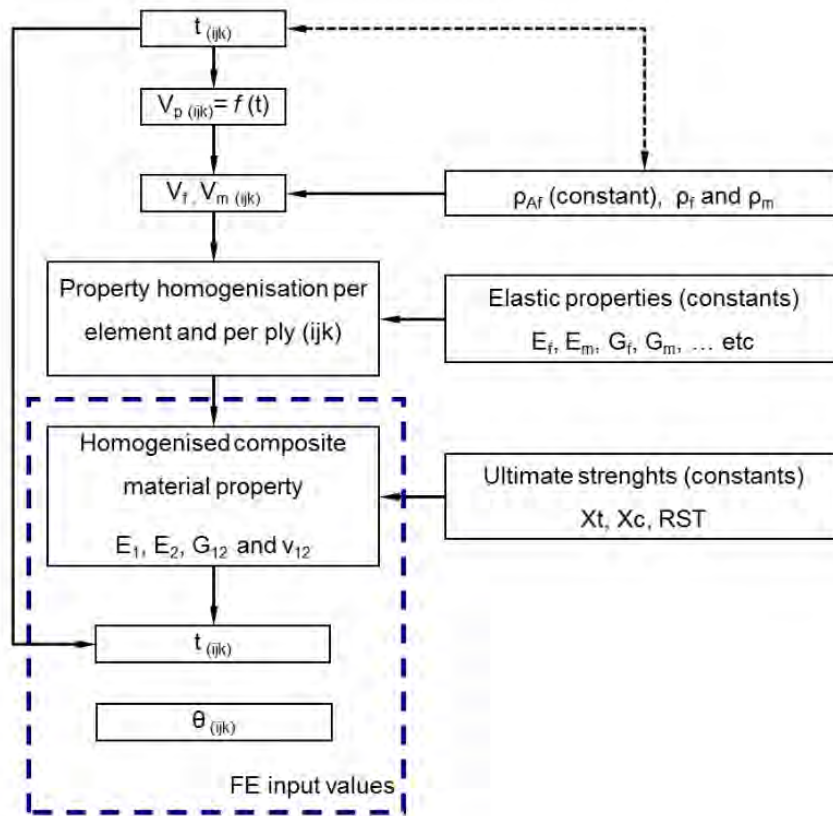
Figure 2-4. Schema generation and assignment of elastic properties in the F.E. model, element per element and ply per ply.

2.3.3 Value-added of the proposed methodology for the design and analysis of composite structures

As explained in Chapter 1 and section 2.1, the usual path to analyse a composite structure by probabilistic analysis is to obtain from the normalised test the material properties and adjust such properties to the probability distribution functions that better describe the experimental data [4,7,8]. It is also noteworthy that the input variables come from material databases obtained during standard test coupons. These coupons deviate from the actual material used in the composite structure in terms of geometry and manufacturing process, thus skewing the values of the material [9]. After the model generation, the solution is usually determined by Monte Carlo simulations. This, however, does not prevent

the use of other types of stochastic analysis, such as reliability based methods [6], optimisation based procedures [10] and stochastic finite element methods [11]. The properties introduced into the model are thus homogenous in the sense that they represent the same set of properties from one point to another in the structure [12]. Nonetheless, the material properties are varied in all elements of the model at each individual simulation. This results in fact that, in the most extreme cases, the model outputs do not have a physical sense, since all the properties are either in the most favourable of the least favourable combination.

This method proposes a thoughtful approach in the construction of the material database and preparation of the model. By introducing geometrical variabilities that are measured on the actual composite structure, such as the ply thickness and the fibre orientation, thus the derived mechanical properties are in agreement with these geometric variations inside the plate. The designer has more control on the assignation of values to each finite element through mathematical laws obtained from the observation of the physical structure. These laws can be modified accordingly with new observations. The input parameters of the mathematical function parameters are drawn from probabilistic distributions. This inhibits the possibility of having gradients of values comparable to a material defect or values that do not have a physical sense.

The proposed method produces results that are in agreement with the physical reality of the structure. Thus, the obtained distributions can help to reduce the model uncertainties especially at the tails of the probability distribution. It is also noteworthy that having a heterogeneous solution can may be indicate a failure probability in a certain point of the structure that can be otherwise overlooked by more traditional methods of probability based approaches.

2.4 Measurements of variability in a composite structure cured in autoclave

2.4.1 Choices for the identification and quantification of sources of variability in a CFRP structure

Few research efforts are interested in the determination and measurement of sources of variability in order to give a physical meaning. The influence of these variabilities in the material properties before and after manufacturing is also scarcely studied. Potter [13–15] has worked in the identification of defects in the aeronautic structures produced from unidirectional prepregs. These defects include variation in density, fibre undulations (due to the storage of prepreg roll), wrinkles from folding and lay-up of curved forms, residual stresses and effects of 'spring in/out' after polymerization. Therefore the identification and quantification of variability must be performed during the manufacturing stage of composite parts.

The composite materials are multi-scale systems with complex interactions of variables through the different scales of the composite. One of the challenges that arise when dealing with this type of materials is the adequacy of such data to the scale at which this data is being assessed.

2.4.2 Challenges in the multi-scale characterisation of the variability in composite structures

The study of the variability in composite materials represents a challenge from the point of view of the measuring techniques, since it must take into account all the interdependencies among the variables, as well as the way they are coupled of all the scales of the composite material. Therefore, the main problem regarding the data collection deals with the methods needed to characterise any given property at a certain composite scale which is most probably incompatible with the measurement of the same property at another scale.

Considering the example of determination of the fibre volume fractions in the composite at a ply level and at the structure scale as depicted in Figure 2-5. The first step to determine the fibre content by volume in a composite material is to obtain a specimen from the mother plate. At this moment, due to the tools and technique to obtain the specimen, its exact position in the plate can only be known within certain margin. This can be critical if the zone of interest is near to singularity in the composite material. At this point, decisions must be made in order to determine the technique to evaluate the volume fractions of the elementary constituents. To determine the volume fractions at ply scale, the most common technique used is the micrographs of the cross-section in the composite. This implies that the specimen has to be placed in a mounting resin and prepared for optical or scanning electron microscopy to obtain images of the polished cross section of the specimen. The determination of the volume fractions is done by image analysis of the obtained micrographs. The results depend on the quality of the images, including the finishing quality of the cross section, the size of the images, and the ability of the operator to apply the correct filters and ceiling levels to determine the fibre, matrix and voids content. Conversely, for the determination of the volume fractions of the composite constituents of the whole specimen, one of the used methods for a carbon/epoxy system is by chemical digesting the composite matrix. This implies the measurement of the specimen density and applying the procedure indicated in the applicable standards (see NF EN 2564 [16] or ASTM D3171 [17]). The uncertainties in the measurements depend on the ability of the operator, the equipment employed, and the assumed values of the density of water and constituent materials.
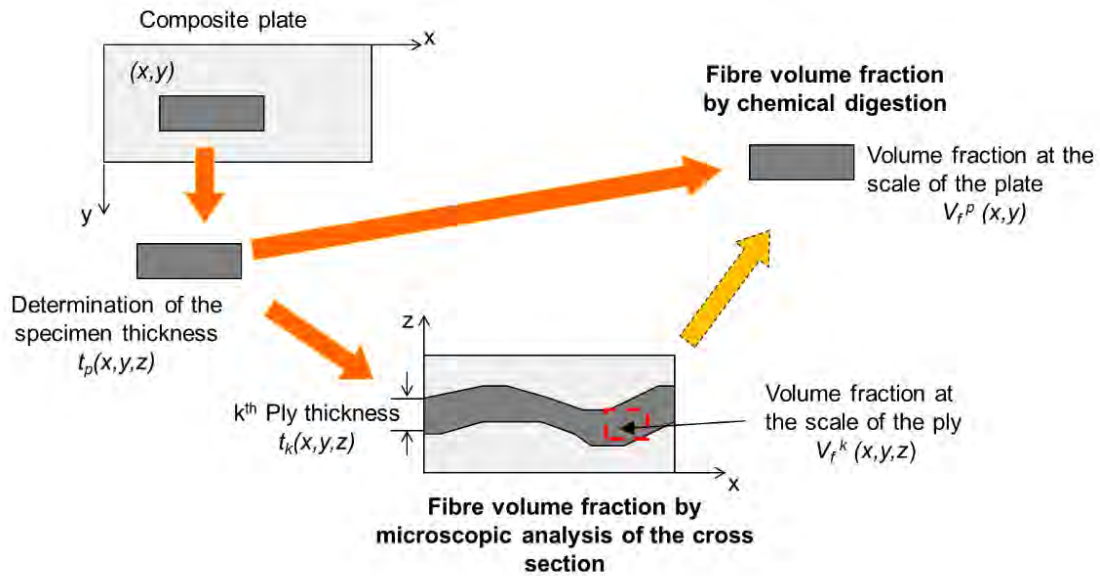
Figure 2-5. Challenges in the determination of the volume fractions of the constituent material at local scale (ply scale) and global (specimen) scale.

The obtained values for each scale cannot be cross-checked with the same specimen within an acceptable tolerance, since both techniques are mutually exclusive. The micrograph analysis implies the addition of an external material to the existing specimen (mounting resin) to facilitate the polishing of the cross-section, as well as its observation in the microscope. In case that one would like to obtain the volume fractions at the scale of the ply by means of matrix digestion of this particular specimen, the additional resin must be removed prior to the procedure. Nonetheless, the complete removal of the mounting resin is not guaranteed, and an impact on the measured values is therefore expected. On the other hand, the matrix digestion implies the destruction of the specimen as the determination of the ratios of the composite constituents are functions of the initial weight of the specimen and the final mass of the remaining fibres after the complete consumption of the resin. This hypothetical scenario does not take into account the use of a special mechanical mounting of the specimens for their preparation for microscopic observation, since the use of such equipment might not be available for every laboratory.

The measurement of the volume fractions, as explained above, is only an example to illustrate the difficulties to retrieve certain information at two different material scales. This kind of difficulty is present when measuring other physical variables at different scales of the composite material.

2.5 Overall description of the methodology

The autoclave curing of unidirectional (UD) prepregs remains the standard in the manufacturing of aircraft parts. Thus, the methods presented in this document are presented for this manufacturing method.

The process of identification, quantification and modelling of variability in a composite structure is performed through the fabrication of composite plates (12) of dimensions 615 x 300 mm. The material used in this process is the HexPly® M10.1/38%/UD300/CHS which is a carbon/epoxy UD prepreg. The prepreg plies are cut and laid-up by hand. The chosen lay-up is a 16 ply quasi-isotropic with a stacking sequence of $[90/-45/0/(+45)_2/0/-45/90]_s$. The stacking sequence is chosen since it is representative of industrial parts.

On one hand, since there are many variables and factors interdependent with each other, to quickly allow and to facilitate a physical interpretation of the data, the calculations and the statistical analysis are carried out with probabilistic distributions such as the uniform distribution and normal distribution. On the other hand, this does not mean that these distributions are the most adequate to represent the parameter variations. Other types of probability distribution functions, such as the 2-parameter Weibull and the lognormal distributions, can fit better the experimental data. Nevertheless, the scope of this work is not to perform an in-depth statistical analysis of the material properties, but to provide a methodology than can be used to enrich the material databases by providing a manner to control the parameters gradient within a structure composite and can be variable during multiple simulations.

All statistical moments (average, standard deviation, etc.), unless otherwise indicated, are reported with a 95 % confidence level. Additionally, the alpha value, which serves as a ceiling for the rejection of the null hypothesis in various statistical tests is 0.05.

2.6 References

[1] US Department of Defense, "MIL-HDBK-17-3F: Composite Materials Handbook. Polymer matrix composites: materials usage, design, and analysis." US Department of Defense, 2002.

[2] C. C. Chamis, "Probabilistic simulation of multi-scale composite behavior," *Theor. Appl. Fract. Mech.*, vol. 41, no. 1–3, pp. 51–61, Apr. 2004.

[3] C. C. Chamis, "Probabilistic Design of Composite Structures," *Int. Conf. Comput. Exp. Eng. Siences*, 2007.

[4] S. Sriramula and M. K. Chryssanthopoulos, "Quantification of uncertainty modelling in stochastic analysis of FRP composites," *Compos. Part A Appl. Sci. Manuf.*, vol. 40, no. 11, pp. 1673–1684, Nov. 2009.

[5] A. Shaw, S. Sriramula, P. D. Gosling, and M. K. Chryssanthopoulos, "A critical reliability evaluation of fibre reinforced composite materials based on probabilistic micro and macro-mechanical analysis," *Compos. Part B Eng.*, vol. 41, no. 6, pp. 446–453, Sep. 2010.

[6] M. Di Sciuva and D. Lomario, "A comparison between Monte Carlo and FORMs in calculating the reliability of a composite structure," *Compos. Struct.*, vol. 59, no. 1, pp. 155–162, Jan. 2003.

[7] D. J. Lekou and T. P. Philippidis, "Mechanical property variability in FRP laminates and its effect on failure prediction," *Compos. Part B Eng.*, vol. 39, no. 7–8, pp. 1247–1256, Oct. 2008.

[8] T. P. Philippidis, D. J. Lekou, and D. G. Aggelis, "Mechanical property distribution of CFRP filament wound composites," *Compos. Struct.*, vol. 45, pp. 41–50, 1999.

[9] L. S. Sutherland, R. A. Shenoi, and S. M. Lewis, "Size and scale effects in composites : I. Literature review," *Compos. Sci. Technol.*, no. 59, pp. 209–220, 1999.

[10] M. Bouhafs, Z. Sereir, and A. Chateauneuf, "Probabilistic analysis of the mechanical response of thick composite pipes under internal pressure," *Int. J. Press. Vessel. Pip.*, vol. 95, pp. 7–15, Jul. 2012.

[11] N. Hyuk-Chun, "Stochastic finite element analysis of composite plates considering spatial randomess of material properties and their correlations," *Steel Compos. Struct.*, vol. 11, no. 2, pp. 115–130, 2011.

[12] M. C. Shiao and C. C. Chamis, "Probabilistic evaluation of fuselage-type composite structures," *Probabilistic Eng. Mech.*, vol. 14, no. 1–2, pp. 179–187, Jan. 1999.

[13] K. D. Potter, M. Campbell, C. Langer, and M. R. Wisnom, "The generation of geometrical deformations due to tool/part interaction in the manufacture of composite components," *Compos. Part A Appl. Sci. Manuf.*, vol. 36, no. 2, pp. 301–308, Feb. 2005.

[14] K. D. Potter, C. Langer, B. Hodgkiss, and S. Lamb, "Sources of variability in uncured aerospace grade unidirectional carbon fibre epoxy preimpregnate," *Compos. Part A Appl. Sci. Manuf.*, vol. 38, no. 3, pp. 905–916, Mar. 2007.

[15] K. D. Potter, B. Khan, M. R. Wisnom, T. Bell, and J. Stevens, "Variability, fibre waviness and misalignment in the determination of the properties of composite materials and structures," *Compos. Part A Appl. Sci. Manuf.*, vol. 39, no. 9, pp. 1343–1354, Sep. 2008.

[16] AFNOR, "NF EN 2564: Série aérospatiale - Stratifiés de fibres de carbone - Détermination de la teneur en fibres en résine et du taux de porosité.," 1998.

[17] ASTM International, "ASTM D3171: Standard Test Methods for Constituent Content of Composite Materials," 2011.

Chapter 3: Variability in a CFRP part cured in autoclave

3.1 Material and process

The structural properties are heavily linked to the used material system (fibre and resin types), since many of the intrinsic characteristics of the final piece are given by the interactions between the resin, fibre architecture and other additives or elements present, such as the thermoplastic nodules contained in the HexPly® M21/T700GC prepreg.

In this work, the employed material is the unidirectional prepreg HexPly® M10.1/38%/UD300/CHS from Hexcel Composites. It is a CFRP having mechanical properties similar to the UD M21/T700GC prepreg which is extensively used in the aerospace industry for the production of structural components. Indeed the M10.1/CHS is a non-controlled flow resin system, contrary to the M21 that is a quasi-net prepreg system. Table 3-1 shows the principal characteristics and the main differences between these two materials. The stated values are nominal values without information on their variability (e.g. standard deviation, or coefficient of variation).

Two different batches of the prepreg rolls are investigated. The first roll (*L-1,* Lot No.: 10502F02) has a width of 0.46 m, a length of 110 m for a total area of 50.6 m². The second roll (*L-2,* Lot No.: 2144E002A) has a width of 1 m and a length of 40 m, hence an area of 40 m².

Table 3-1. Nominal properties of the prepreg s UD M10.1/CHS and M21/T700GC.

Property	*M10.1/38%/UD300/CHS* [1]	*M21/35%/268/T700GC* [2]

Reinforcement	High strength carbon UD	Toray T700GC (high strength carbon) UD
Mass per unit area of the reinforcement	300 g m^{-2}	268 g m^{-2}
Matrix	M10.1 (epoxy)	M21 (epoxy)
Curing temperature	120°C	180°C
Mass fraction of resin in the prepreg	38 %	35 % (quasi-net)
Density of prepreg	484 g m^{-2}	412 g m^{-2}
Nominal thickness of the ply	0.320 mm	0.262 mm
Volume fraction of the reinforcement	0.524	0.569
Young modulus *.	130 GPa	148 GPa
Ultimate tensile stress *.	1700 MPa	2375 MPa

* Values "normalised" to $V_f = 0.6$

After preparation, the plates are put in the autoclave. M10.1 resin is an epoxy system that cures at a temperature of 120 °C. The typical cure cycle is shown in Figure 3-1. For a correct material consolidation and reduction of porosity, the cycle has two temperature dwells: the first is maintained at 80 °C (1) for 30 minutes, and the second at 120 °C for 60 minutes (2). A hydrostatic pressure is also applied by maintaining two dwells, the first at 2 bar (3) from the beginning of the cycle until the end of the second heating ramp, and the second pressure dwell of 5 bar (4) is applied until the end of the cycle. In order to avoid residual stresses, as well as thermal damage due to the exothermic peaks during polymerization, heating (5 and 5') and cooling (6) rates are set to 2 °C min^{-1}. A vacuum load of - 0.9 bar (7) is applied throughout the curing cycle to ensure a good ventilation of the volatiles and a good compaction of the material. The total duration of the cycle is roughly 200 to 220 min.
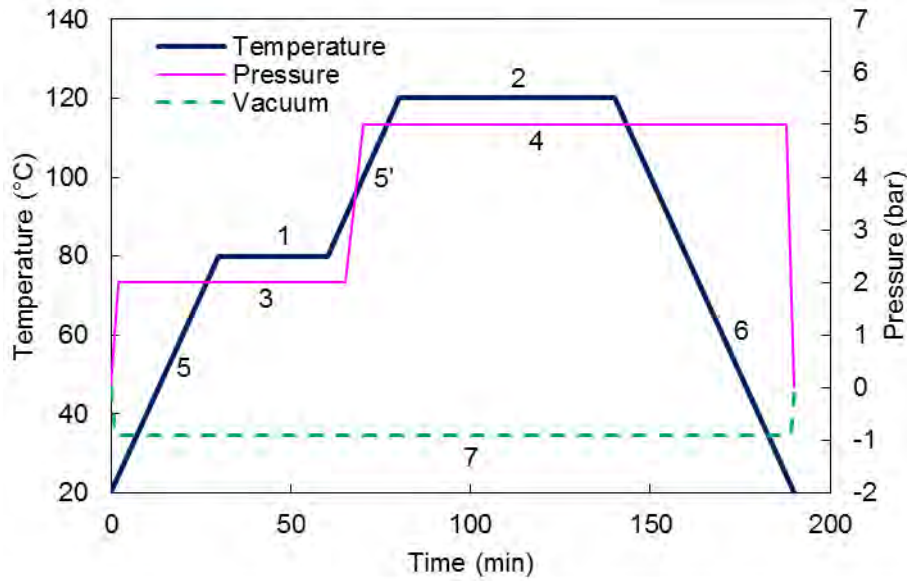
Figure 3-1. Typical cure cycle for a thick plate manufactured in M10.1/38%/UD300/CHS.

3.2 Determination of the mass per unit area of the UD prepreg

3.2.1 Measurement protocol

The density is a property of the material; it is also a source of variability related to the volume fractions of the fibre and matrix. Due to the difficulty to obtain the actual thickness of the prepreg films, this property cannot be easily assessed. Instead, as the mass of the prepreg m_0 and the ply area A_0 can be obtained separately, the mass per unit area ρ_A is determined by a simple relationship (cf. eq. 3-1). Therefore, this property can be used as an indicator of prepreg variability.

$$\rho_A = \frac{m_0}{A_0} \tag{3-1}$$

However, both, the mass and the ply area, cannot be obtained directly because the material is very flexible and its manipulation makes it unusable. Hence, to obtain the ρ_A two indirect methods are used. The first method involves the prepreg plies that will be used in the manufacturing of composite plates. The second method uses dedicated samples of material for the

determination of this property. The ply area, in both cases, is obtained indirectly by measuring the area of the white protective film (silicone paper), which is removed during the lay-up procedure (cf. Figure 3-2). Such protective paper is cut at the same time that the prepreg, thus sharing the same dimensions and it is only separated from the prepreg at the moment of the lay-up.
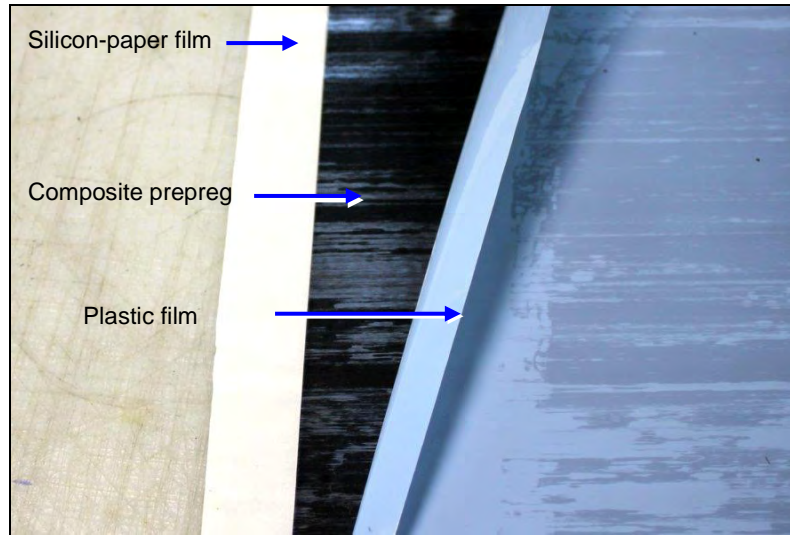
Figure 3-2. Prepreg M10.1/38%/UD300/CHS (view from below).
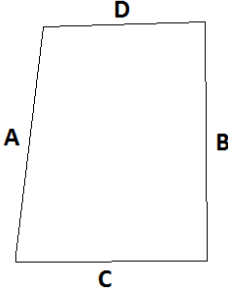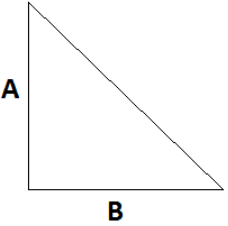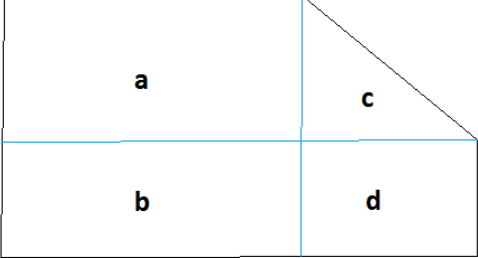
Method 1 - Ply prepregs for the manufacture of composite parts

The mass of prepreg ply is determined indirectly by weighing it with its protective silicone film m_{f+p} (cf. Figure 3-2). After the ply has been laid onto the stratification, the removed protective film is weighed (m_f). The mass of the prepreg composite is obtained by subtracting these two values (cf. eq. 3-2). Since this method can be used to weigh a complete ply of dimensions 600 x 300mm that itself can weigh several hundred grams, the measurement was done in a weighing scale with a precision of 0.1 g. This was the only scale available at the moment of the mass determination that could handle the ply sizes.

$$m_0 = m_{f+p} - m_f \qquad (3\text{-}2)$$

To obtain the ply area, the perimeter of the protective films is measured using a steel rule. Then the area of the ply is calculated using simple geometric formulae (cf. Table 3-2).

Table 3-2. Types, forms and formulas used for calculating the area.

Type	Shape	Formula for calculating the area
Type A (quadrangle)		$A_0 = \left(\dfrac{A+B}{2}\right)\left(\dfrac{C+D}{2}\right)$ (3-3)
Type B (triangle)		$A_0 = \left(\dfrac{A \times B}{2}\right)$ (3-4)
Type C (polygon)		Sum of the areas $A_0 = (A_a + A_b + A_c + A_d)$ (3-5)

Method 2 - Samples not used for the manufacture of parts

Prepreg specimens of dimensions up to 100 x 100 mm are weighed directly in scale of precision of 0.0001 g without their protective films. The reasons of using a higher precision scale are that the prepreg specimens are not going to be used in the fabrication of composite plate, thus they can be deformed; and that the weight of the specimens are in the order of 1.5 g.

The determination of the area of the ply is made by the digital scanning of the protective film (cf. Figure 3-3). The protective film is placed against a black background to improve the contrast at the edges of the film. The image is then processed in 'Image-J'. The area of the prepreg is determined by a correlation between the number of pixels in the image and the relative size of the pixel.

Protection
film

Dark
background

(a)

(b)

(c)

(d)
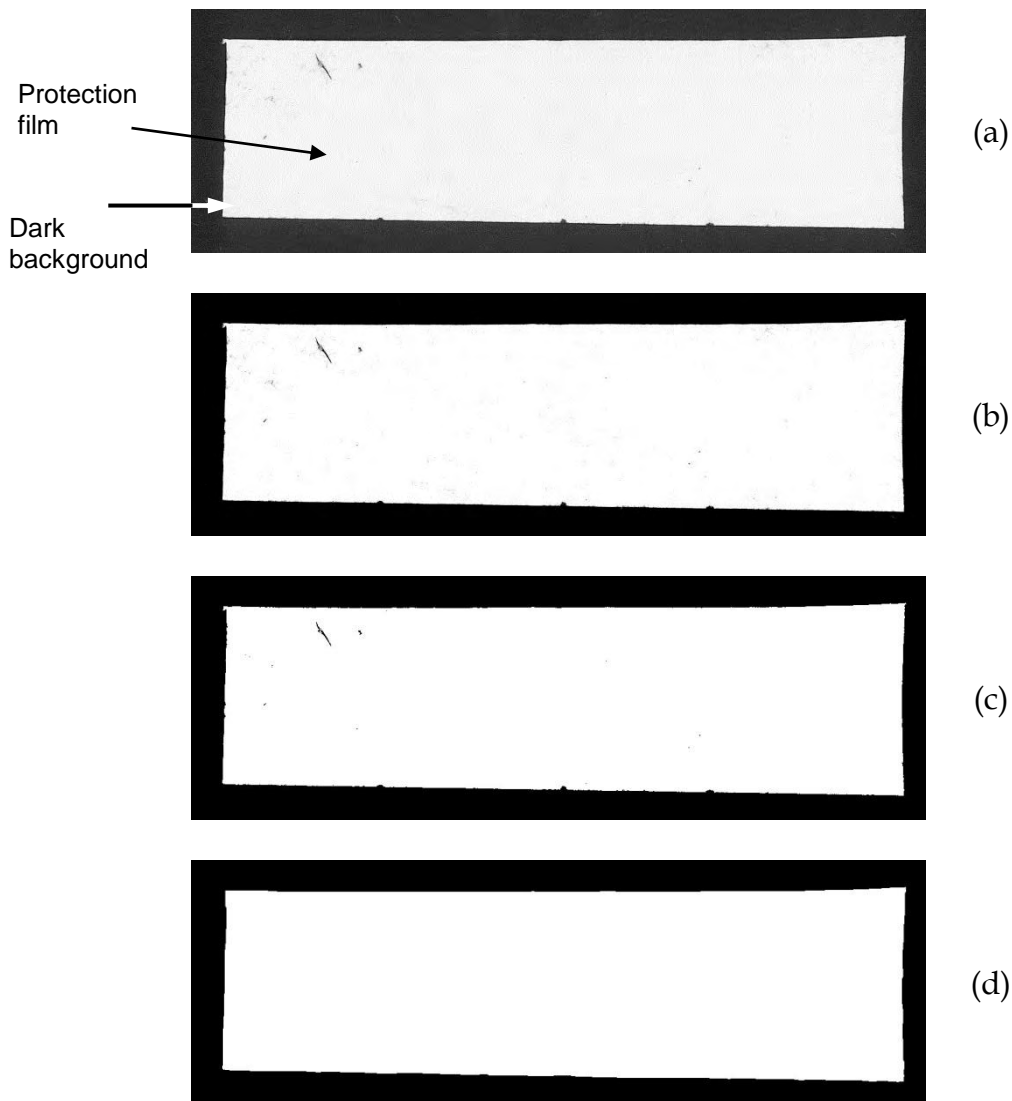
Figure 3-3. Determination of ply areas in protection scan of the image with, (a) the raw image after the scan, (b) correcting the brightness and contrast, (c) binary image and (d) removal of black pixels and smoothing the edges.

For the calibration of the pixel size, a steel rule was also scanned to determine the resolution. The rule is scanned in horizontal and vertical positions to verify that there is no distortion between the horizontal and vertical scan resolutions. The image is scanned using a resolution of 600 dpi (dots per inch) which gives a theoretical equivalence of 23.62 pixel mm^{-1}. The calibration using the rule confirmed this correlation. The area of each pixel corresponds to 1.792×10^{-3} mm^2 or 558 pixels mm^{-2}.

After the scanning of the protective films (cf. Figure 3-3a), the brightness and contrast of images are adjusted to improve the sharpness of the edges (cf. Figure 3-3b). Next, a binarization operation is performed on the image to obtain only white and black pixels (cf. Figure 3-3c). Then the black pixels remaining within the white area are removed as well as a few pixels around the edges (cf. Figure 3-3d). Using the histogram of the image, the number of white pixels is counted. The area of the film is therefore calculated from the correlation of the size of the pixel specified previously, by the number of white pixels N_{px} (cf. eq. 3-6).

$$A_0 = \frac{N_{px}}{558} \text{ or } A_0 = N_{px}\left(1.792 \times 10^{-3}\right) \tag{3-6}$$

3.2.2 *Sampling*

Since the mass per unit area is the ratio of the mass of prepreg divided by the area of the ply, this property does not depend neither on the size of the coupon nor on its shape. The samples have areas ranging from 1 000 mm² to 200 000 mm². To be consistent with the literature, the area density is reported in g m⁻².

Due to the use of several methods for the measurement of the mass and area of the prepreg composite, several types of samples were used. Table 3-3 presents the definition of each measured sample, the method used for the determination of the area density and the number of elements contained in that sample.

Samples *A* and *B* are obtained from the material cut to manufacture the plates of autoclave batches *A* and *B*. The sample *DR* is taken during the material cutting used in the repair of composite structure tests [3]. These three samples are controlled with *method 1*. Using *method 2*, a sample E of 35 elements is then considered. This sample is also used to check that the determined area density is not related to the size or shape of each element.

A sample for more precise control of this property has been measured using the standard NF ISO 10352 [4]. According to this standard, the samples are cut

using a template with an area of 0.01 m² (100 x 100 mm). Then they are weighed in a balance with a precision of 0.0001 g. Due to the dimensions of the used template, which does not correspond to those specified in this standard (i.e., the template has approximate dimensions of 90 x 90 mm), the areas of the protective films are determined by *method 2*. It is also noted that there are differences in the size of the template and of the prepreg cut. Thus, the use of *method 2* allows better accuracy of the measurement. This sample is named *R1*. It has 35 elements which are randomly taken from prepreg roll. On the roll L-2, a series of 10 samples (R2) are taken to verify if, indeed, there is a difference between the two batches of material. The number of elements in this series is limited depending on the available material after cutting and manufacture of composite plates. Samples, such as those from R1 and R2, were taken at random locations on the prepreg rolls.

Table 3-3. Identification of groups for the determination of the mass per unit area.

Group	Method	Description	Number of elements
A	1	Material cut to manufacture batch A plates	91
B	1	Material cut to manufacture batch B plates	87
DR	1	Material cut to manufacture the evaluators of repair from the plates of the batches A and B	72
E	2	Sample to evaluate method 2	34
R1	2	Sample roll R1 (ISO 10352) 90 x 90 mm	35
R2	2	Sample of control of roll R2 (ISO 10352) 90 x 90 mm	10

3.2.3 Results

Table 3-4 shows the measurements taken during the manufacturing of composite parts of autoclave batches *A* and *B*, and the material cutting for repair. It must be observed that there is a significant difference in the average value for each sample. It was noted that variability is lower than the expected 2 %, even if the method for the measurement of the properties is not the optimum.

Table 3-4. Mass per unit area obtained with method 1.

Sample	Number of elements	Average ($g\ m^{-2}$)	Standard deviation ($g\ m^{-2}$)	CV (%)
A	91	502.5	8.24	1.64
B	88	500.7	6.89	1.38
DR	72	501.1	9.30	1.86
Total method 1	**251**	**501.5**	**8.13**	**1.62**

Sample *E* is used to assess the impact of the size and the shape of the elements on the variability of the area density of the material. Samples of group E have an area between 658 mm² and 19 725 mm² (i.e. a difference of 19 067 mm²). However, the shape and the size of the elements that correspond to the R1 sample almost does not vary, i.e. the area of the plies is between 7 785 mm² and 8 251 mm². As noted above, there is no correlation between the dispersion of the mass per unit area and size of the ply. The two samples show very different shapes of ply areas although they have a similar mass per unit area dispersion (cf. Figure 3-4). The differences between the average value and standard deviation of the area density, as shown in Table 3-5, are possibly due to the accuracy of the measure of each of the properties, i.e. the mass and area of the protective film. However, this difference is not statistically significant, and the values of the mass per unit area are independent from the size and shape of the specimen.

Table 3-5. Mass per unit area of material lot L-1 obtained with method 2 samples.

Sample	Number of elements	Average ($g\ m^{-2}$)	Standard deviation ($g\ m^{-2}$)	CV (%)
E1	14	500.8	7.58	1.51
E2	10	505.5	7.59	1.50
E3	10	506.8	8.87	1.75
Total E	**34**	**503.9**	**8.20**	**1.63**
R1	**35**	**500.7**	**6.05**	**1.21**
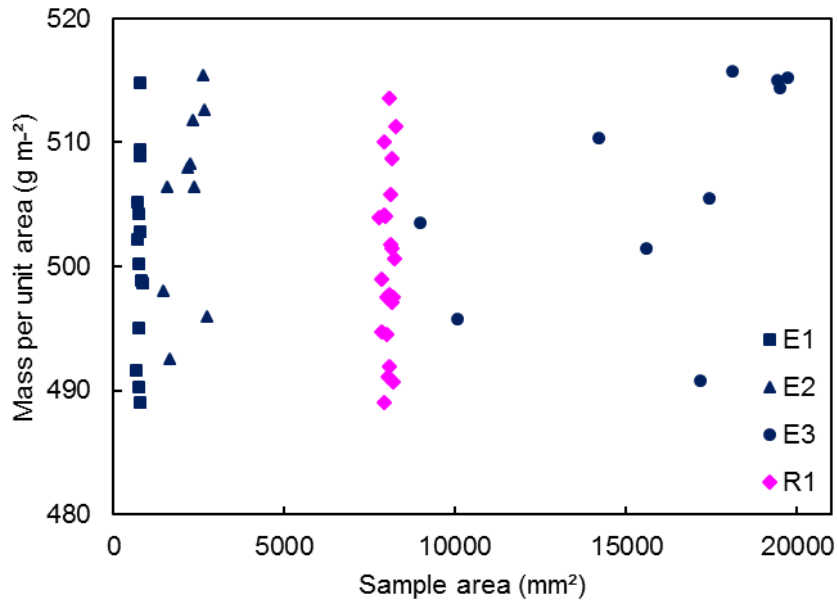
Figure 3-4. Mass per unit area compared to the area of the ply of samples E and R1.

Figure 3-5 shows the average values for each sample and their confidence intervals for the mean. It is observed for samples obtained from material lot L-1 (A, B, DR, E and R1) the average values have a good correlation with the sample R1, which is the sample measured with better precision. By contrast, the R2 sample, used to control the prepreg roll L-2 shows a very different mean value of that observed for samples from the roll L-1. Since the values of the area density do not depend on the size of the specimen, as illustrated by the average values of the *A* and *B* samples compares to the R1 sample, the difference between the R2 and the rest of the specimens is purely due to the nature of the material of the roll L-2.
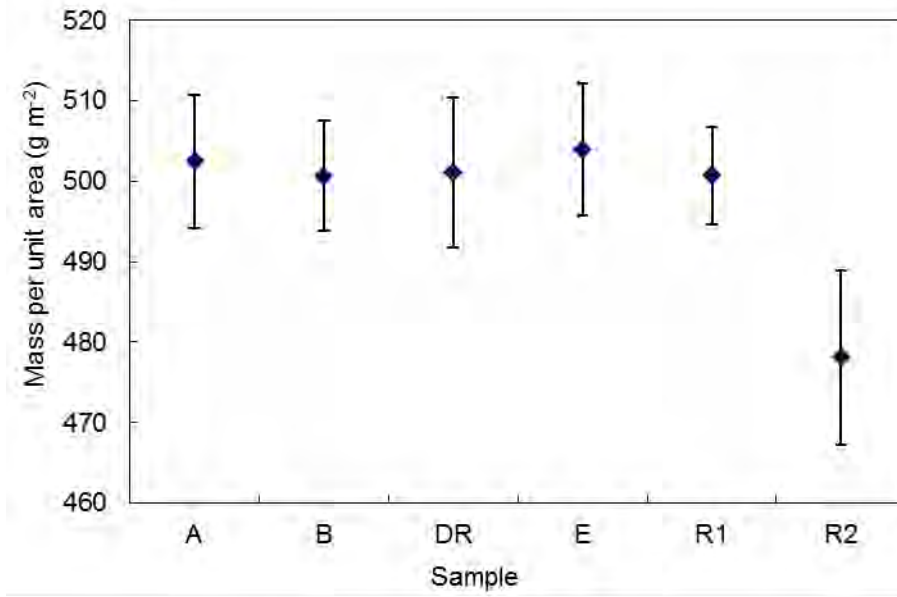
Figure 3-5. Average of the mass per unit area for each specimen with ± 1 standard deviation.

A more precise comparison between R1 and R2 samples is presented in Table 3-6. The standard deviation of each batch of material is a priori different, with a value of 6.05 g m⁻² for lot R1 and 10.76 g m⁻² for lot R2. However, the average of the mass per unit area remains statistically different for these two lots: 500.7 g m⁻² for R1 compared to 478.1 g m⁻² for R2. It is noted that the "nominal" value for this material is 484 g m⁻² [1]. The difference between the values of the standard deviation is feasibly explained by the reduced number of elements of R2 compared to the R1s sample, 10 elements for the former and 35 for the later. However, it is also probably influenced by the nature of the material, since there is no specification for the actual type of fibres included in the M10.1/CHS.

Table 3-6. Summary of samples for comparison between the values of the MS for R1 and R2.

Sample	Number of elements	Average (g m⁻²)	Standard deviation (g m⁻²)	CV (%)
R1	35	500.7	6.05	1.21
R2	10	478.1	10.76	2.25

To corroborate the mean values for each batch of material, a comparison between the actual weight and the theoretical is carried out in Table 3-7. The theoretical mass of the plate is calculated from the average mass per unit area (depending on the used lot of prepreg) and the theoretical surface of material draped to each plate. In any case the difference is not greater than 0.5 % of the actual weight of the plate, despite the differences between the theoretical and real surfaces.

Table 3-7. Comparison between theoretical mass and the actual mass of the plates.

Plate	Roll	MS average (g·m^{-2})	Theoretical plate area (m²)	Theoretical mass (g)	Measured mass (g)	Difference (g)	Difference (%)
A-1	L-1	500.7	2.952	1478.07	1477.7	0.37	0.02
A-2	L-1	500.7	2.952	1478.07	1476.1	1.97	0.13
A-3	L-1	500.7	2.952	1478.07	1477.6	0.47	0.03
B-1	L-1	500.7	2.952	1478.07	1483.2	-5.13	0.35
B-2	L-1	500.7	2.952	1478.07	1483.2	-5.13	0.35
B-2	L-1	500.7	2.952	1478.07	1485.1	-7.03	0.47
C-11	L-2	478.1	2.961	1415.77	1415.1	0.67	0.05
C-12	L-2	478.1	2.961	1415.77	1419.3	-3.53	0.25
C-13	L-2	478.1	2.961	1415.77	1414.3	1.47	0.10
C-21	L-2	478.1	2.961	1415.77	1415.4	0.37	0.03
C-22	L-2	478.1	2.961	1415.77	1414.9	0.87	0.06
C-23	L-2	478.1	2.961	1415.77	1418.9	-3.13	0.22

From the gathered data, one can conclude that variability intra roll of the mass per unit area is lower than expected, approximately 2 %. By contrast, the difference in average value of the mass per unit area between two batches of material is large. The mass per unit area for *lot 1* is 500 g·m^{-2} with a coefficient of variation (CV) of 1.3 %, and for the *lot 2* it is 478 g·m^{-2} with a CV of 2.2 %. For reference, an aeronautical material has an average area density of 406 g·m^{-2} and a standard deviation 4.22 g·m^{-2} (i.e. a CV of 1.04 %) [5]. In this study, several batches of material were controlled (14 material batches in 127 different rolls). In our case, a comparison to this prepreg material is difficult due to the material availability.

However, in this study, several samples per roll have provided better accuracy for the mean and dispersion of the mass per unit area.

3.3 General description of the polymerization cycle for the M10.1/CHS

Composite plates are manufactured in autoclave batches called chronologically *A*, *B* and *C*. The first two batches include 3 plates each, identified as A-1, A-2 and A-3 for the first one, and B-1, B-2 and B-3 for the second one. The plate denominated *-1* is placed at the bottom of the autoclave and the plate *-3* is placed closest to the autoclave door (Figure 3-6). Additionally to the six plates produced in batches A and B, six additional plates are produced in batch C at the same time by arranging them on two levels. The plates are thus identified C-11, C-12, C-13 for the lower level and C-21, C-22 and C-23 for the upper level.
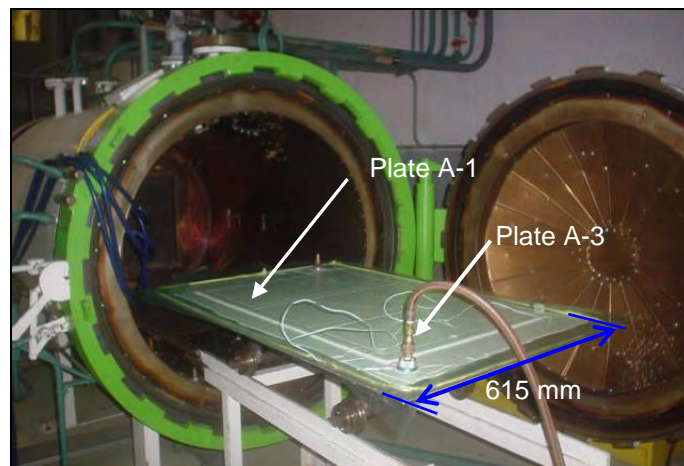
Figure 3-6. Picture of the composite plates prior to introduction into the autoclave.

For precise temperature control of the composite curing cycle, the plates placed at the centre of the tool (plates A-2, B-2, C-12 and C-22), were instrumented with thermocouples. One thermocouple is placed between the plate and the mould (identified as TC-1) and the second one is placed between the top plate and

vacuum bagging products (identified as TC-2, cf. Figure 3-7). These two thermocouples measure the temperature in the thickness of the composite. A priori, the TC-1 thermocouple measures the mould temperature, while TC-2 measures the temperature between the composite plate and the vacuum bag products. An important difference between the temperatures measured by TC-2 and TC-1 indicates an exothermic peak due to the polymerization reaction of the resin. For plates B-2, C-12 and C-22, a third thermocouple is installed in the core of the composite plate (identified as TC-3, cf. Figure 3-7) placed between the 8th and 9th ply for more accurate tracking of the variation of temperature inside the composite during the curing cycle and the verification of the presence of exothermic peak.
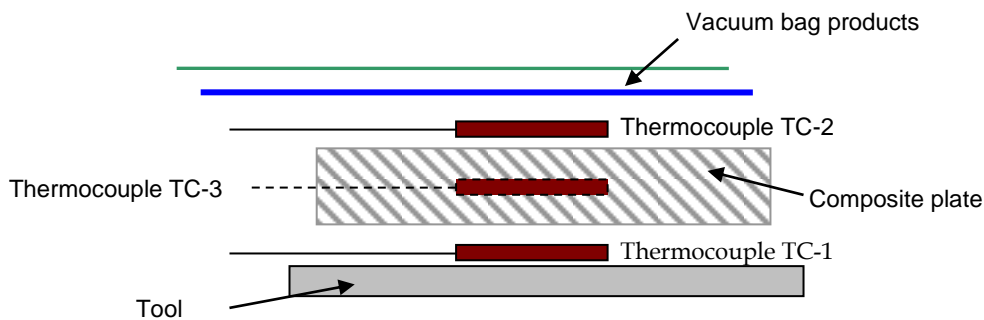
Figure 3-7. Diagram indicating the placement of thermocouples TC-1, TC-2 and TC-3 in the composite plates.

Figure 3-8 shows the cycles of temperature for autoclave batches *A*, *B* and *C*. There is a difference of 10 min of the cycle *A* relative to cycle *B* due to a cooling at the beginning of the cycle. Apart from this variation in the ramps of warming at the beginning of the cycle, there are no significant differences between these two curves. The exothermic peak due to polymerization is greater for cycle *B* compared to cycle *A*. This peak is highlighted in Figure 3-9 which shows the differences in temperature between the thermocouples TC-1 and TC-2 (cf. Figure 3-7). For cycle *B*, the difference of temperatures between TC-2 and TC-1 remains zero most of the time, but for cycle *A*, TC-2 remains warmer for the

40 min mark (after the first isothermal dwell) till the end of the cycle. This difference can be explained by the fact that there is twice as much resin in the bleeder fabric and the breather. Finally, for cycle *B*, Figure 3-10 shows the difference in temperatures between the TC-2 placed between the upper plies and the vacuum products and TC-3 placed in the core of the composite. There are no significant differences between these two temperatures, except at the beginning of polymerization where one can observe a peak of 1° C between the two temperatures.
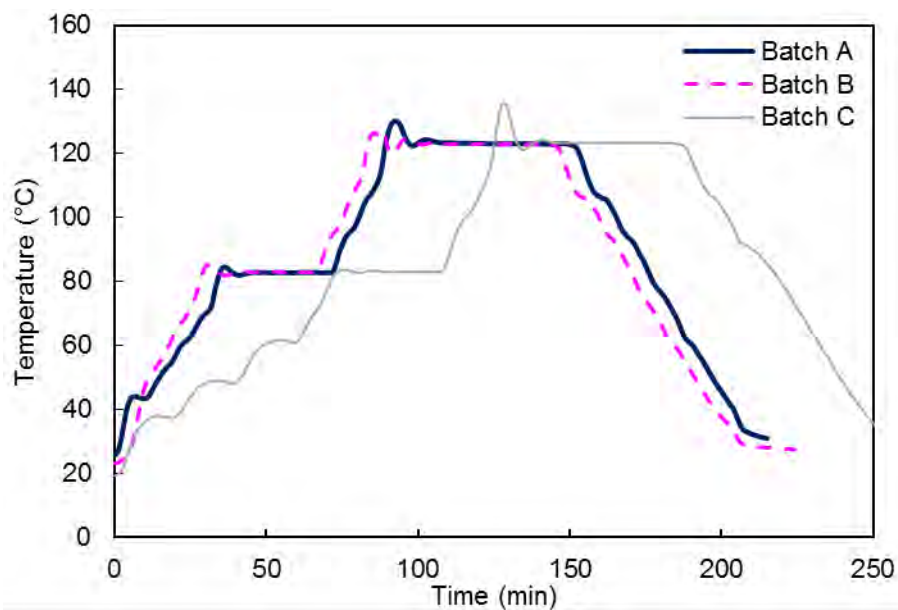
Figure 3-8. Actual cycle of temperature for autoclave batches A, B and C.
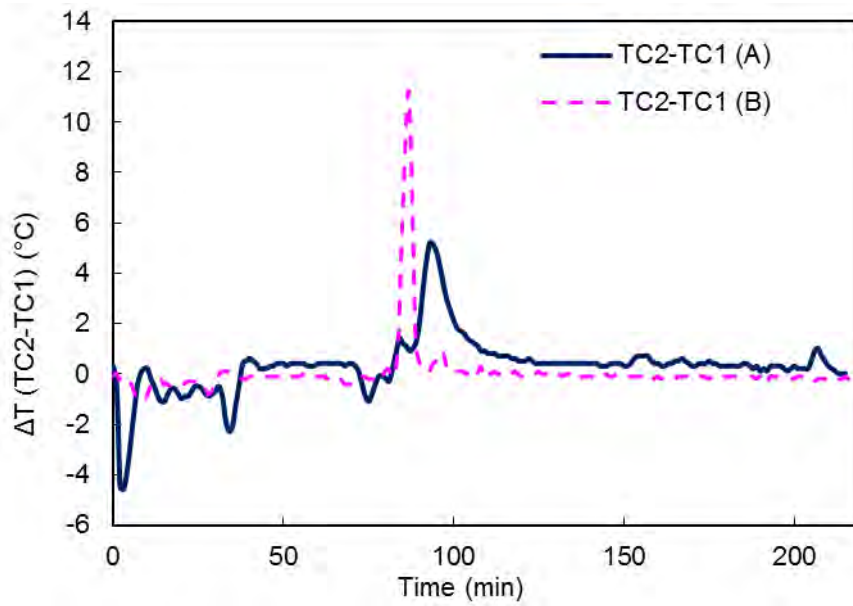
Figure 3-9. Difference between the temperatures measured by thermocouples TC-1 and TC-2 to autoclave batch A and B.
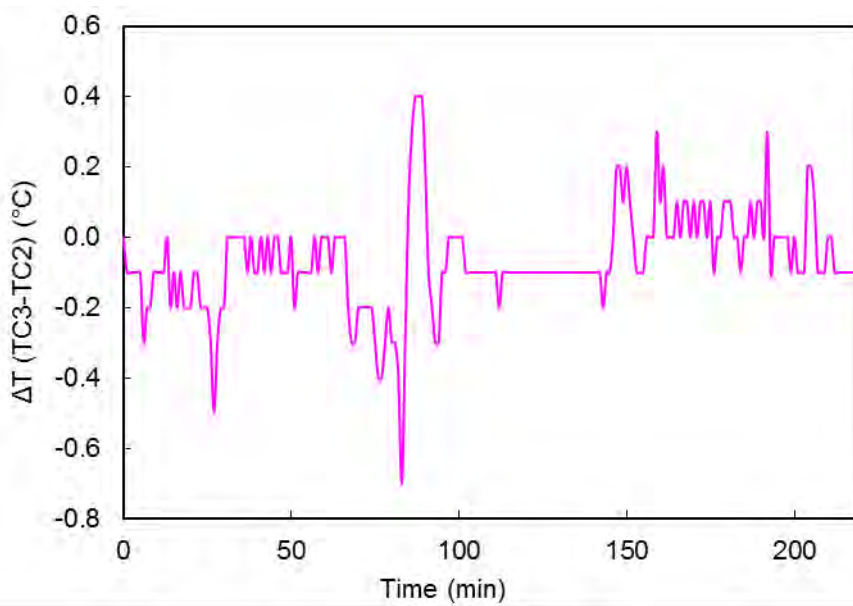
Figure 3-10. Temperature difference between TC-2 and TC-3 thermocouples for autoclave batch B.

3.4 Impact of the configuration of vacuum bagging on the thickness of the plates

3.4.1 Vacuum bagging sequence

The sequence of the vacuum bagging products has an influence on the properties of the cured piece.

After the lay-up, the composite plates are placed in a mould and prepared for autoclave polymerization. Figure 3-11 shows the typical pattern of vacuum bagging to produce a composite part in the autoclave. The composite structure (4) is placed on a steel or aluminium tool (1) over a release agent or Teflon based release film between the mould and the laminate (2). A peel ply is placed below and above the composite (3 and 5) and it serves to improve the demoulding of the piece. It also produces a rough surface which can be employed for possible future surface treatment and the placement of tabs for mechanical testing. A perforated release film (6) is then placed to allow the ventilation of volatile fumes and the flow of excess resin into the bleeder fabric (7), which is typically made of fibreglass. A micro perforated release film (8) is placed between the bleeder fabric and the breather mat (9) to allow the evacuation of volatiles. The breather mat allows a uniform application of the vacuum (12) over the composite plate. A mosite barrier (11) is placed around the prepreg to ensure the dimensions of the plate by avoiding the lateral flow of the resin. Finally, the system is covered by the vacuum bag (10). A seal (13) ensures the correct fixation of the bag to the mould while providing an effective isolation from the ambient exterior.
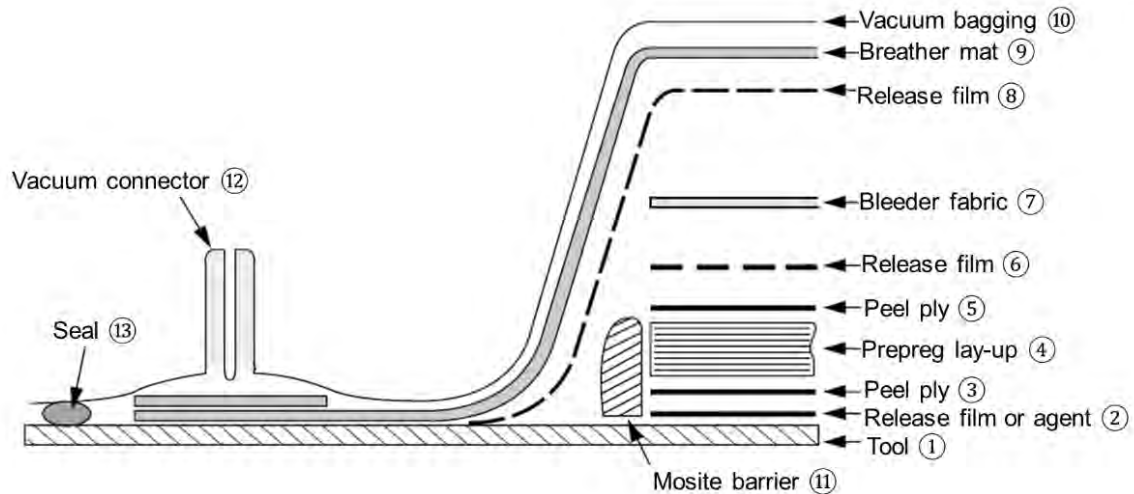
Figure 3-11. Schematic of vacuum bagging for the autoclave polymerization.

The preparation of the mould is based on our experience with a prepreg similar UD, the M21/T700GC. However, this prepreg is a quasi-net system, i.e. the resin flow remains minimal compared to the prepreg M10.1. Indeed, the M10.1 resin has a lower viscosity of 0.4 Pa·s at 110 °C compared to 1 Pa·s at 140 °C for the M21, and higher mass fraction for the prepreg system M10.1/CHS, 38 % versus 34 % of the M21/T700. In batch *A*, the bleeder fabric was not sufficient to contain the resin. Moreover, the excess of resin "filled" the breather mat (cf. Figure 3-12). Since the breather mat is essential to maintain a uniform application of the vacuum on the surface of the plates, it is necessary to prevent resin from flowing and clogging. In order to avoid this situation for batch *B*, the number of layers of the bleeder fabric is increased and the perforated release film is changed to a micro perforated type film to further block the flow of resin. This configuration, which effectively prevents the resin flowing in the breather, is retained for batch *C*. The vacuum bagging was conducted with the following differences:

- except for plate B-3 (taken to the debulking station after the placement of 8 consecutive plies), plates of batches *A* and *B* are debulked after laying 4 plies. For logistical reasons, the debulking of the six plates of batch C is made after the placement of 8 consecutive plies;

- for plates manufactured in the batch *A*, mosite has been placed around the plates so as to contain the side overflow of resin. Having observed that this lateral overflow has no significant impact on the thickness in the middle of the plate, the rest of the plates do not make use of mosite;

- a single layer of bleeder fabric and a perforated release film were used between the bleeder fabric and the breather in batch *A*. For autoclave batches B and C, two layers of bleeder fabric and a micro perforated film were used.
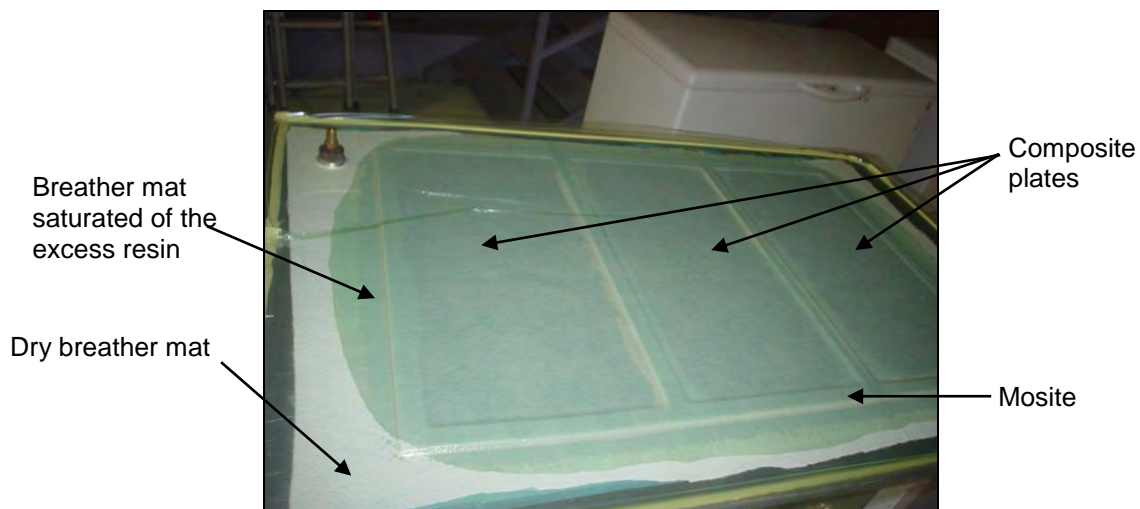
Figure 3-12. The batch "A" plates after being taken out from the autoclave and the excess flow of resin impregnated the breather mat.

After polymerization of composite plates, it was observed that the difference between curing cycles and vacuum bagging layers used for each autoclave batch, both have an influence on the final properties of the plates. Plates of batch *A* have lost on average 13 % of resin weight of compared with 6 % for those of batch *B*. There is a slight reduction in the plate thickness, and therefore in the average thickness of the ply. This observation allows the conclusion that manufacturing conditions have a direct influence on the geometry of the part.

3.4.2 Resin flow

Table 3-8 presents the results of the weighing of the plates before and after curing. In batch A, the use of a release film perforated between the absorber and the breather as well as the application of a single bleeder fabric caused a flow of resin in the breather until saturation (cf. Figure 3-12). This 13 % loss of resin by mass is assumed the product of a phenomenon of capillary action on the contact of the resin and the breather mat. There is also considerable variation between the quantities of resin lost by the plates, especially between the first two plates and the plate A-3. The origin of this variation in the mass of the plates is unclear. It is certainly linked to the saturation of the breather and the application of the vacuum during the curing cycle.

Table 3-8. Weighing composite plates before and after curing.

	Batch A			Batch B		
	A-1	A-2	A-3	B-1	B-2	B-3
Weight plates before curing (g)	1477.7	1476.1	1477.6	1483.2	1483.2	1485.1
Weighing plates after curing (g)	1290.1	1284.3	1261.3	1392.3	1392.4	1388.7
Resin lost by plates (g)	-187.6	-191.8	-216.3	-90.9	-90.8	-96.4
Lost resin ratio / plate weight (%)	12.7	13.0	14.6	6.1	6.1	6.5
	Batch C					
	C-11	C-12	C-13	C-21	C-22	C-23
Weight plates before curing (g)	1415.1	1419.3	1414.3	1415.4	1414.9	1418.9
Weighing plates after curing (g)	1347.3	1361.1	1349.3	1347.4	1347.3	1341.7
Resin lost by plates (g)	-67.8	-58.2	-65.0	-68.0	-67.6	-77.2
Lost resin ratio / plate weight (%)	4.8	4.1	4.6	4.8	4.8	5.4

When, in batch B, the perforated film between the absorber fabric separator, and the breather is replaced by a micro perforated film and the addition of a second fabric absorber, the loss of resin by mass is then limited to 6 %. This implies that the plates from the batch *A* have the double of the average resin flow of batches *B* and *C*.

3.5 Measure of the thickness of plates

In order to know the influence of the flow of resin on the geometry of the batches *A* and *B* plates, their thicknesses are controlled using a 3D coordinate-measuring machine (CMM). In this procedure, the composite plates are placed on a marble table and fixed it using clamps. The machine measures the thickness of the plate following a mesh of size of 30 x 30 mm. This mesh covers almost the entire surface of the plate by performing between 190 and 220 measurement points.
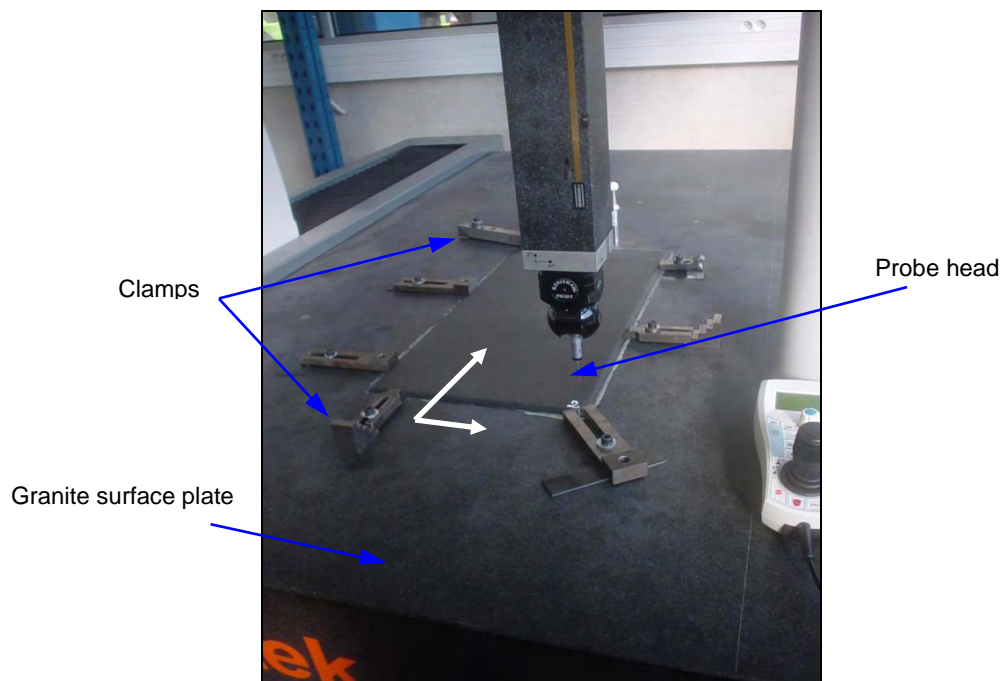
Figure 3-13. Positioning and clamping of a plate in the coordinate-measuring machine (CMM).

After the demoulding of the plates, it is observed that they are not completely flat. They have a certain curvature that is due to residual strains caused by the mismatch between the tool thermal expansion and the composite plates, or by other effects [6]. This curvature is more evident on the plates of batch *B*. At this point, there is no interest in measuring the warpage of the composite plates but their raw thickness. Thus, the plates are fixed to the marble by using 6 or 7 clamps (cf. Figure 3-13).

The edges of the plates also present a different morphology regarding the use or not of the mosite to retain the lateral resin flow. On the plates where the mosite was used, the edges are flat and perpendicular to the tool with a slight increase of the thickness near the edge, as shown in Figure 3-14a. For plates fabricated without mosite, the edges are concave with a progressive reduction of the thickness near the edges of the plate (cf. Figure 3-14b). Both types of edge shapes are not too significant since the edges of the plates are trimmed before employing them for constructing a technological evaluator.

(a)   (b)
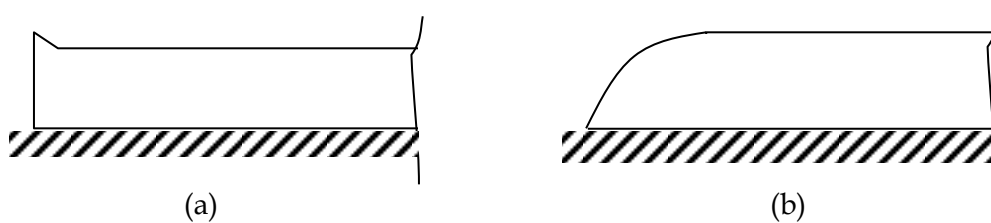
Figure 3-14. Schematic drawing of the profile of composite plates with, (a) with mosite and (b) without mosite.

Due to the irregular nature of the edges of the plates, it was necessary to find a reference point for the coordinate-measuring machine. This reference was made by drilling two perforations near the corners of the plate which are used by the measuring machine to define the reference axes (cf. Figure 3-15). The y-axis is defined by the straight line passing through the centre of the two perforations. The x-axis is perpendicular to this straight line and parallel to the granite surface. The z-axis is thus perpendicular to the plane defined by x and y. The origin of the reference system is located arbitrarily in the centre of the left hand side perforation.
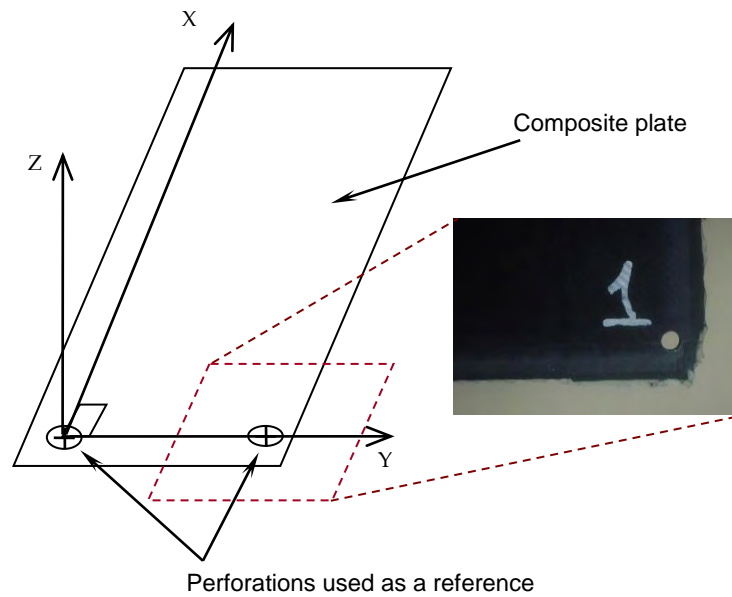
Figure 3-15. Reference system for the coordinate-measuring machine (CMM).

The results of the measurement of thicknesses are shown in Table 3-9. As expected by the plates weighing, the average thickness of those manufactured first is lower compared with batch *B*, 4.700 mm compared to 5.100 mm. Thus, the average thickness of the plies for the plates of the batch *A* is 0.290 mm and 0.320 mm for batch *B*. The nominal thickness for material M10.1/CHS is 0.322 mm [1]. Anyhow, the coefficients of variation associated with the thickness of the plates are in the same order of magnitude among the plates within the same autoclave batch.

Table 3-9. Measurement of thickness of composite plates.

	Batch A			*Batch B*		
	A-1	*A-2*	*A-3*	*B-1*	*B-2*	*B-3*
Thickness of plate $\bar{t}_{plate}$ (mm)	4.720	4.690	4.580	5.110	5,110	5.080
Standard deviation (mm)	0.315	0.190	0.203	0.159	0.161	0.157
CV (%)	6.7	4.1	4.4	3.1	3.2	3.1
Average ply thickness $\bar{t}_k$ (mm)	0.295	0.293	0.286	0.319	0.320	0.317

After having measured the thickness of the plates of batches *A* and *B* in the CMM, the average thickness is equal to 4.700 mm for the plates of batch *A* and 5.100 mm for batch *B,* as shown in the mapping of the A-2 (cf. Figure 3-16) and B-2 (cf. Figure 3-17) plates. It is evident that these plates do not have a constant thickness. The maximum thickness is located in the central section of all plates manufactured in this study, while the minimum thickness is always located in the corners. A similar effect was reported by Olave [7] for a 2/2 twill woven textile fabricated using a HexPly® M10.1/T700.
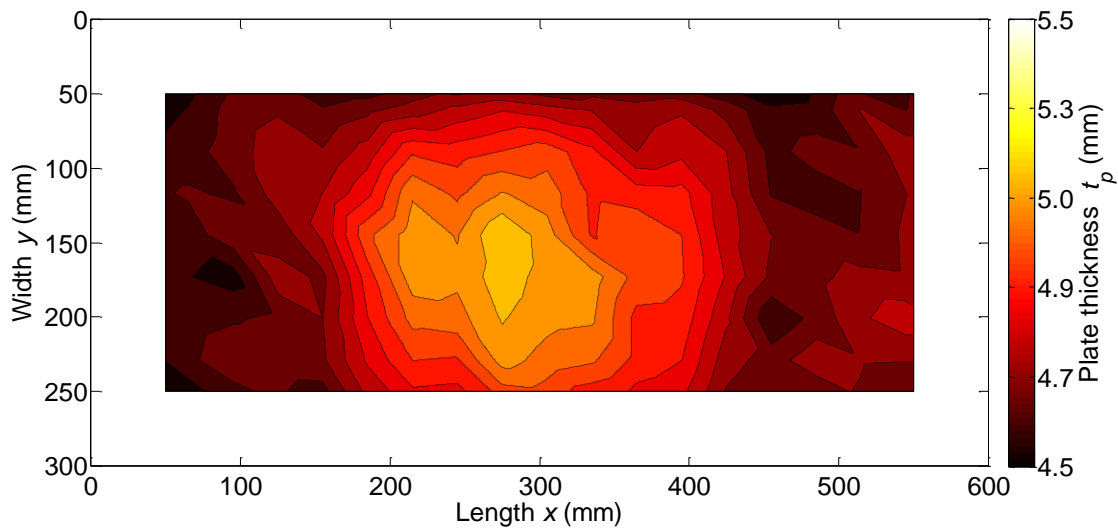
Figure 3-16. Thickness map of the A-2 plate.
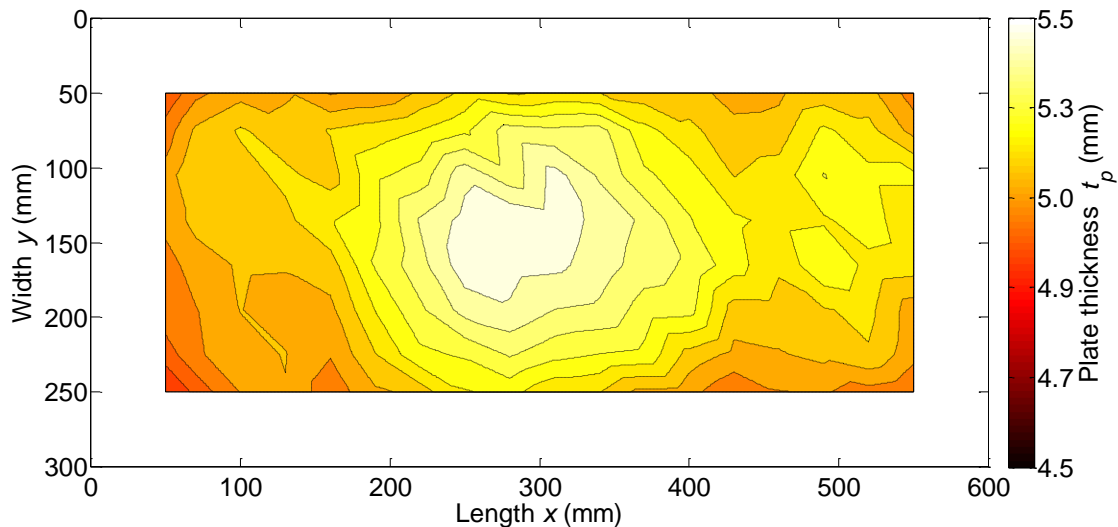
Figure 3-17. Thickness map of the plate B-2.

It is important to mention that the UD prepreg M10.1/CHS has a nominal cured ply thickness of 0.320 mm. The difference in thickness between the minimum located at the edges of the plate and maximum values in the centre of the plate is 1.061 mm for the plate A2 and 0.706 mm for the plate B2. Thus, the variation in the thickness of the plate is 2 to 2.5 times the nominal thickness of a single ply. This difference can cause difficulties for the dimensioning of parts.

It is assumed that the thickness variation of the plate is carried over the ply thickness. This variation can be modelled through the equation of a 3D sine wave or a 3D parabola. An example of a mathematical model that controls the evolution of the variation of the plate thickness through the ply δt_{plate} is shown in equation 3-7.

$$\delta t_{plate}(x, y) = \frac{A_{plate}}{4}\left[\cos\left(\frac{2\pi}{\lambda_{pla\cdot x}}(x + X_c)\right) + \cos\left(\frac{2\pi}{\lambda_{pla\cdot y}}(y + Y_c)\right)\right] \tag{3-7}$$

where A_{plate} is the difference between the maximum and minimum thickness value, $\lambda_{pla\,x}$ and $\lambda_{pla\,y}$ are half the plate length and width respectively, and X_c and Y_c are the coordinates of the thicker zone. The generated thickness can be then used in the finite element model with a thickness variation (cf. Figure 3-18).
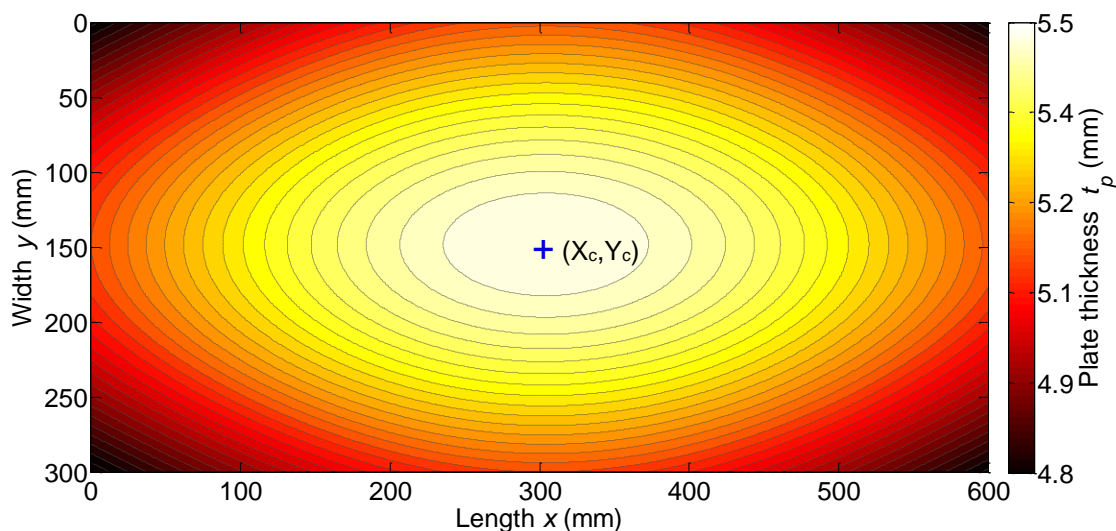
Figure 3-18. Plate thickness generated using eq. 3-7.

3.6 Volume fractions of the cured plate

In order to link the mechanical properties to the geometrical properties of the composite material, the volume fractions of the constituent materials, fibre, resin and porosity must be determined. To maintain continuity in the modelling, the hypothesis that the quantity of fibres in a ply does not change from one element to another is made. Thus the fibre mass per unit area ρ_{Af} of M10.1/38%/UD300/CHS has a nominal value of 300 g·m^{-2}. However, to test this assumption and to determine the relationship between the ply thickness and the volume fractions of the composite plate, a physical characterisation of the real structure is made. Eight specimens are obtained from one of the fabricated plates (C-11). The volume fractions of their constituent materials are obtained using the standard test EN NF 2564 [8]. This method allows the separation of the reinforcement fibres by means of chemical digestion of the matrix. Initially, the specimens, being 20 mm long and 10 mm wide are weighed and their density calculated using the water displacement principle. After the chemical decomposition of the matrix, the fibres are then weighed. The weight difference between the specimen before and after the chemical decomposition indicates the quantity of the resin contained in the composite. An assumed density of the fibre (1 800 kg·m^{-3}) and the matrix (1 200 kg·m^{-3}) are used to calculate the volume fractions of the fibre and resin, being the difference between these two values the ratio of the porosity in the material. Since this type of measurement covers the whole specimen, these properties are considered to be distributed homogeneously through the 16 plies of the stratification.

Figure 3-19 shows the plate porosity as function of the plate thickness. The trend of the least square fit indicates that effectively the porosity varies with the plate thickness. For these measurements, the thicknesses data set ranges from 4.830 to 4.930 mm. A linear variation of the porosity is assumed with a zero porosity region for plate thicknesses less than to 4.800 mm (cf. eq. 3-8). Above the assumed zero porosity thickness, the increase in the plate thickness can be

explained by an accumulation of resin and an increase of the volume fraction of the entrapped voids in the resin.

$$V_{p \cdot plate} = \begin{cases} 0 & \text{if} \quad t_{plate} < 4.800 \\ 0.102 t_{plate} - 0.490 & \text{if} \quad t_{plate} \geq 4.800 \end{cases} \tag{3-8}$$

where $V_{p \, plate}$ is the volume fraction of the porosity and t_{plate} is the plate thickness. The coefficients 0.102 and 0.409 are obtained from a linear regression from the experimental data (cf. Figure 3-19).
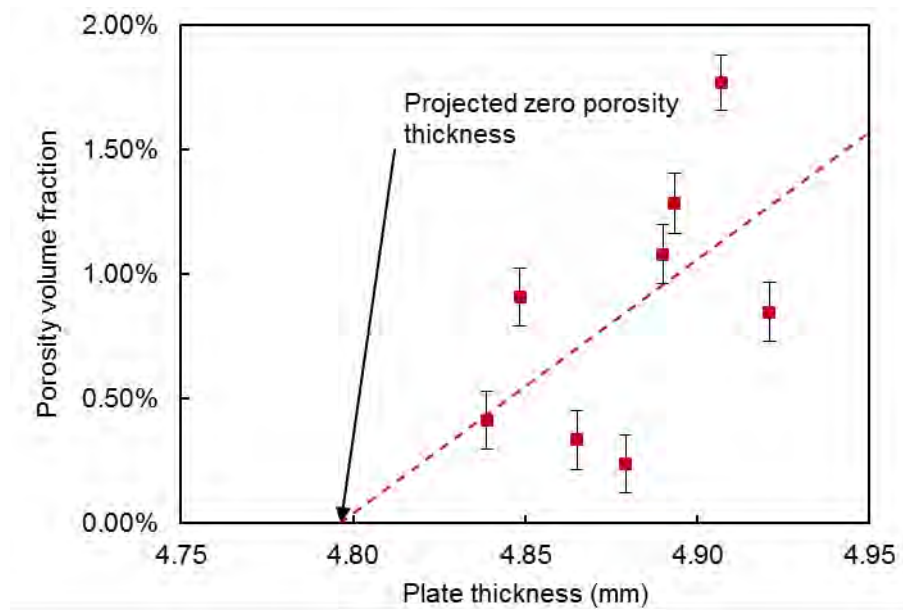
Figure 3-19. Evolution of the volume fraction of the porosity through the plate thickness.

From experimental data, the actual fibre mass per unit area is calculated. The obtained value is 304.5 g·m⁻², which is within 2 % of the nominal value. Using the new mean ρ_{Af}, recalculated volume fractions of the constituent materials are obtained (cf. Figure 3-20 to Figure 3-22).
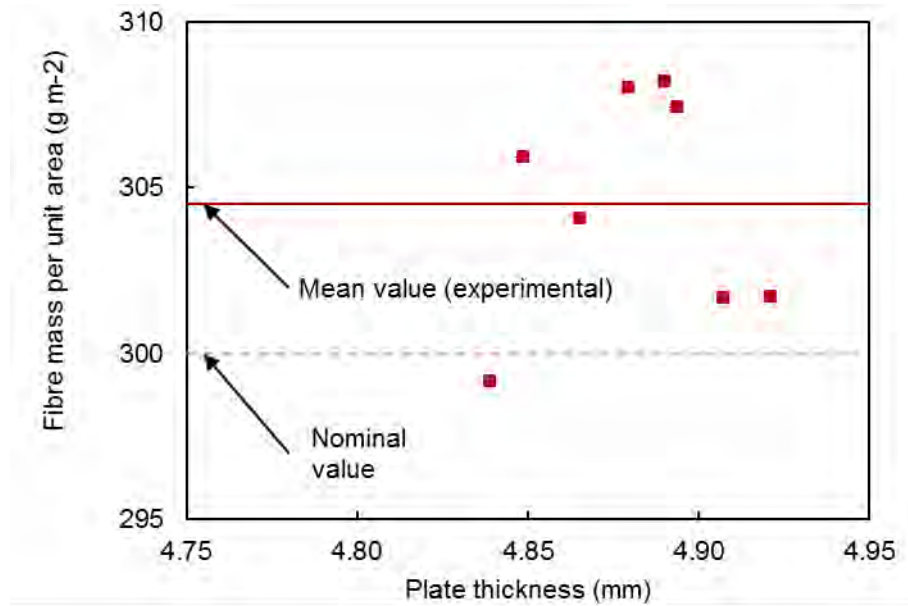
Figure 3-20. Evolution of the fibre mass per unit area ρ_{Af} with the ply thickness

As shown in Figure 3-20, the mean value of the fibre mass per unit area shows a shift from the nominal data. This change in the fibre mass per unit area can be due to the use of a specific type of reinforcements. Unfortunately, the M10.1/CHs prepreg does not specify the exact type of reinforcement. The value of ρ_{Af} used in the calculations is thus 304.5 g·m^{-2}. The expected values of the constituent materials using the actual ρ_{Af} are in better agreement with the experimental data with a 1 % gain in the fibre volume fraction than the values calculated using the nominal data. The fibre volume depends only on the thickness of the composite and not on the porosity (cf. Figure 3-21). For the matrix volume ratio, since the variation of the resin content is linked to the presence of voids, an inflexion point of the calculated trend is present at 4.800 mm thickness. Beyond this point, the matrix volume fraction exhibits a rate of variation lower than in the first part of the curve. This is an indication that the change in the matrix is more dependent on the presence of voids (cf. Figure 3-22). Again, the difference between the nominal value and the experimental value for a ρ_{Af} is approximately 1 % of the volume fraction.
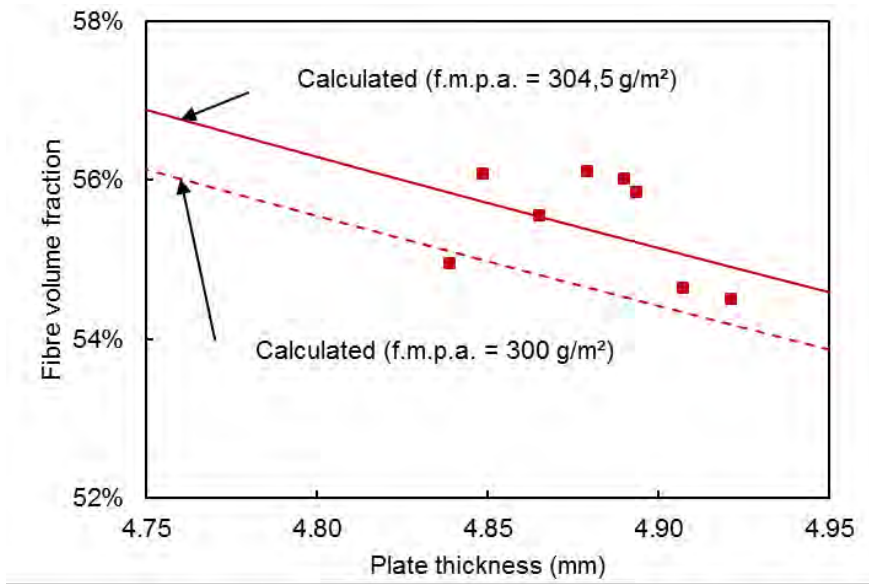
Figure 3-21. Change of the volume fractions of the fibre with respect the plate thickness.
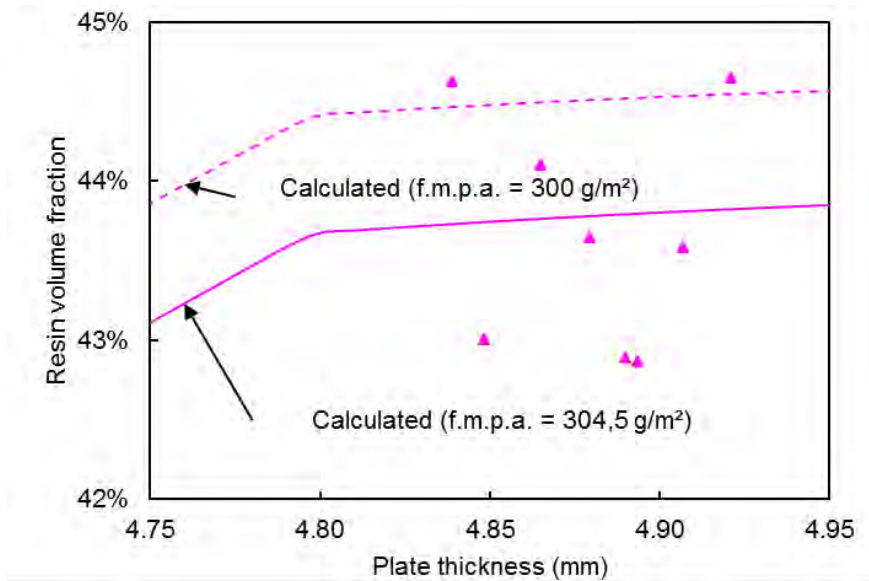
Figure 3-22. Change of the volume fractions of the resin respect the plate thickness.

3.7 Conclusions

The variability in composite structures is strongly influenced by all the stages in its manufacturing, including the raw materials. In this chapter, the sources and effect of variabilities have been exposed.

In a first stage, the variability of the prepreg plies is studied through the measurement of the mass per unit area. In this measurement campaign, several sets of information have been obtained during the different campaigns of fabrication procedures of composite plates. Also, a more precise method to measure the surface of the ply was proposed. The variability of the mass per unit area using the two exposed methods gives similar results, both in terms of means and variances. Two different lots of material were controlled. The lot L-1 has a mean value of 500.7 $g \cdot m^{-2}$ with a CV of 1.21 % and the lot L-2 having a mean of 478.1 % and a CV of 2.25 %. The variability between the different lots of material is more important than the variability from one point to another in the same material lot.

However, to project an influence of the variability of the prepregs into the cured plate is difficult since the resin flow during the cure cycle is strongly dependent on the vacuum bagging products, the cure cycle and the stratification employed, as shown by the different quantities of resin lost during the cure cycle by changing the conditions of manufacturing and using another material lot. This does not inhibit the possibility of quantifying the effects of each change in the polymerised structures.

As a direct effect of the resin loss between batches A and B, there is a significant difference in the plate thickness. The plates of batch A have an average thickness of 4.60 mm, while the plates of batch B have an average of 5.10 mm. It is also found that the composite plates do not have a constant thickness. These variations in thickness can affect the ply thickness and thus the local volume fractions of fibre.

Finally, the values of the plate porosity were obtained for a set of specimens by chemical digestion of the resin. It is noteworthy that the obtained values are very dependent on the assumed density for the fibre and matrix. It was measured that the porosity changes are maybe proportional to the plate thickness, indicating that, if the quantity of fibre filaments is constant, the porosities are effectively evacuated by the exceeding resin flow of this material. The measured volume fractions of porosity are less than 2 %.

3.8 References

[1]   Hexcel Composites, "HexPly M10.1 Product data. FTU287." 2009.

[2]   Hexcel Composites, "HexPly M21 Product data. FTA002c." 2007.

[3]   L. Crouzeix, Y. Davila, F. Collombet, B. Douchin, Y. Grunevald, and R. Zitoune, "Study of double step lap composite repairs on CFRP evaluators," in *ECCM 15*, 2012.

[4]   AFNOR, "NF EN ISO 10352: Plastiques renforcés - Préimprégnés - Détermination de la masse surfacique." 2010.

[5]   K. D. Potter, C. Langer, B. Hodgkiss, and S. Lamb, "Sources of variability in uncured aerospace grade unidirectional carbon fibre epoxy preimpregnate," *Compos. Part A Appl. Sci. Manuf.*, vol. 38, no. 3, pp. 905–916, Mar. 2007.

[6]   M. Mulle, F. Collombet, P. Olivier, and Y.-H. Grunevald, "Assessment of cure residual strains through the thickness of carbon–epoxy laminates using FBGs, Part I: Elementary specimen," *Compos. Part A Appl. Sci. Manuf.*, vol. 40, no. 1, pp. 94–104, Jan. 2009.

[7]   M. Olave, A. Vanaerschot, S. V Lomov, and D. Vandepitte, "Internal Geometry Variability of Two Woven Composites and Related Variability of the Stiffness," *Polym. Compos.*, pp. 1335–1350, 2012.

[8]   AFNOR, "NF EN 2564: Série aérospatiale - Stratifiés de fibres de carbone - Détermination de la teneur en fibres en résine et du taux de porosité.," 1998.

Chapter 4: Determination and modelling of the in-plane local misalignments during a manual lay-up procedure of a CFRP laminate

4.1 Introduction

Variations in fibre orientation have an important impact on the composite structure performance [1]. These variations are the result of several factors present during the different stages of the structure manufacturing, resulting in global and local misalignments. A global misalignment happens when the mean orientation of the ply or fibre bundles differs from the intended ply orientation. Local misalignments are produced by the periodic undulations present in the prepregs and dry preforms [2], as well as the preform manipulation to give shape to the composite structure [3].

Arao [4] suggests that ply misalignment can be assumed to be normally distributed with a mean of 0° and a standard deviation of 0.4°. These values have been confirmed by an inverse method while comparing a numerical analysis of the curvature induced to a composite plate subjected to a moist environment. Two values of SD of the fibre orientation, 1° and 0.4° respectively, using a Monte Carlo method were assessed. The model results were then compared against experimental data. The calculation using a SD 0.4° yielded the best correlation against the experimental points even though no actual measurements have been performed on the fibres.

In order to measure the actual fibre orientation in a cured composite, Yurgartis [5] proposed a method in which a composite specimen is cut along the cross-section in a known angle. By observing the ellipsoidal form of the fibres, it

can be calculated the actual fibre misalignment along its intended axis. As a result of measuring a carbon/APC-2 composite a mean angle of 3.71° with a standard deviation of 0.794° was obtained. However, his method is sensitive to the assumed fibre diameter, which must be obtained by observing another cut from the composite cross-section perpendicular to the fibre axis. In any case, this method can be used to measure the in-plane and out-of-plane misalignment of the fibre bundles. Also, in this case there is no indication on the specimen manufacturing process. This technique has been used to identify fibre misalignment for pultruded composites identifying the number of fibres which present a higher misalignment than other fibres bundles in the same section [6]. Olave [7] used this technique to quantify the misalignment on woven composites with values of 1.71° and a SD of 0.69° for a 3K fibres/yarn material and 2.88° with a SD of 1.23° for the 12K fibres/yarn material. This technique is used to compare the fibre orientation of flat specimen to curved specimen flat formed [8]. In this case, the materials and the manufacturing processes are not disclosed.

The major drawback of this technique is that it requires a quality surface of the observed specimen, as well as the resolution and image quality. The variation in the fibre orientations must be calculated by the obtained mean of several hundreds to thousands of fibres (1.5 million in the case of [6]). Also, since the images are taken with microscopes, the measured zones are relatively small, in the range of 0.015 mm² to maximum 100 mm² (after assembling 6 624 micrographs), compared with the size of an industrial part. In order to overcome these drawbacks and reduce the analysis time, Sutcliffe [9–11] proposed the use of a fast Fourier transform (FFT) on low resolution images of the cross-sections coupled to an autocorrelation function to obtain the mean fibre orientation on a specific zone. To measure the orientation of a group of fibres, the use of the FFT coupled with filtering techniques means that the quality of the images of the cross-section can be lower and thus can be taken by other means than optic microscopy, like X-rays. Also, this methodology permits the measurement of the fibre waviness when observing the specimen along the fibre axis.

These techniques are applied to determine the fibre orientations at the cutting plane. To obtain the 3D behaviour of a fibre, a micro tomography technique (µCT) has been used [12] where 3D synchrotron tomography images are used in composite specimens to determine the local volume fractions and fibre orientations in their 3 major axes. The specimens have 1 x 1 mm² cross-section and a length of 6 to 10 mm. However the observable length accounts only for 1.43 to 1.64 mm. In this study, misalignments of fibres were observed to have a preferential orientation of 7° with respect of the vertical axis of the sample with variations up to 20°.

As can be seen, all these techniques depend on the specimen size, and cutting precision, since all these measurements are referred to the cutting plane of the specimen. Also, due to the size of the micrographs, a broad study of a composite part would be intensive time and resource consuming, in order to determine the actual trends of the orientation variability.

In order to have a better understanding of the spatial variation of the fibre orientation, a set of images of the prepreg are used. Skordos [13] mounted a digital camera into a coordinate measuring machine to take a set of photos of a woven prepreg. The images covering each 100 mm² must be assembled into a grid. The 630 images must be assembled to cover a surface of 103 500 mm² (300 x 345 mm). Each image is then processed using a FFT and an autocorrelation function was used to determine the angle of the warp and weft orientation and as well as the length of each unit cell. For the orientations, it was found that the mean warp direction was -0.1° with a standard deviation of 0.36°, and for the weft direction the orientation was 86.68° with a SD of 0.95°. The same methodology was applied by Mesogitis [14] for a ±45 non-crimp fabric (NCF) studying a prepreg using 748 images over an area of 18 700 mm² (170 x 110 mm). The results yield a standard deviation of 1.22° for both directions. The mean in both cases is equal to the specified value. In these cases, the analysis time was not indicated. Regardless, processing the images with the FFT and the autocorrelation function can take several seconds per image. In both cases, only the fibre misalignments on the

composite fabric were studied. A great number of images were taken for a single layer, supposedly to reduce the image distortion due to the camera lens. Also the characteristics of the camera were not disclosed.

Potter et al. [2,15] identified that the reinforcement of UD prepreg presents an undulation in the form of a sinusoidal wave. This effect is due to the fact that the composite prepreg is stored in rolls, and thus, there is a difference in length between the internal and the external side at the moment of rolling the prepreg onto the drum. The sine wave identified has a mean amplitude of 0.03 mm and a wavelength of 3 mm.

In order to have an understanding of the effects caused by the fibre misalignment on the composite structure, a Finite Element Model (FEM) is proposed here, having these global and local misalignments. The inputs of the proposed model are based on the actual configuration of the material. Since the values obtained for the misalignment are highly depend on the manufacturing process of the composite structure, a methodology is developed to measure the actual fibre orientation in the stratification.

The methodology described focuses on the ply lay-up before the curing of the plates and permits not only the evaluation of the local and global misalignments of the prepreg plies, it can also be used to assess the accuracy of the manufacturing technique to establish a benchmark for other types of lay-up techniques, operators and structure shapes.

4.2 Optical analysis and image treatment

4.2.1 Experimental setup and image treatment description

A series of images are taken during the manufacturing of composite plates. The plates are fabricated by manual stacking of unidirectional plies of a carbon/epoxy prepreg. The images are taken by a DSLR camera Canon EOS 550D with an EF 50MM/macro lens mounted 1.7 m above the work area (cf. Figure 4-1).

The resulting images have a resolution of 5 184 x 3 456 pixels. The relationship between the image size and the work area is 6.48 pixels/mm with a pixel aspect ratio of 1. The working area includes a reference grid purposely made to lay up the composite plate in order to determine the location of defects and reduce the distortion in the images (cf. Figure 4-2). The grid dimensions are 700 x 400 mm (or 4 536 x 2 886 pixels).
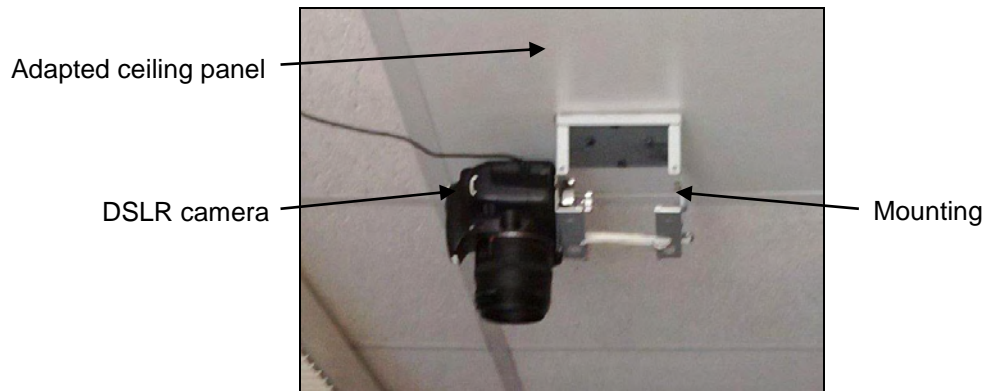
Figure 4-1. DSLR Camera mounting on an adapted ceiling panel.
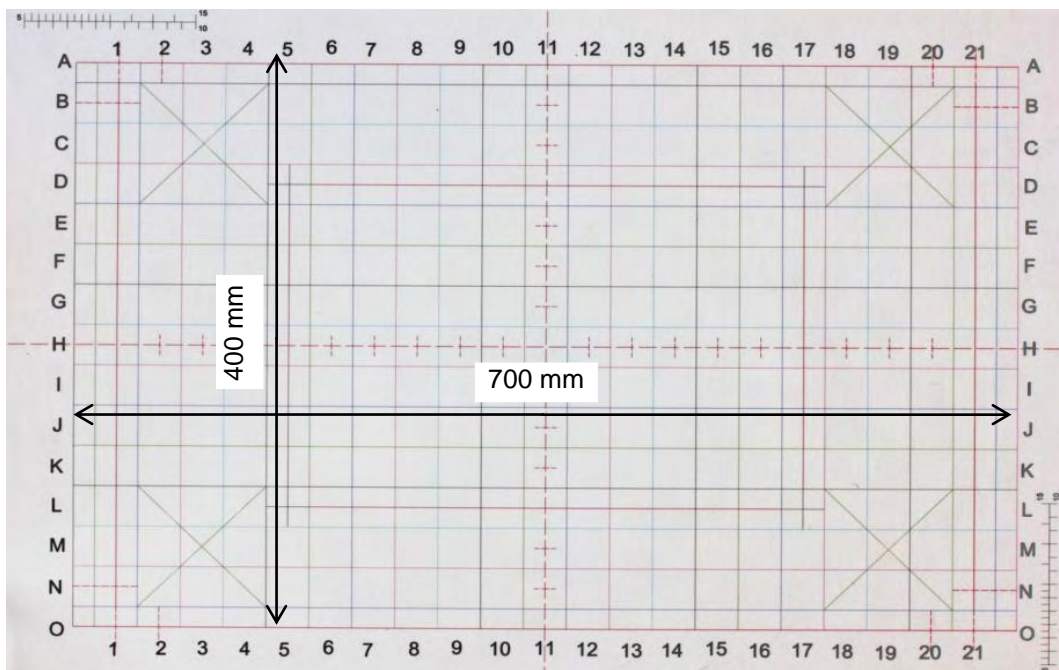
Figure 4-2. Working area (reference grid).

The principle of the measurement of ply orientation is based on the line detection of the fibre bundles in the surface of the prepreg by means of a Hough

transform on the filtered image based on the methodology proposed by Shi and Wu [16]. This technique is coupled with a convolution mask to enhance the edge detection along the intended fibre direction. The description of the steps to obtain the fibre orientation is as follows (cf. Figure 4-3):

- since the image covers both the composite lay-up and the grid, the core of the prepreg must be selected as zone of interest. The boundaries of the plies can affect the measurement by disrupting the cut-off ceilings of pixel intensity (cf. Figure 4-3a and Figure 4-3b);

- the images are then segmented into a predefined number of elements where the mean orientation is calculated. These elements are not constrained by a fixed size nor aspect ratio. This gives more flexibility to the calculation (cf. Figure 4-3b);

- a Laplacian of Gaussian (LOG) kernel is created to enhance the edges created by the fibre bundles by filtering the image noise. The LOG filter is coupled with a series of compass convolution masks (type Robinson) to further filtering the image in the orthogonal directions to the desired orientation. For quantifying the misalignment at 0° direction, the convolution masks are applied in the +45°, -45° and 90° directions [17] (cf. Figure 4-3c);

- an edge detection function is then applied to obtain the lines formed by the fibres [18] (cf. Figure 4-3d);

- a Hough transformation is then performed in the resulting image to extract the lines following the fibre bundles. The lines obtained by the Hough transformation are used to obtain the angle of each fibre bundle. A test is performed in order to remove all the lines that have angles which are not within a tolerance set for the intended orientation. This is necessary since some of the Hugh lines are generated for all the orthogonal directions 0°, ± 45° and 90°. To prevent abnormal values, a test is implemented to assure that the Hough line falls within a 7° tolerance of the intended measurement.

For each element, a mean and standard deviation of the Hough lines are obtained (cf. Figure 4-3e);

- the properties of the element are obtained by averaging the value of the angles of the Hough lines at each element. It is difficult to determine the real uncertainty of the measurement. Besides, the Hough lines can present values which are not contained within the expected value due to a lack of clarity in certain zones of the image, mostly due to reflection of the light source in the prepreg.
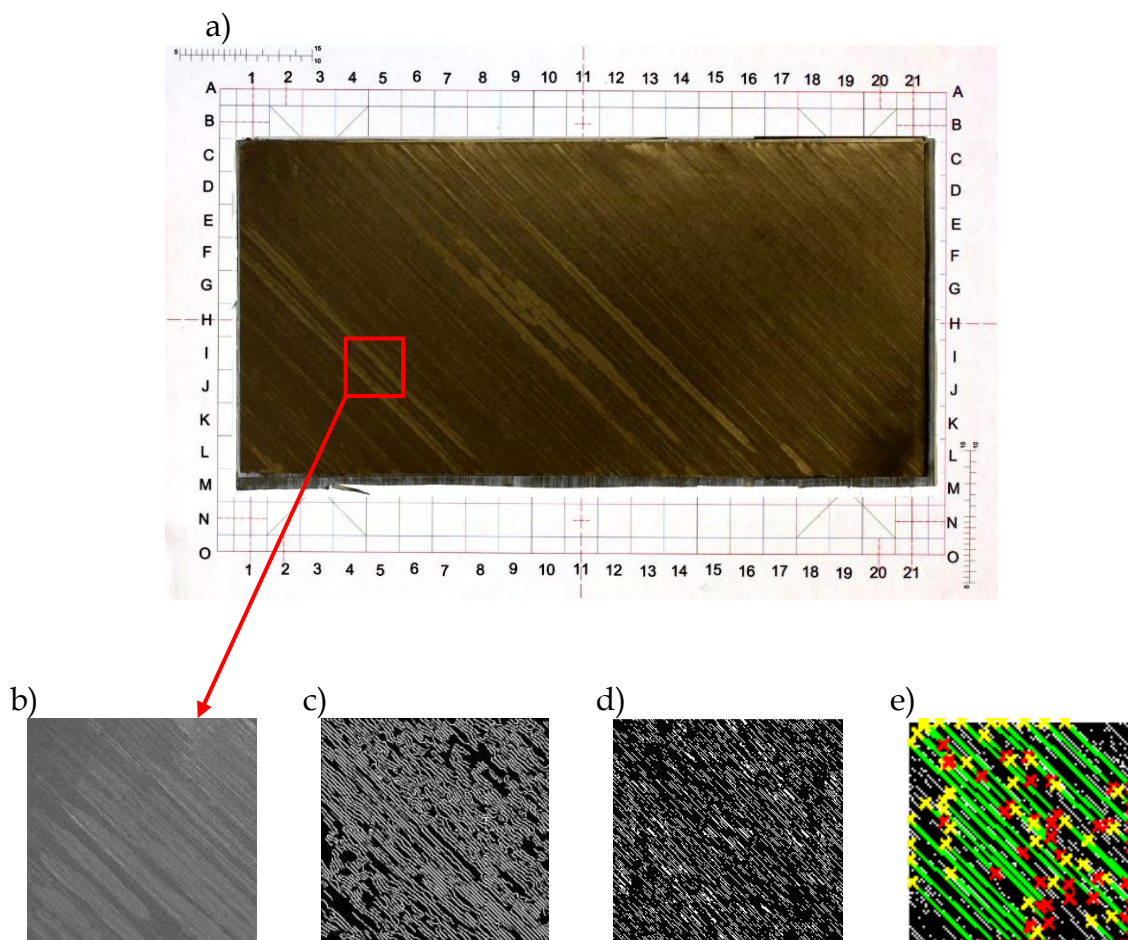
Figure 4-3. Fibre orientation measurement in a composite prepreg with, a) laid ply onto the work zone, b) detail of an element image, c) the image after the application of the LOG filter and convolution masks, d) edge detection and e) Hugh lines along the fibre direction.

4.2.2 *Precision of the measurement and selection of the size and number of elements*

The capabilities of the proposed method are tested by using a generated pattern at known angle variations. The calibration patterns consist of groups of lines oriented in a known angle at 8 different quadrants. The patterns are designed to measure very small angle increments (less than 1°) and more significant increments up to 3° difference from the intended orientation. Figure 4-4 shows the map of the obtained angle variations. For the 0° direction, the measurement is not too sensitive, because the lighting conditions make the image fuzzier at these orientations. For the 45° orientation, the sensitivity of the measurement is more adequate since the measured angles are closer to the predetermined directions.

Since the measurement is based on the relative position of the start and end points for each Hough line along the fibres, the precision of the measurement is proportional to the image size. Likewise, the measurement precision changes accordingly to the intended direction. The minimum angle that can be measured is given by the change of one pixel over the distance between the start and the end points of the Hough line along the *x* or *y*-directions. Thus, this distance *L* can be either the length or the height of the image. For the 0° and 90° directions the minimum resolution is given by the relationship $tan^{-1}(1/L)$. For the ± 45 directions the relationship is $tan^{-1}[(L-1)/L]$. Figure 4-5 shows the evolution of the angle resolutions through the image length. Indeed the lines created by the Hough's function do not cover in any case the total length of the element. It must be considered that the value found in each element is the mean value of all Hough lines inside each element.
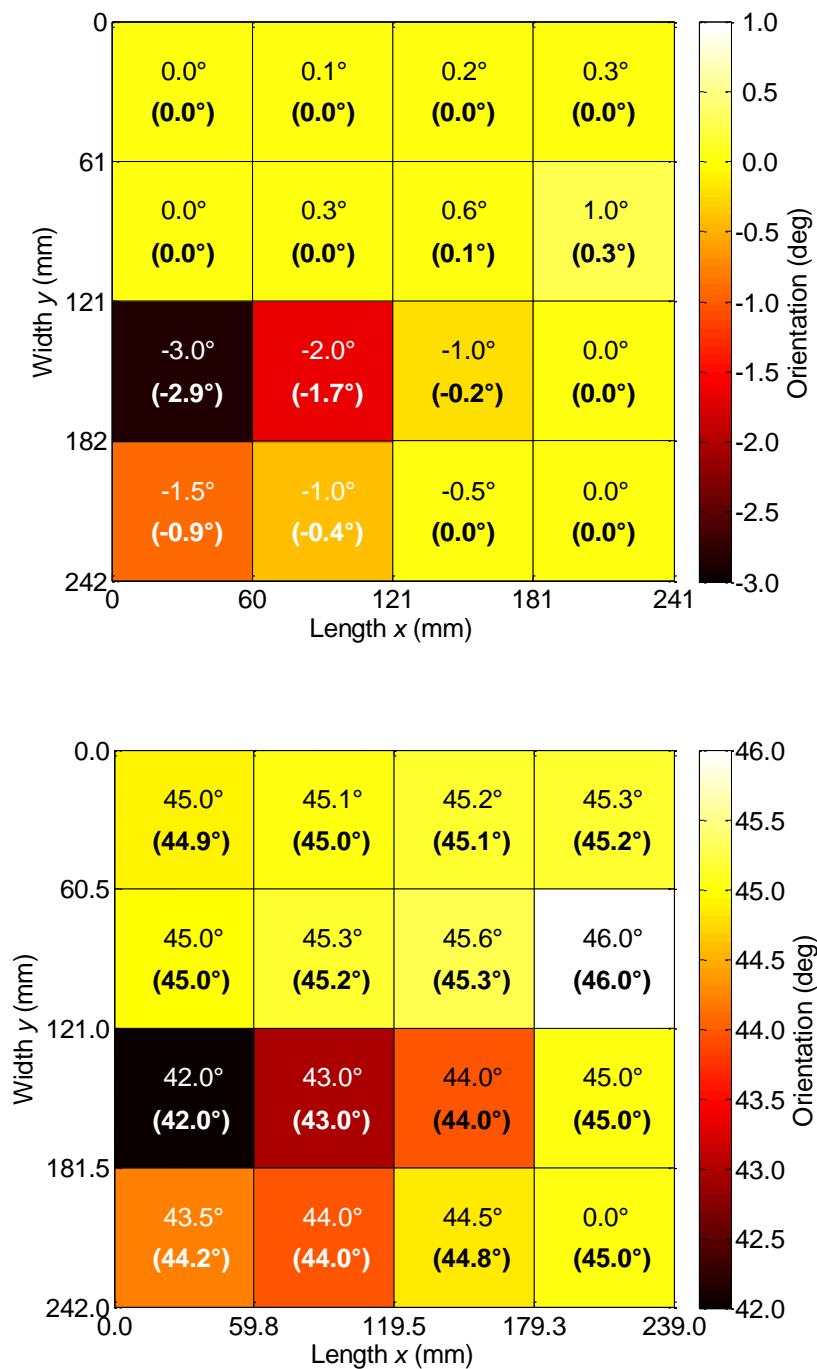
Figure 4-4. Precision test on the orientation method by Hough lines comparing the theoretical value (written top) to the measured value (written between parentheses), each quadrant representing a different mean value with, (top) the 0° orientation and (bottom) the 45° orientation.
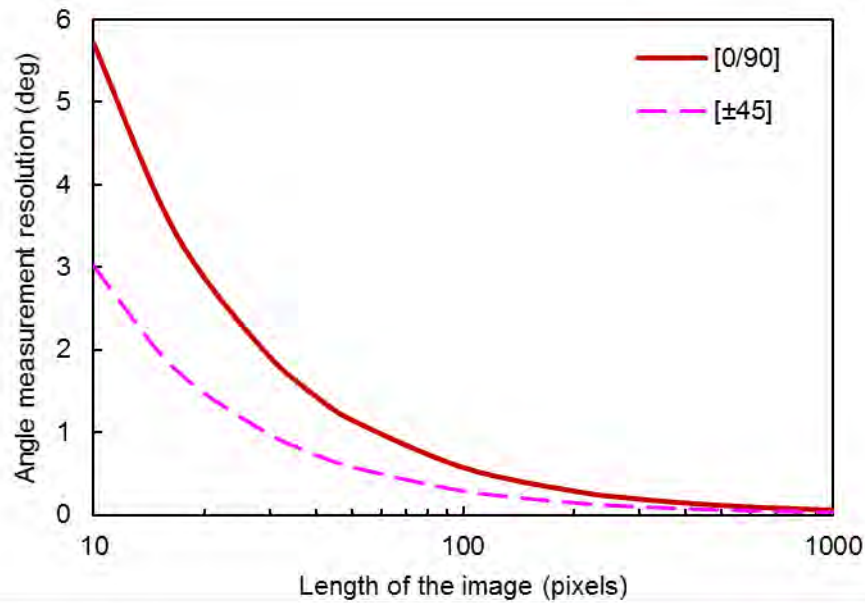
Figure 4-5. Maximum resolution of the determined angle for a single Hough line according to the maximum length of the image.

To determine the optimal number of elements in the real images of the laid plies, several tests are performed varying the number of elements. Increasing the number of elements logically leads to a reduction of the size of the element, and thus, affecting the element average orientation since there is a variation in the number and length of the Hough lines. For the sake of simplicity, it is chosen that the number of vertical elements to be equal to half of the horizontal elements. Hence, the total number of elements in which the ply is divided increases by a factor of $a^2/2$, being a the number of elements in which the ply is divided horizontally (*x*-direction). As shown in Figure 4-6, the number of Hough lines initially increases when increasing the number of elements from 50 to 200. From this point, the number of Hough lines decreases. Conversely, the average length of the Hough lines decreases with the augmentation of number of the elements.
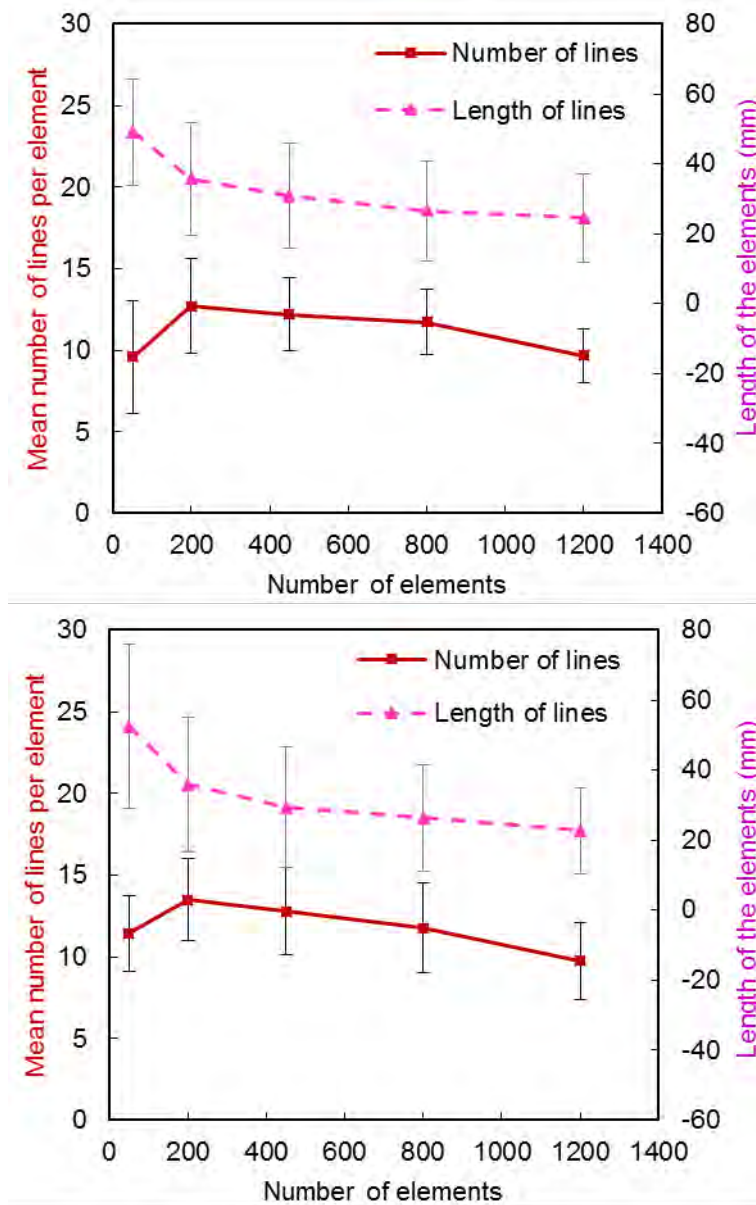
**Figure 4-6. Mean number of Hough lines per elements (error bars for ±1 SD from the
mean value) and its length in function of the number of elements with, (top) a ply
oriented at 0° and (bottom) a ply oriented at -45°.**

Figure 4-7 shows the average ply orientation of all the elements contained
within a ply. In the case of the ply oriented at 0°, the mean value does not exhibit a
significant change in value above the 200 elements. There is a 0.3° variation
passing from 50 elements to 200 elements. On the contrary, the standard deviation
goes from 0.5 to 1.0°. This means that the dispersion of the orientation has
increased. It is not clear at this stage if the uncertainty increases due to the increase
of the length and number of Hough lines, or if it is due to the variability of the

fibre orientations. It is evident when increasing the number of elements, the standard deviation does not show a significant change. On the contrary, for the -45° orientation, the mean value varies from -45° to -44.5°. Conversely, the standard deviation continues to grow from 0.2° at 50 elements towards 1.2° at 1200 elements. It seems that the standard deviation increases linearly with the number of elements across the length. This indicates an instability created by the Hough lines discarded at each element that are not contained between the tolerances set.

The selection of the number and size of elements depends on the capacity to determine a trend in the variation of the fibre orientation along the ply surface. For example, an element that is relatively small can contain a single Hough line, in which case, its determined value can diverge from the expected values beyond the tolerance set in the angle of the fibre. Meanwhile a small number of elements can be used to determine a mean orientation with more accuracy, but at the same time, neglecting local changes in the fibre orientations. As previously mentioned, this method is very dependent on the lighting conditions since the patterns generated by the fibres reflect the lights in different directions.
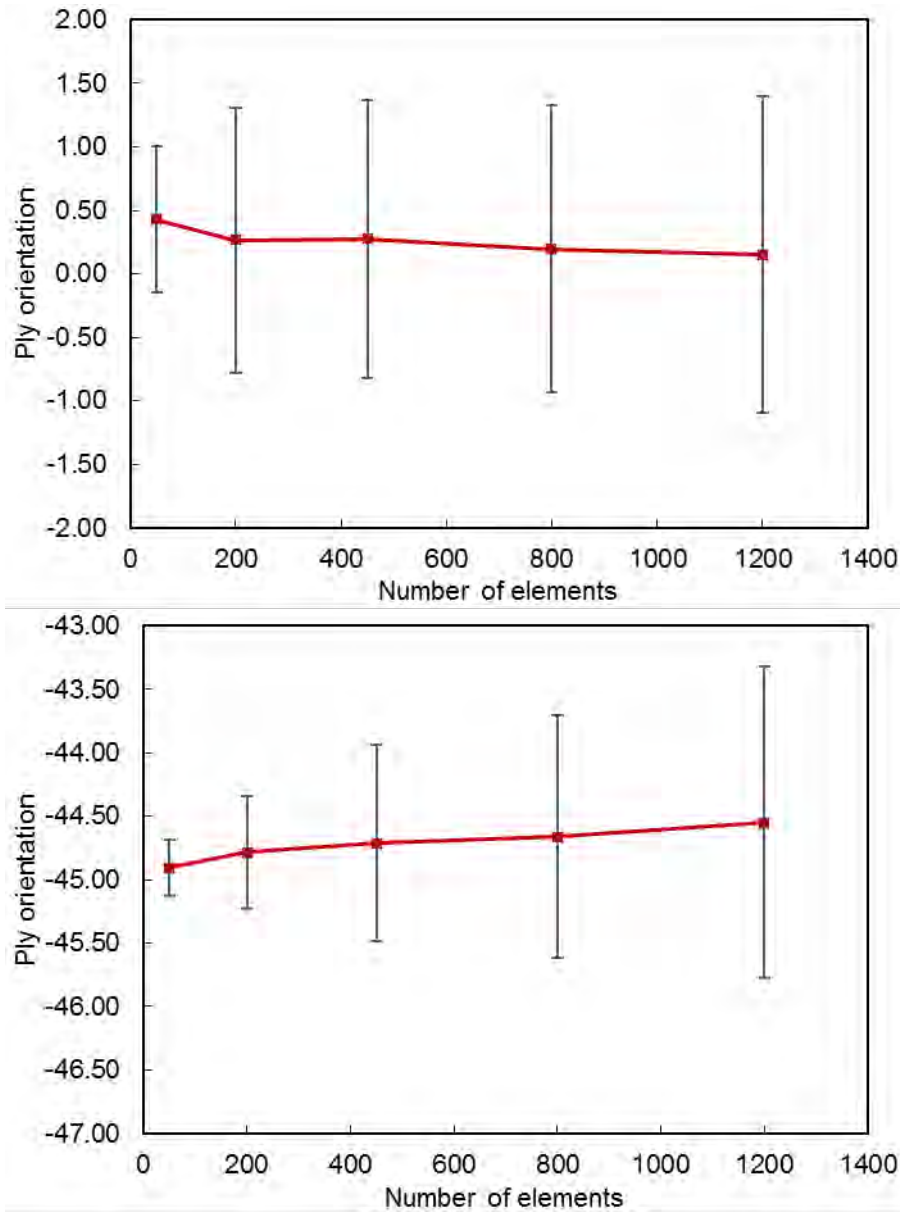
Figure 4-7. Mean ply orientation in function the number of elements (error bars for a ±1 SD from the mean value) with, (top) a ply oriented at 0° and (bottom) a ply oriented at -45°.

A 20 by 10 elements grid (200 elements in total) is chosen as a good compromise between the accuracy and the uncertainty of the measurements and the localisation of the deviation in the fibre orientations. One of the advantages of using the algorithm in 4.2.1 is the possibility of sectioning the image into elements having arbitrary sizes and shapes that are not limited to be in function of power of 2. The dimensions of the elements are approximately 30 x 30 mm. Unfortunately, this element size does not allow the identification of small variations in the fibre

direction such as the waviness in the fibre. Regardless, this size is more than enough to characterise the overall variations in the fibre orientations due to in-plane shear forces when laying-up the ply. To accurately determine a localised defect, a clear image should be taken with better resolution. However this operation can overlook the global misalignment of the fibres.

The image analysis is not computationally intensive as it can process a large quantity of images in relatively short time, even though there must be a careful memory management. The time of the calculation is roughly constant per element image, therefore, it only depends on the number of analysed images. The processing time for each image at full resolution is approximately 40 s using a 64 bits "Core i3 processor" running at 2.40 GHz and 4 GB in RAM.

4.3 Materials and methods

The variability of a composite plate is very dependent on the manufacturing process, materials and geometry of the structure. The presented results are derived from the methodology explained in section 4.2 and are valid for the manufactured plates as described below. However, the methodology is still valid for other types of material and lay-up techniques.

A batch of six composite plates are produced by manually stacking the unidirectional carbon/epoxy prepreg HexPly® M10.1/38%/UD300/CHS, furnished by Hexcel Composites. The dimensions of the manufactured plates are 615 mm long and 300 mm wide. The 16 ply stratification is chosen to be quasi-isotropic with the lay-up sequence $[90/-45/0/(+45)_2/0/-45/90]_s$. The plates are cured in an autoclave using the recommended cure cycle, with a consolidation dwell at 90°C for 15 minutes and a cure dwell at 120°C for 120 minutes. The heating and cooling rates were set to 2 °C min^{-1}. The consolidation pressure and curing pressure are set to 2 and 5 bar, respectively.

The procedure to form a composite plate starts with cutting the prepreg plies from a roll of the prepreg M10.1/38%/UD300/CHS. The size of the plies is given by the dimensions of the composite plates, 615 x 300 mm. The plies are cut following a pattern designed to reduce material waste. Some of the plies need to be assembled from two or more pieces increasing the probability of a change of the fibre direction within a single ply. After the preform cut, the ply lay-up is done manually by two operators. Each operator is placed at one side of the work zone and holds the composite plies at his (her) own side. All the composite plates were laid by the same operators using the same technique to reduce operator induced variability. The plate must be moved from the working area after the placement of 8 plies to the debulking area to remove the entrapped air ensuring a better contact between the plies prior to the curing phase. The replacement at the exact position of the composite plate on the work zone after the debulking operation cannot be assured. Thus, the lay-up must be self-referenced at any moment during the fabrication in order to have a common reference for all the 16 plies forming each single plate. The first ply (oriented at 90°) is 10 mm larger than the rest of the plies, having dimensions of 625 x 310 mm. Plies 2 to 16 are then referenced to this ply #1.

An image of each ply is then taken after it is laid onto its position for all six manufactured plates. The optics of the DSLR camera and its relative positioning to the work zone generate optical distortions (barrel and perspective) on the acquired images. To reduce the error in the fibre orientation measurement, DxO Optics Pro® commercial software was used to reduce these distortions before the analysis of the images. After a correction of the images, these are then treated in an in-house program to determine the orientation angles of each ply described in section 4.2.

4.4 Results analysis of the optical measurements

4.4.1 Overall ply misalignment

During the lay-up procedure, the complete stratification can be moved from its starting position, mostly due to transporting the lay-up to the debulking area after the placement of 8 plies. In order to determine the true orientation of all the plies with respect to the composite plate, all the measurements are referenced to the first ply which is 10 mm longer than the rest of the plies in order to be visible in all the images taken of the lay-up procedure. Figure 4-8 shows the differences between the actual ply orientation and its theoretical orientation, the dashed lines show the mean squares linear fit for each plate. For plates C-11 through C-22 these differences range between -0.5° to 0.5°. The standard deviation of the ply misalignment ranges from 0.34 to 0.41° for each plate. As it is shown in the figure, the overall misalignment is shifted towards a positive angle. This effect is more noticeable in the plate C-23. However, for the rest of the plates this derive is not significant and no correlation was found between the ply theoretical orientation and its measured misalignment.
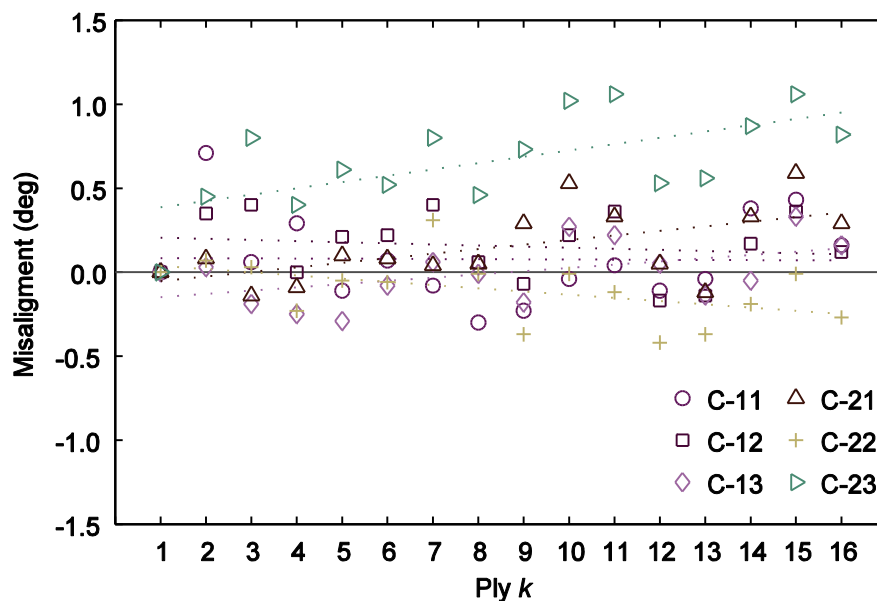
Figure 4-8. Difference between the theoretical orientation and the measured orientation in the ply.

To ensure that the values are valid and representative, the misalignments are verified by manual measurements of the ply orientation. This procedure is performed by manually tracing a line following the fibre lines [19]. The comparison between the manual and the automatic procedure yields the same results. The dispersion compared to the manual measurements is negligible with a difference lower than 0.2°. The global differences between the intended orientation and the measured fibre directions are lower than the expected values. The obtained values are lower than the values reported by Yurgartis [5] and Olave [7], and are in good agreement with the values obtained by Skordos [13].

The low value of ply misalignment is partly due to the size of the ply, since a misplacement of 10 mm in a 600 mm long ply is noticeable. This ratio of 1 to 60 is roughly 1° of difference. Nevertheless in much smaller plies, the global misalignment could be more significant, since the errors in the ply positioning are less noticeable [20].

This characterisation is proper to our own lay-up technique. The zones with internal variability can exhibit more significant changes than the global misalignments of each ply compared to its mean and theoretical orientation. Nevertheless the local changes in the fibre direction cannot be described by this technique.

4.4.2 Local misalignments

To evaluate the internal dispersions of the composite plate, the standard deviation of the ply angles is determined by 200 elements. At first sight, the most deformed plies are the 0° plies with a mean of 1.02°. The least scattered ply undulations are for the ± 45° orientations. However, plies oriented at 0° and 90° exhibit a large number of elements to be discarded since any of the Hough lines of the element falls within the imposed tolerance. In average, 48 elements for the 0° direction and 19 elements for the 90° orientation are thus discarded. For both of ± 45° directions, none of the elements have been discarded. Another effect that

must be taken into account is that the elements surrounding the discarded elements exhibit a significant dispersion in the measured orientation, while the elements in the core of the plate have the narrowest range of values closer to the mean ply orientation (cf. Figure 4-9).

For the plies oriented at 0°, the highest variations are found on the left hand and upper part of the ply. This is not explained by the internal variation of the fibre bundles, but by the lighting conditions. Since having the objective of the camera and the light source in a fixed position, the reflecting light and shadows in the composite rend these zones unable to determine the fibre direction. The few elements that can be measured exhibit great uncertainties. This effect is not found in the other directions. Nevertheless, the central zone and right hand side corner are not affected and exhibit the least variability of the ply. This effect is thought to be the same for all the plates of the same type. This is due to the architecture of the 0° plies. Since they are more rigid than the other preform cuts in the other directions, hence they have better support for handling and placing onto the lay-up structure.

Plies oriented at ± 45° shows a greater variability at the corners of the ply. For the +45° the variations are more significant in the lower left and the upper right hand side corners. It could be thought that the variations are more predominant in the upper left and lower right hand side corners since the fibres at the corner are shortened towards the corner. Also these fibres are more prone to being deformed during the lay-up sequence.

For the plies oriented at 90°, it is more difficult to define a zone that exhibits more variability since the preforms have a very low transverse rigidity compared to the plies oriented at 0°. Also, the nature of the ply cutting implies the use of strips of composite prepreg laid side by side.
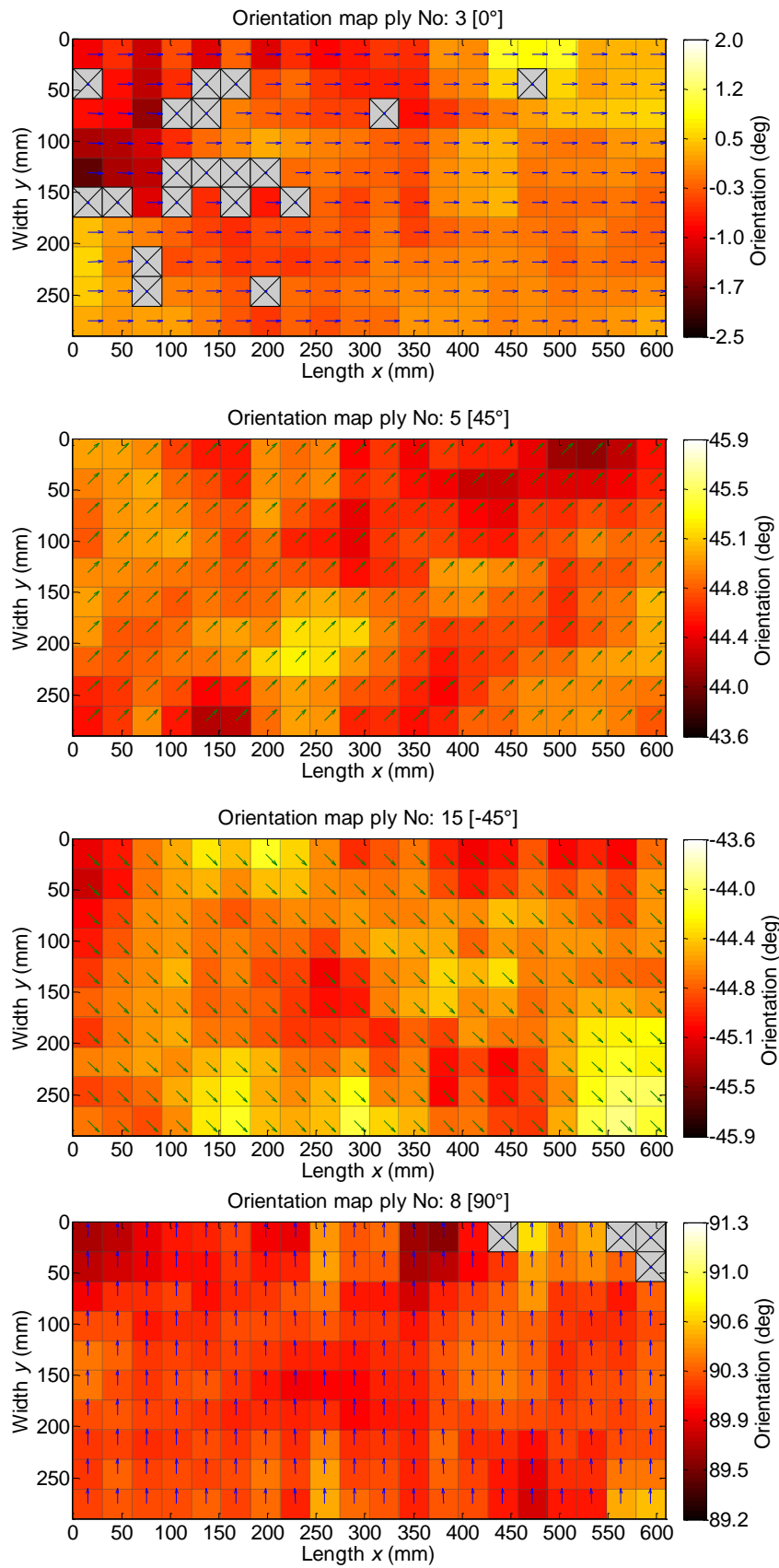
**Figure 4-9. Orientation maps of 4 different plies from plate C-11 oriented, from top to
bottom 0°, +45°, -45° and 90° respectively.**

The measurements of the local misalignments within a ply (due to the juxtaposition of prepreg strips) are strongly correlated to the ply orientations. A 0° orientation offers the largest stiffness and best support along the fibres. Thus, it is more difficult to deform while performing the lay-up. By contrast, the ± 45° directions offer the least support and are more prone to deformation due to the manipulation of the prepreg. This is more evident in the corners of the ply or in zones where there is juxtaposition of two or more ply strips.

4.5 Modelling the fibre misalignments

4.5.1 General description of the mathematical model

In order to evaluate the effects of the variability of fibre orientation θ in a composite part, the fibre misalignments are introduced into a finite element (FE) model as the sum of three different scales (cf. eq. 4-1). The first scale is the mean ply misalignment $\delta\theta$ which is the average deviation for all the plies from the theoretical ply orientation θ_{th} ("th" for theoretical). The second scale is the local variability due to the deformation θ_{pert} ("pert" for perturbation), and finally, a continuous variability produced by the fibre in-plane undulations θ_{wav} ("wav" for waviness).

$$\theta_k(x, y) = \theta_{k \cdot th}(k) + \delta\theta_k + \theta_{wav}(\theta_{k \cdot th}) + \theta_{pert}(x, y) \tag{4-1}$$

The global ply misalignment values are obtained in section 4.4. While the local continuous undulations are obtained from the literature, the undulation in form of a sinusoidal wave has a mean amplitude of 0.03 mm and a mean wavelength of 3 mm being its extreme values found between 2.2 and 4 mm [2,15].

To model the in-ply fibre orientations observing a continuity in the orientation values, the local variation of the misalignment can be described as a sum of ith pseudo-Gaussian surfaces (cf. eq. 4-2 and Figure 4-10), having a central point with coordinates X_i and Y_i, the length and the width of each perturbation is described by the parameters a_i and β_i, homologues to the standard deviation in a

normal distribution. The amplitude of this perturbation is controlled by the parameter B_i. This set of equations allows the modelling of a continuous change in the fibre orientation properties [21].

$$\theta_{pert}(x, y) = \sum_{i=1}^{12} B_i e^{-\left(\left(\frac{x-X_i}{\alpha_i}\right)^2 + \left(\frac{y-Y_i}{\beta_i}\right)^2\right)} \tag{4-2}$$
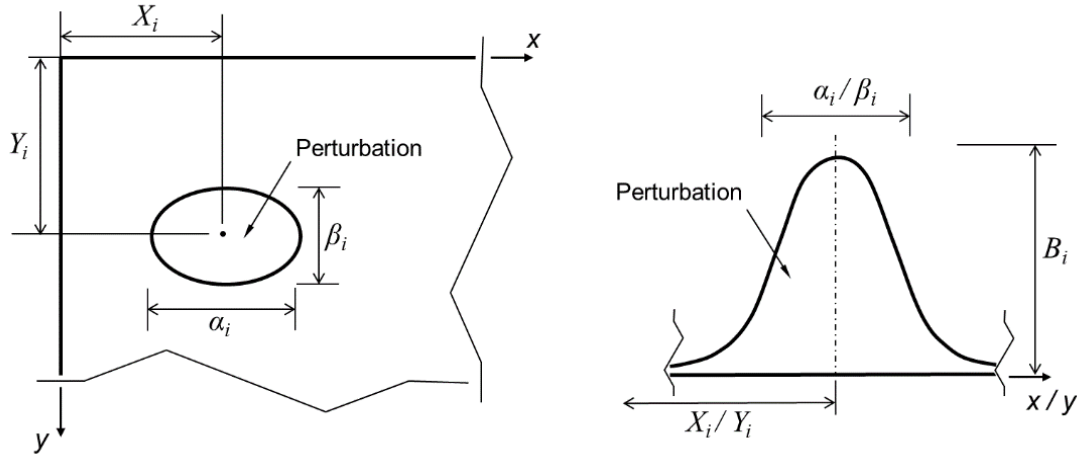
Figure 4-10. Schematic description by a pseudo-Gaussian surface (on right) of a localized zone of fibre orientation perturbation (on left).

4.5.2 Data set analysis for the continuous misalignment

To obtain the values of the representative peaks of the perturbation that define the fibre misalignment, an optimisation algorithm is applied to the amplitude, position and shape of the perturbations. This algorithm is performed by minimizing the values of the function in eq. 4-2 under a series of constraints (minimum and maximum limits) of the variables in this function. In this case, 12 peaks have been chosen in a trade off or matching the original pattern, the calculation time and convergence of the algorithm. The computation time is between 60 to 80 seconds for each ply in a CPU with the characteristics explained in section 4.2.

Before applying the detection algorithm, the mean value of the ply orientation is subtracted from the elements in order to consider only the local

misalignments. The centre of the ith perturbation can be located anywhere between -60 and 660 mm in the x-direction and -60 and 360 mm in the y-direction. The placement of the centre of the perturbation can be outside the plate since a part of it can be modelled. The size of the perturbations a_i and β_i are set between +30 and 210 mm. The perturbation amplitude is maintained between -1 and 1 mm. The reconstructed surface using the values found by the optimisation algorithm is shown in Figure 4-11 as an example. In this example, the extreme values are not correctly predicted by the optimisation algorithm. Nonetheless, these extreme values can be a result of errors of the image processing. The shape of the surfaces is however in good agreement with the experimental data.

Ply #15 [-45°] Measured

Ply #15 [-45°] Identified
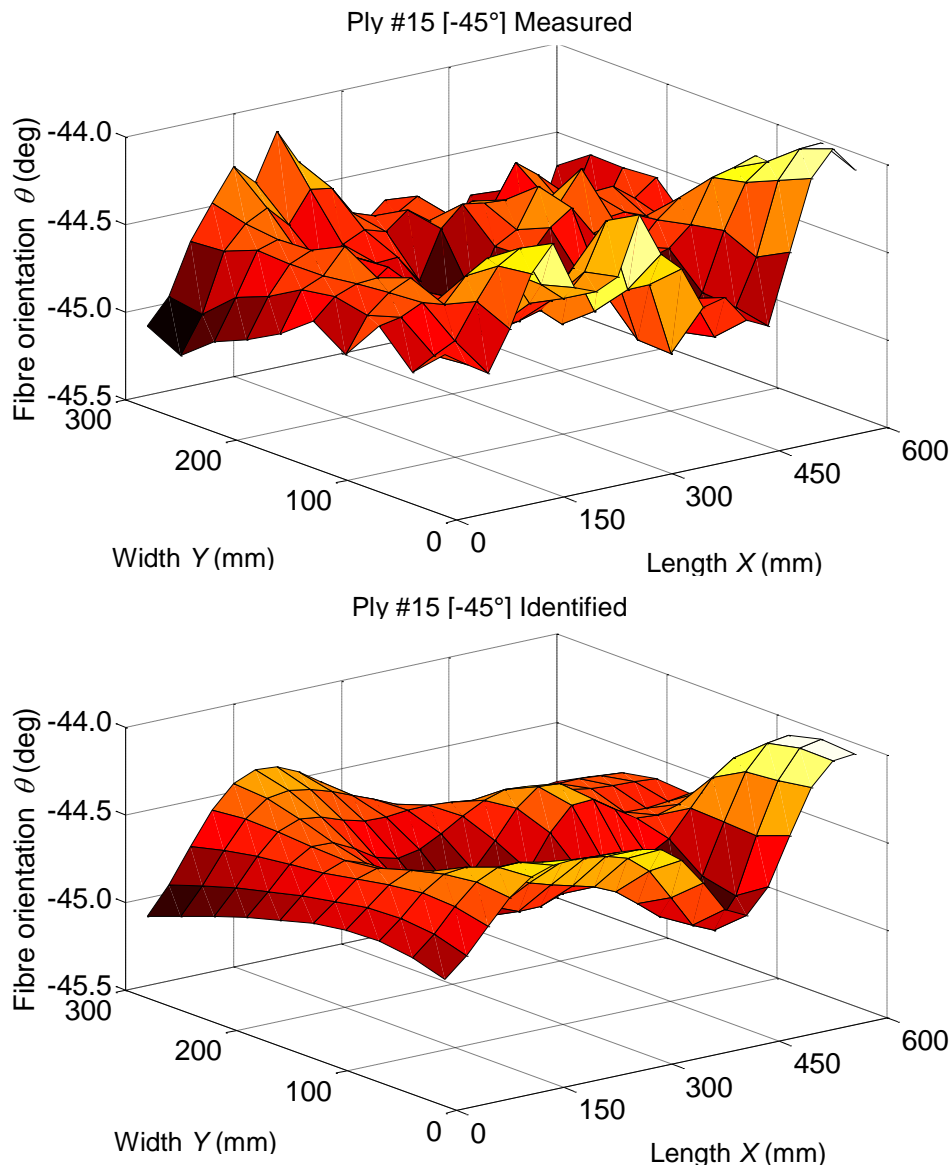
**Figure 4-11. Comparison of the misalignment maps for the plate C-11 ply #15 oriented
at -45° with, (top) the measurements and (bottom) the ply reconstructed using the
identification algorithm.**

The generation of a data set to produce a digital fibre misalignment using
equation 4-2 is challenging since there is an interaction between the different
variables. Also, the in-ply misalignment is the product of pre-existing local
prepreg misalignments coupled with its manipulation during the cutting and
lay-up phases. Zones that exhibit a larger variability can be identified, for
example, on the ply corners, where the fibres have less support from the
contiguous prepreg. The mathematical interpretation of these local misalignments

is thus produced by the interdependency of five variables: the amplitude of the perturbation that can be either positive or negative, the position of the perturbation and the shape of the perturbation, both parameters varying in two dimensions. To keep the calculation and analysis of the identification results as simple as possible, the shape of the perturbation is only considered for its major and minor axis with no rotation with respect to the z-axis.

The values of B_i are obtained by the identification algorithm, ranging from -0.800 to 1.000 mm. A gap in the values near the amplitude of 0 mm is found (cf. Figure 4-12). Nevertheless, these values are not important since the variation of the peak is small. The values are found in the negative side ranges from -0.800 to -0.106 mm and in the positive side from 0.173 to 1.000 mm. Additionally, 44 % of the values are negative and 56 % positive.

To draw the amplitudes, both negative and positive values are brought into a continuous distribution by removing the gap between the highest negative value and the lowest positive value. The continuous distribution of B_i has a mean of 0.049° and a standard deviation of 0.340°. A normal distribution is used to draw the amplitude values. The amplitude B_i gap is restored by subtracting 0.106 mm if the drawn value is less than or equal to 0, or adding 0.173 mm if the draw value is greater than 0. If after restoring the gap, the amplitude B_i is less than -0.800 mm or greater than 1.000 mm, the value of B_i is substituted by its corresponding limit.
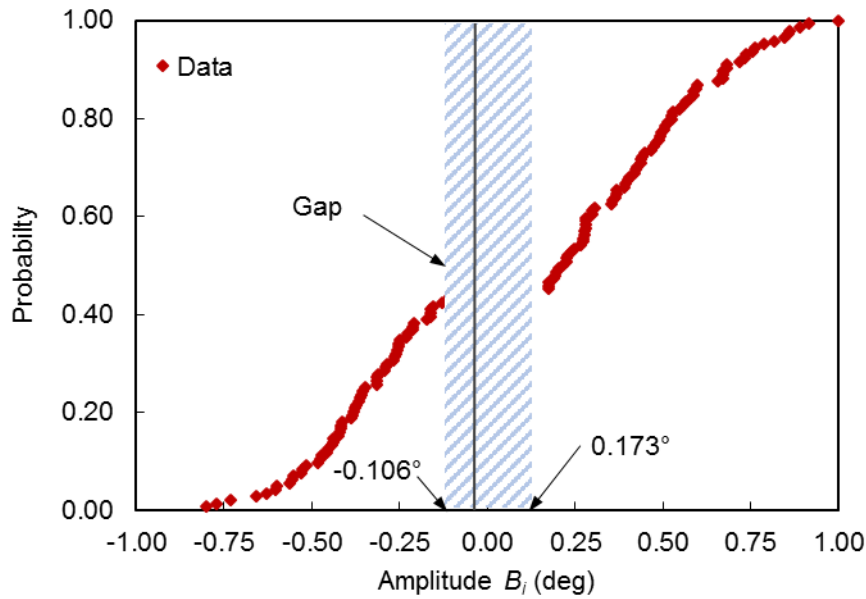
Figure 4-12. Cumulative distribution function of the Amplitude B_i acquired by the optimisation algorithm.

The amplitudes a_i and β_i are generated independently, and are drawn from a uniform distribution with its limits ranging from 30 to 210 mm. The data are chosen from 46 different plies.

The positions of the centre of each perturbation are also drawn from a uniform distribution. Since the original identification algorithm accounts for a perturbation that has its maximum value outside the plate, with limits ranging from -30 to 660 mm in the x-direction and from -60 to 360 mm in the y-direction. To avoid the superposition of two peaks, a minimum distance between the centres of each peak of d = 15.6 mm is introduced for the generation of the digital perturbations, which is coherent with the experimental results. To achieve this condition, a first peak is generated inside the boundaries of the composite plate (within a range of 60 to 540 mm in the x-direction and 60 to 240 mm in the y-direction). After the insertion of the next peak, the minimum distance is calculated between all the existing points. This cycle is continued if the distance is less than the cut of distance d = 15.6 mm. 12 peaks are considered to be spread over a surface of 500 x 800 mm (the plate dimensions plus the overrun area to accommodate a peak external to the plate). In this analysis, the number of peaks is

chosen as a compromise between the accuracy of the mathematical representation and computation time.

4.6 Generation of a digital misalignment

The main goal of the procedure is to create a data set that will be introduced into a finite element model to take into account the variability in fibre orientations. Using the recompiled data from sections 4.4 and 4.5, the fibre orientations are generated using the proposed algorithms. The reconstructed misalignment using the variables from the identification algorithm shows that the mean in all the cases is zero, as shown in the cumulative distribution function (CDF) of the analysed plies (cf. Figure 4-13). On the contrary, the generated misalignments have a different distribution with a minimum mean value of -0.5° and a maximum mean value of 0.8°. This means that the algorithm to generate the different sets of values is not optimised. The CDF of the standard deviation of the ply misalignment within a ply exhibits a similar value, even though the CDFs do not completely match. This mismatch is due to the random generation of the pair of values. However for modelling the fibre orientation, the difference between the standard deviation CDF for experimental data and for generated data is not significant. Since the mean ply orientation is introduced into the model as an independent variable (cf. eq. 4-1), the generated misalignments can be forced to have a zero-mean orientation by subtracting its own mean. This procedure does not impact the standard deviation of the ply misalignment but only the maximum and minimum misalignments, as shown in Figure 4-14. A gap between the CDF for the original values and the generated values is observed. Also the shapes of the distributions do not match. Nevertheless after subtracting the mean value from the obtained misalignment, the maximum and minimum misalignments are in better agreement with the experimental distribution at the exception of the tails of the distributions.
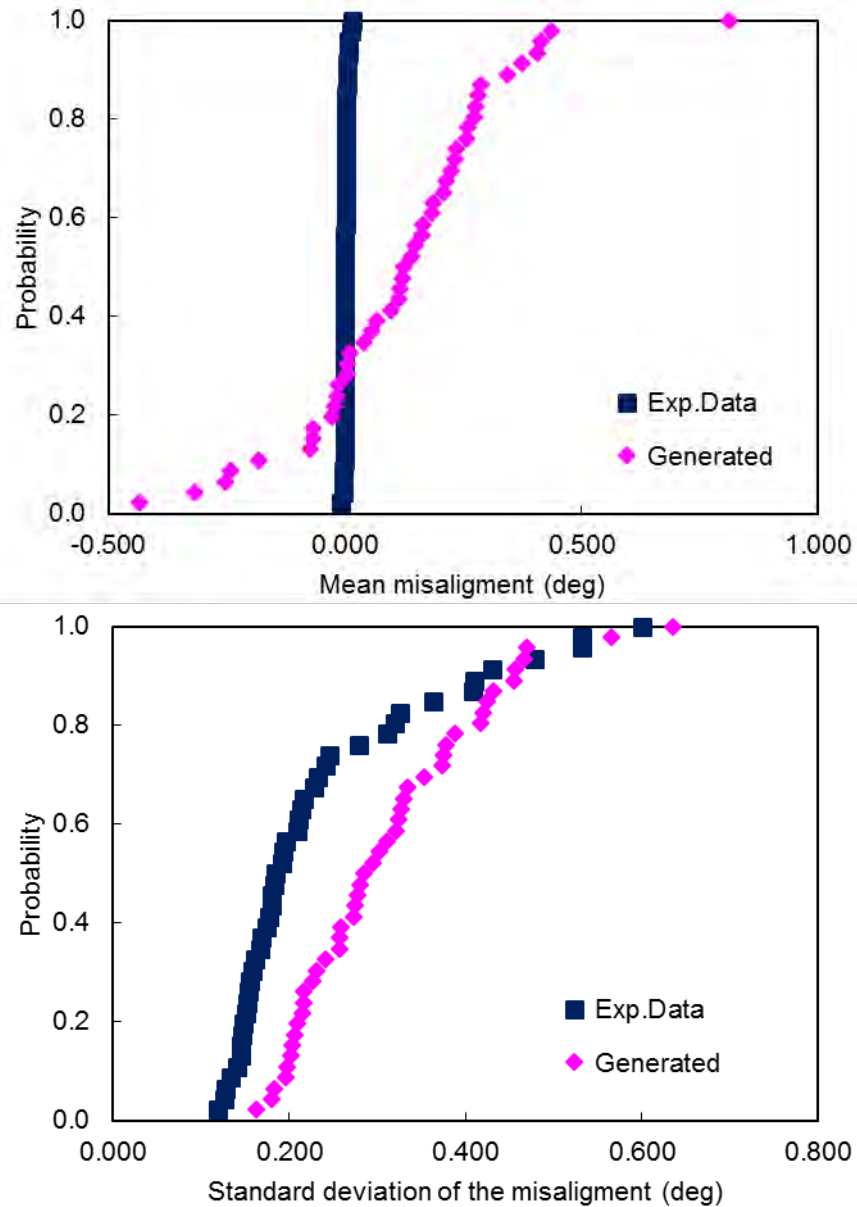
Figure 4-13. Cumulative distribution functions for the reconstructed misalignment using equation 5-2 (square markings) compared to experimental data (diamond markings) with, (top) the mean misalignment and (bottom) the standard deviation of the in-ply misalignment.
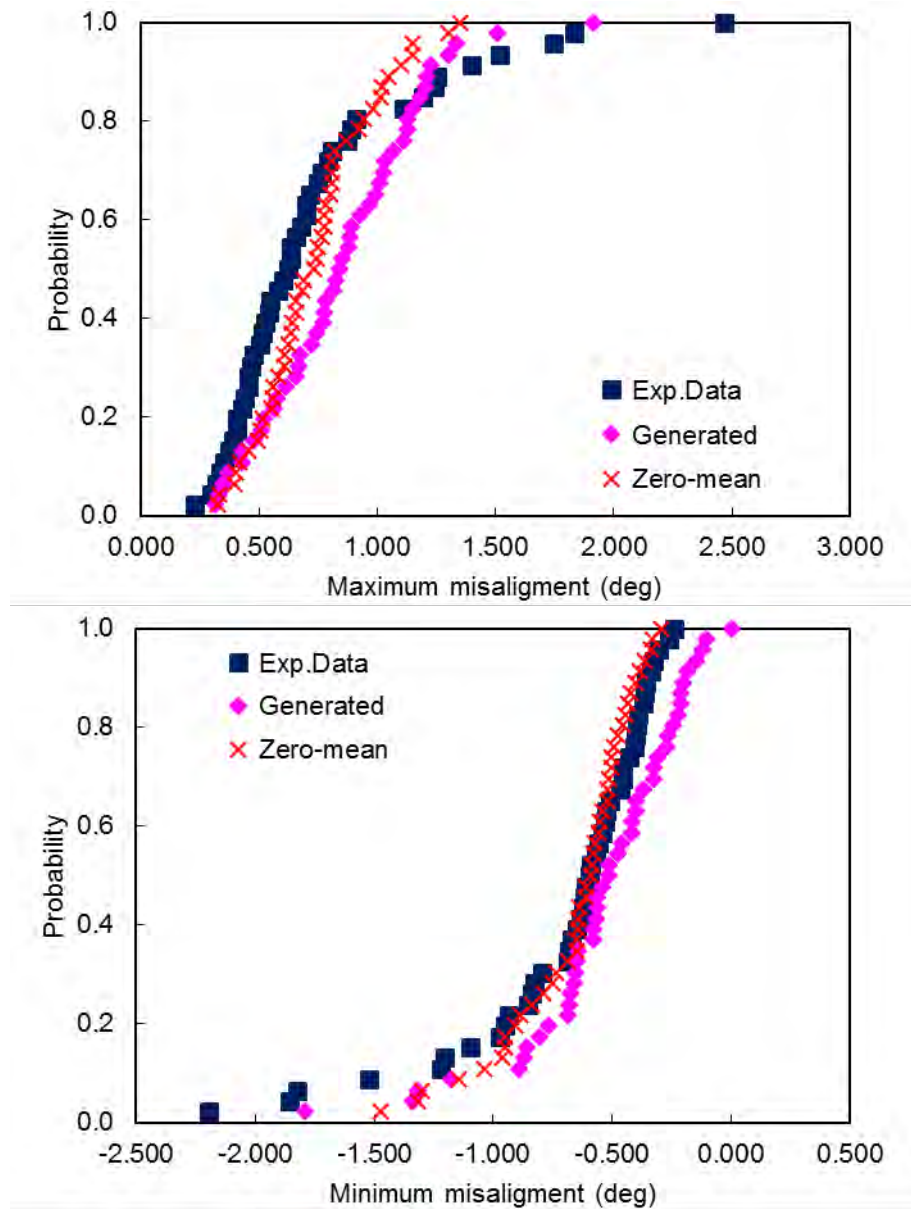
Figure 4-14. Cumulative distribution functions for the reconstructed misalignment using equation 5-2 (square markings), corrected for a zero mean (cross markings) compared to experimental data (diamond markings) with (top) the maximum values and (bottom) the minimum values.

This methodology can be used to draw different sampling for Monte Carlo simulations. Figure 4-15 shows the location and the amplitude B_i for the 12 peaks randomly generated within the imposed restrictions. The reconstructed misalignments (cf. Figure 4-16) show lower in-plane variability than the rest of the studied plate, with values ranging from 1° to -0.5°. The resulting misalignment map can be further optimised to obtain values closer to the reality. Regardless, as a

first approach to model the local change in the fibre orientation accounting for a
spatial variability the results are encouraging.
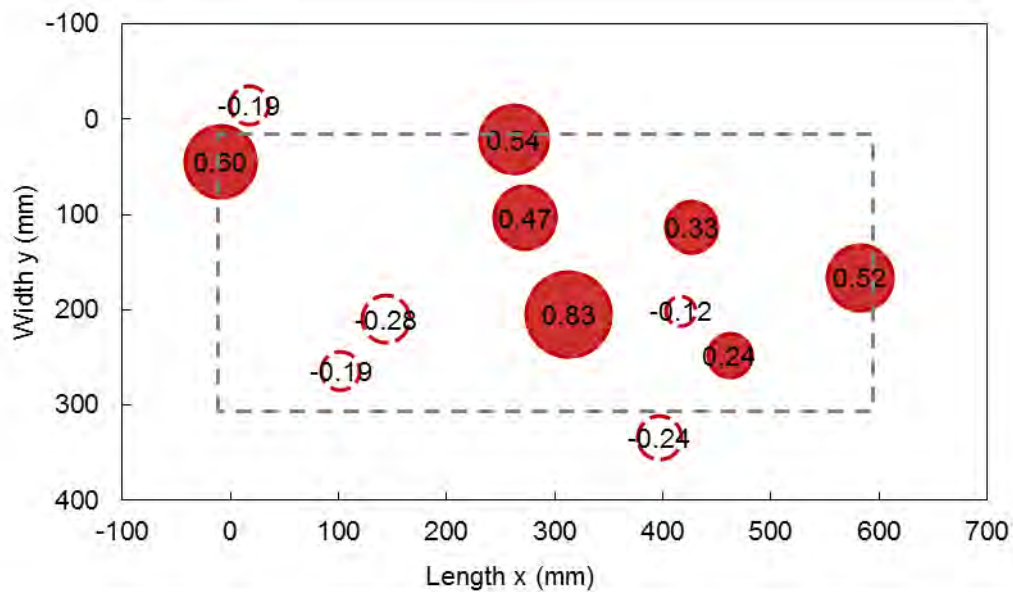
**Figure 4-15. Localisation and amplitude of the 12 perturbation peaks used to generate
digital in-plane misalignments, the diameter of the circles indicating the values of the
amplitudes B_i in degrees.**
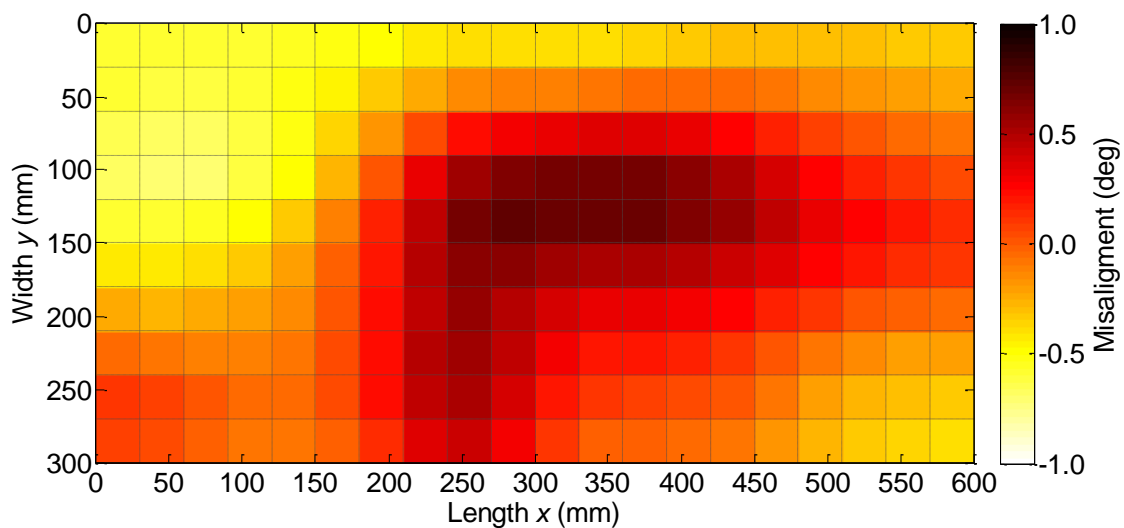
**Figure 4-16. Map of the generated in-plane fibre misalignment with the size of the
element of 30 x 30 mm.**

4.7 Conclusions

The variability in the fibre orientation was measured on the uncured prepreg during the lay-up procedure of a composite plate. The orientations are assumed to be unchanged during the curing phase of the composite material. However, this hypothesis cannot be proven, since the determination of actual fibre orientation after curing involves destructive techniques to measure the fibre in the composite cross-sections.

An optical method has been proposed using the Hough transform in order to detect the fibre orientation using images of the complete ply (600 x 300 mm). The method yields good results in terms of calculation time and overall misalignments. The use of the Hough transform allows the selection of any arbitrary element size. In our case, the selected elements size is approximately 30 x 30 mm.

The variation in the mean ply orientation is found lower than the expected values, ranging from -0.5 to 0.5°. The standard deviations for the overall misalignment within the 16 plies lead to stratification ranges between 0.34 and 0.41°. No correlation was found between the overall ply misalignment and the intended orientation of such ply. An increasing misalignment is noted through the lay-up sequence.

A model was proposed for the fibre misalignments where the fibre misalignment is due to the overall ply misalignment, the local perturbations formed during the prepreg manipulation and the fibre periodic undulations. The values of fibre orientations will be used in a finite element model with the inclusion of variability.

An identification algorithm of the local perturbations is also proposed, in which the geometrical parameters of a pseudo-Gaussian surface are obtained. Using these parameters, a model of local perturbations is provided. The resulting misalignments have the same behaviour as the real ply.

4.8 References

[1]   C. C. Chamis, "Probabilistic Composite Design," *Compos. Mater. Test. Des.*, vol. 13, pp. 23–42, 1997.

[2]   K. D. Potter, B. Khan, M. R. Wisnom, T. Bell, and J. Stevens, "Variability, fibre waviness and misalignment in the determination of the properties of composite materials and structures," *Compos. Part A Appl. Sci. Manuf.*, vol. 39, no. 9, pp. 1343–1354, Sep. 2008.

[3]   R. S. Trask, S. R. Hallett, F. M. M. Helenon, and M. R. Wisnom, "Influence of process induced defects on the failure of composite T-joint specimens," *Compos. Part A Appl. Sci. Manuf.*, vol. 43, no. 4, pp. 748–757, Apr. 2012.

[4]   Y. Arao, J. Koyanagi, S. Utsunomiya, and H. Kawada, "Effect of ply angle misalignment on out-of-plane deformation of symmetrical cross-ply CFRP laminates: Accuracy of the ply angle alignment," *Compos. Struct.*, vol. 93, no. 4, pp. 1225–1230, Mar. 2011.

[5]   S. W. Yurgartis, "Measurement of small angle fiber misalignments in continuous fiber composites," *Compos. Sci. Technol.*, vol. 30, no. 4, pp. 279–293, Jan. 1987.

[6]   S. Barwick and T. Papathanasiou, "Identification of fiber misalignment in continuous fiber composites," *Polym. Compos.*, no. 3, pp. 475–486, 2003.

[7]   M. Olave, A. Vanaerschot, S. V Lomov, and D. Vandepitte, "Internal Geometry Variability of Two Woven Composites and Related Variability of the Stiffness," *Polym. Compos.*, pp. 1335–1350, 2012.

[8]   K. Engel, P. Horst, T. Hundt, C. Schmidt, and B. Deneka, "Effect of manufacturing process induced fiber waviness on mechanical properties of composite structures by example of a prepreg forming process," in *ECCM 16*, 2014.

[9]   C. J. Creighton, M. P. F. Sutcliffe, and T. . Clyne, "A multiple field image analysis procedure for characterisation of fibre alignment in composites," *Compos. Part A Appl. Sci. Manuf.*, vol. 32, no. 2, pp. 221–229, Feb. 2001.

[10]   K. Kratmann, M. P. F. Sutcliffe, L. Lilleheden, R. Pyrz, and O. Thomsen, "A novel image analysis procedure for measuring fibre misalignment in unidirectional fibre composites," *Compos. Sci. Technol.*, vol. 69, no. 2, pp. 228–238, Feb. 2009.

[11]   M. P. F. Sutcliffe, S. L. Lemanski, and A. E. Scott, "Measurement of fibre waviness in industrial composite components," *Compos. Sci. Technol.*, vol. 72, no. 16, pp. 2016–2023, Nov. 2012.

[12] G. Requena, G. Fiedler, B. Seiser, P. Degischer, M. Di Michiel, and T. Buslaps, "3D-Quantification of the distribution of continuous fibres in unidirectionally reinforced composites," *Compos. Part A Appl. Sci. Manuf.*, vol. 40, no. 2, pp. 152–163, Feb. 2009.

[13] A. A. Skordos and M. P. F. Sutcliffe, "Stochastic simulation of woven composites forming," *Compos. Sci. Technol.*, vol. 68, no. 1, pp. 283–296, Jan. 2008.

[14] T. S. Mesogitis, A. A. Skordos, and A. C. Long, "Non-crip fabrics geometrical variability and its influence on composite cure," in *ECCM 16*, 2014.

[15] K. D. Potter, C. Langer, B. Hodgkiss, and S. Lamb, "Sources of variability in uncured aerospace grade unidirectional carbon fibre epoxy preimpregnate," *Compos. Part A Appl. Sci. Manuf.*, vol. 38, no. 3, pp. 905–916, Mar. 2007.

[16] L. Shi and S. Wu, "Automatic Fiber Orientation Detection for Sewed Carbon Fibers," *Tsinghua Sci. Technol.*, vol. 12, no. 4, pp. 447–452, 2007.

[17] C. Redon, L. Chermant, J. Chermant, and M. Coster, "Automatic image analysis and morphology of fibre reinforced concrete," *Cem. Concret Compos.*, vol. 21, pp. 403–412, 1999.

[18] J. Canny, "A computational approach to edge detection.," *IEEE Trans. Pattern Anal. Mach. Intell.*, vol. 8, no. 6, pp. 679–98, Jun. 1986.

[19] Y. Davila, L. Crouzeix, B. Douchin, F. Collombet, and Y.-H. Grunevald, "Quantification of sources of variability in CFRP plates cured in autoclave," in *International Conference on Composite Materials 19*, 2013.

[20] M. Torres, B. Douchin, F. Collombet, L. Crouzeix, Y. Grunevald, and R. Bazer-bachi, "Valeur ajoutée d'une encapsulation de capteurs silicium pour l'instrumentation à cœur des structures composites," in *JNC 17*, 2011, pp. 1–10.

[21] A. Goshtasby and W. D. Oneill, "Curve Fitting by a Sum of Gaussians," *CVGIP Graph. Model. Image Process.*, vol. 56, no. 4, pp. 281–288, Jul. 1994.

Chapter 5: Spatial evolution of the variability of ply thickness over a CFRP laminated structure

5.1 Introduction

For design purposes, the structure thickness is given by the sum of the ply thicknesses that form the laminate, or alternatively the thicknesses of the plies are obtained by dividing the total structure thickness by the number of plies of the given stratification. The thickness of the structure is thus considered as constant and equal for all plies, provided that there is not a change of the geometry of the cross-section and stratification [1]. In reality, each ply in the stratification does not present a constant thickness (cf. Figure 5-1).
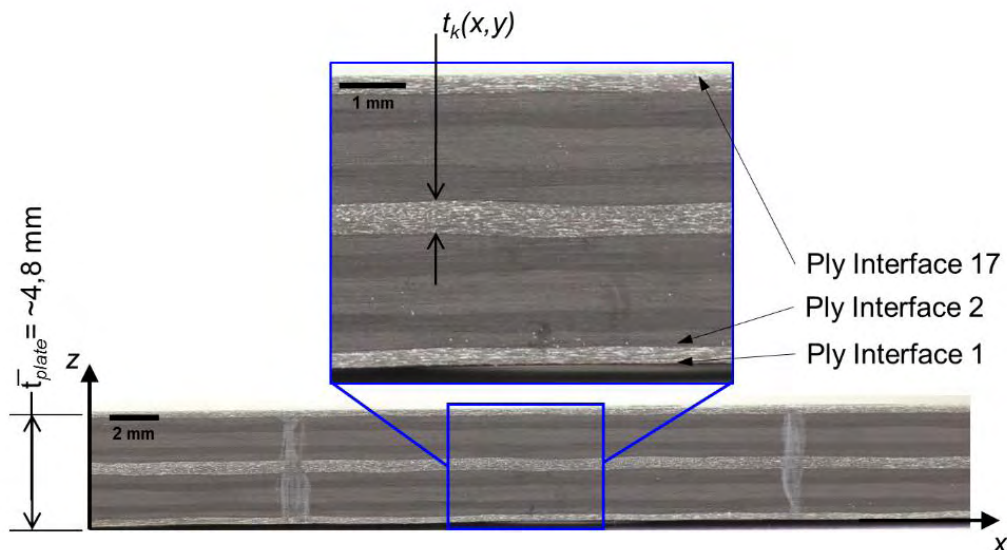
Figure 5-1. Micrograph showing the ply thickness variations spread over a layered composite plate.

The effects of the ply thickness variations have been studied in the literature as localized defects, like wrinkles and warpings [2,3], on thickness variations in the singular zone like L-shaped stringers due to manufacturing conditions [4]. However, there are few publications that address the representation of thickness variations spread over a laminated structures. Collombet et al. [5] reported for a 28-ply M21/T700 carbon/epoxy laminate a mean ply thickness of 0.264 mm with a standard deviation of 0.002 mm, with extreme values of 0.258 and 0.270 mm. However, the determination of the ply thickness was performed through the measurement of the laminate thickness. A further inspection of the cross section of the specimens revealed that the ply thicknesses deviated up to 21 % from the mean ply thickness, with extreme values of 0.245 and 0.314 mm.

As explained, the composite structure cannot be dissociated from its manufacturing conditions. The volume fractions of fibres and porosities are directly linked to the stratification of the composite, the nature of the raw materials and the curing cycle [6, 7]. These changes in the volume fraction can be a source of warpages for thin laminates (global on the scale of the plate and spread on the scale of the plies) [9]. However, a link between the thickness evolution and the spatial distribution of the mechanical properties in a composite structure is another challenge that adds a new layer of complexity that goes beyond the scope of this study.

Daniel et al. [8, 9] have studied the effects of the fibre waviness on thick unidirectional stratifications (up to 150 plies) generated by local and periodic perturbations in the stratification. The proposed method calls for a modification in the compliance matrix by adding an out-of-plane component to the fibre orientation. Nonetheless the problem is treated as a local effect related to a defect present in the material.

During the computational analysis of a composite structure, the magnitude of the ply thickness is changed for a unique value at each simulation for all the elements [10,11]. Conversely in the literature, no methodology was found that

accounts for the local changes spread over the composite structure applied to multidirectional laminates fabricated with UD prepregs.

The aim of this chapter is to propose a modelling strategy which will be used to generate the input parameters of a finite element model based on the reality of the material. A set of digital lay-ups containing the variations of the plate and ply thicknesses is proposed. The main and original contribution of this work is the introduction of a concept of spatial continuity on the ply thickness variation. The main model parameters are obtained by using a discrete Fourier transform (DFT) of the ply thickness profiles of a real composite plate. The generation of a digital lay-up is not done using only a random ply thickness generator, but by proposing a mathematical model based on the actual ply profile. This mathematical model contains parameters that can be modified to generate different digital lay-ups at each simulation while maintaining similar values of dispersion to the original plate.

To retrieve the required information needed for the numerical model, the cross-section of a 16-ply composite plate is analysed to obtain, not only the dispersion in plies and plate thicknesses, but the real profiles of the thicknesses of the plies spread over the plate.

5.2 Materials

The study focuses on composite plates with a constant number of plies and cross sections, without additional structural features, e.g. ply drop-offs. As presented in Chapter 3, we recall that the composite plates are produced by manually stacking a unidirectional carbon/epoxy prepreg HexPly® M10.1/38%/UD300/CHS, supplied by Hexcel Composites. The dimensions of the manufactured plates are 615 mm long and 300 mm wide. The 16 ply stratification is chosen to be quasi-isotropic with the lay-up sequence $[90/-45/0/(+45)_2/0/-45/90]_s$. The plates were cured in an autoclave using the recommended cure cycle, with a consolidation dwell at 90 °C for 15 minutes and a

cure dwell at 120 °C for 120 minutes. The heating and cooling rates were set to 2 °C min^{-1}. The consolidation pressure and curing pressure were 2 and 5 bar for each plateau.

The ply thickness is measured on the cross-section of two different sets of specimens obtained from the cured composite structure. The first set is devoted to the statistical control of the variability in the ply thicknesses regardless of the position along the width (x-coordinate) of the specimen. The second set is dedicated to the determination of a mathematical model of the ply variability maintaining a continuity of the measurement variation over the plate. All the specimens were cut from the composite plates using a cutting disc. The surface of the cross-sections was prepared by grinding the surface with abrasive paper, followed by surface polishing. Figure 5-1 shows the cross-section of the 16 ply laminate exhibiting variability in the ply thicknesses. Due to the lay-up sequence, the pairs of plies 4/5, 8/9 and 12/13 cannot be distinguished individually because the inter-ply of the cured M10.1/38%/UD300/CHS is almost non-existent. For their analysis, the thickness of these dual plies was divided by two.

5.3 Variability of ply thicknesses

5.3.1 Variation in the mean ply thickness

The ply thickness is measured using the micrographs taken from the composite cross-section. An initial set of four specimens of 130 mm long and 20 mm wide was obtained from one of the cured plates. After polishing the cross-section to reveal the stratification, a DSLR camera Canon 550D with an EF-100mm macro lens was used to record the micrographs of the cross-section of the specimens. The image resolution is 150 pixels/mm. The ply thicknesses were measured at 12 different locations in each specimen, for a total of 48 measuring points per ply, considering all 4 specimens.

Figure 5-2 shows the distribution of the ply mean thicknesses with ± 1 standard deviation. As seen in the figure, the mean thicknesses are randomly distributed along the cross-section of the composite plate. It is also shown that the variability of each ply is different and it is uncorrelated to its position within the stratification. The measurements of the cross section reveal that the thicknesses of the plies have coefficients of variation (CV) ranging from 5 % to 11 %. The extreme values are 0.247 and 0.366 mm, which deviate 17 and 22 % respectively from the mean ply thickness which is 0.300 mm. By comparison, the mean thickness of the plate is 4.789 mm with a CV of 1.7 %. This apparent mismatch between the variability of the ply thicknesses and the variation plate is due to the coupling of the local thickening or thinning of the adjacent plies as seen in Table 5-1.
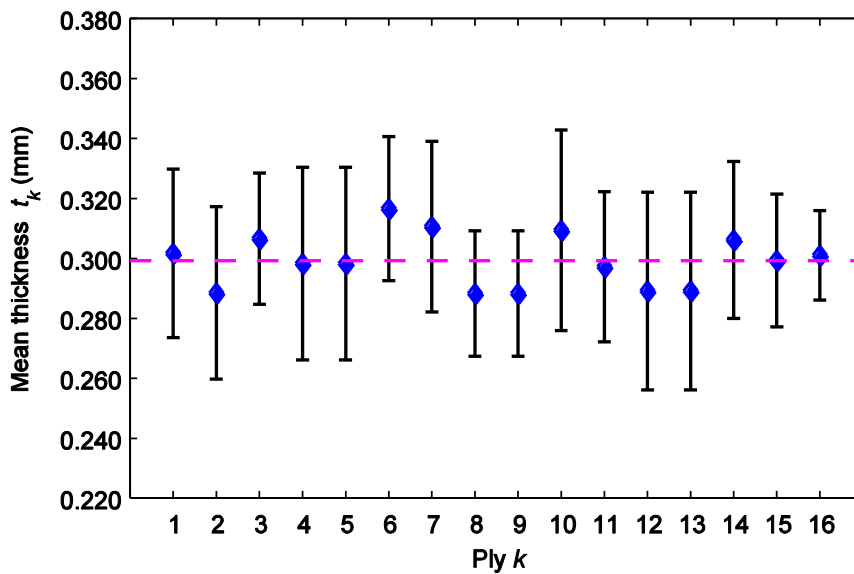
Figure 5-2. Mean ply thicknesses listed for each of the 16 plies ± 1 standard deviation, the measured thickness divided by 2 for the pair of plies 4/5, 8/9 and 12/13.

Table 5-1. Thickness comparison between the ply and the plate averages.

Data	Mean ply (all plies)	Plate
Average thickness (mm)	0.300	4.789
Standard deviation (mm)	0.027	0.081
CV of the ply mean thickness (%)	8.9	1.7

Since the measurements were taken at irregular intervals, the variability of the thicknesses is only expressed by the mean values and standard deviations of the ply thicknesses. However, by observing the cross section of the composite, it is evident that there is a continuity in the variation of the ply thicknesses in the form of waviness spread over the plate. It is also clear that a statistical description of the ply thickness is not enough to describe entirely its behaviour, hence the necessity to consider the spatial evolution of the thickness profiles through the length of the specimen.

5.3.2 *Evolution of the ply thickness profile*

To study the spatial evolution of the thickness variation, a single specimen of 45 x 45 mm was obtained from one of the manufactured plates. The dimensions of the specimen permit a better handling during the preparation of the cross-section of the composite plate by placing the specimen on the mounting resin. A set of micrographs of the cross-section was taken with a Dino-Lite® optical microscope. The micrographs are 1600 x 1200 pixels and have a resolution of 161 pixels/mm. Even though the image resolution is similar to that obtained with the DSLR camera, this method is preferred since images taken with the microscope exhibit a lower distortion than the images captured with the DSLR camera. In addition, the images have lower noise and lower compression improving the quality of the visible ply interfaces.

Each micrograph covers approximately only 7 mm of the length of the specimen. To determine the spatial evolution of the ply thicknesses in a long continuous section avoiding duplicated points on the interface of the plies, the micrographs were assembled into a single image containing the full length of the specimen. In the assembled image, the plies were delimited by a manual selection of the points along the ply interface. A grid on top of the image was used as reference to roughly control the number of points and their spacing. Approximately 220 points were selected for each interface. Nevertheless, these

points were still placed at irregular intervals along the *x*-axis. To obtain the ply thickness profile, it is necessary to subtract the *z*-coordinates of the lower and upper interfaces of said ply at the same *x*-coordinate. To achieve this, the coordinates of the selected points were interpolated into a regular mesh consisting of 1024 points along the *x*-axis. Figure 5-3 shows the ply boundaries delimited by the upper and lower interfaces, while Figure 5-4 shows the resulting thickness profile. The uncertainty of the ply thickness measurement technique is determined to be ± 0.013 mm.
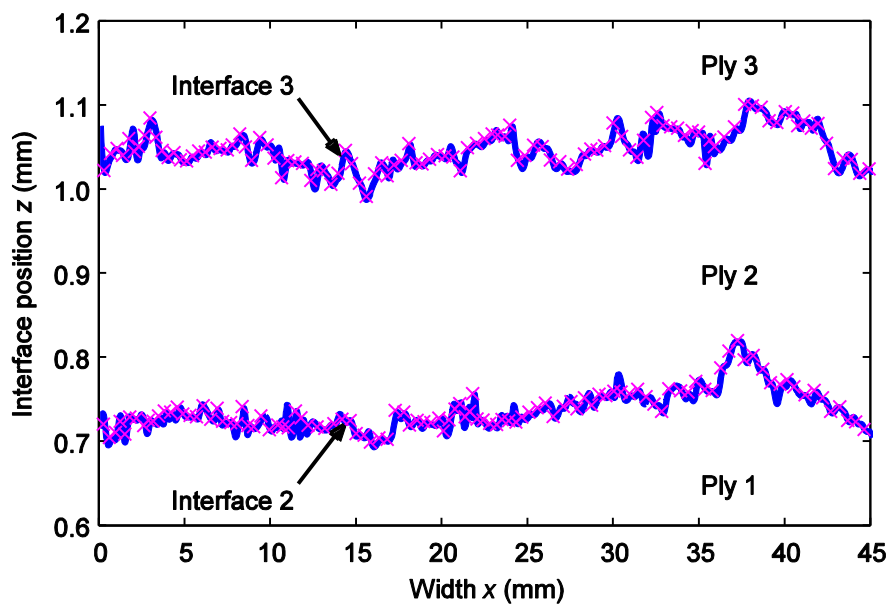
Figure 5-3. Profiles for the #2 and #3 interfaces delimiting the #2 ply, the crosses showing the selection points along the ply interface, while the continuous lines showing the interpolated interfaces.

Using the 45 x 45 mm specimen, the profile of the ply #2 was determined. This ply exhibits a mean thickness of 0.309 mm with a CV of 5.31 %. In this case, both the mean and the CV are calculated by using a sample of 1024 measurement points. It is important to mention that the difference between the maximum and minimum values is 0.097 mm. This difference is approximately 1/3rd of the mean ply thickness.

As mentioned in section 5.3, it is apparent that the variation of the plate and variation of the ply thicknesses have no correlation between each other. However, by tracing a least squares linear fit of the thickness profile of a single ply it t is shown that the slope is not aligned with the mean thickness (cf. Figure 5-4).

By comparing the slopes of the linear fits of the ply profiles to the one of the plate, the slopes of the linear fits follow the same direction (cf. Figure 5-5). As expected the sum of the least squares slopes of the plies is equal to the slope of the plate profile. Indeed, the variation of the overall plate thickness contributes with a certain variation for each ply thickness profiles. This contribution can be expressed in the form of a function $\delta t_{plate}(x)$.
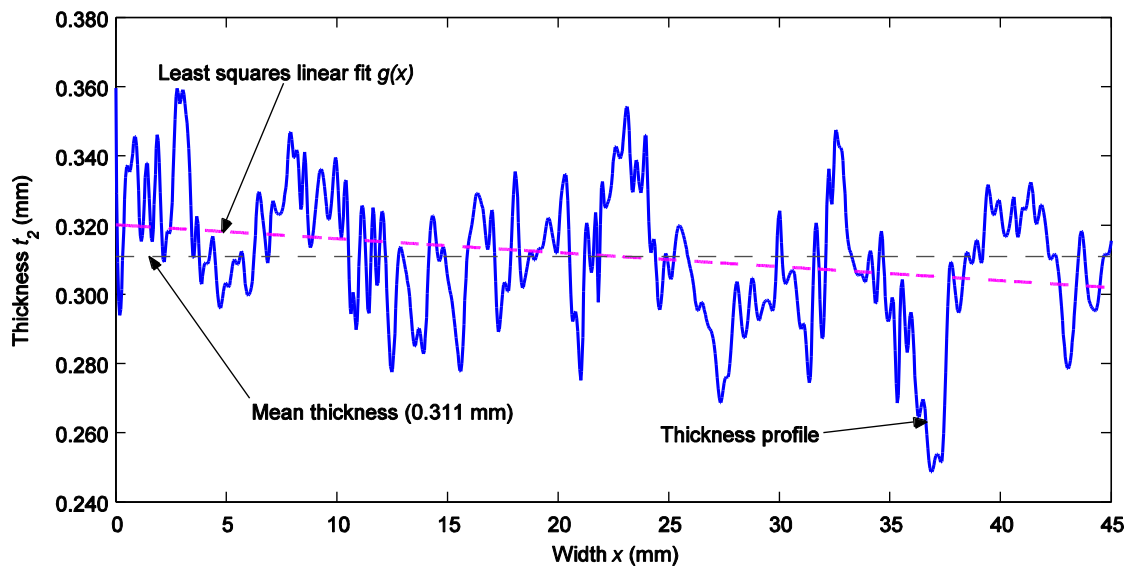
Figure 5-4. Thickness profile for the #2 ply and the least squares linear fit (dashed line) and the mean thickness fit (dashed horizontal line).
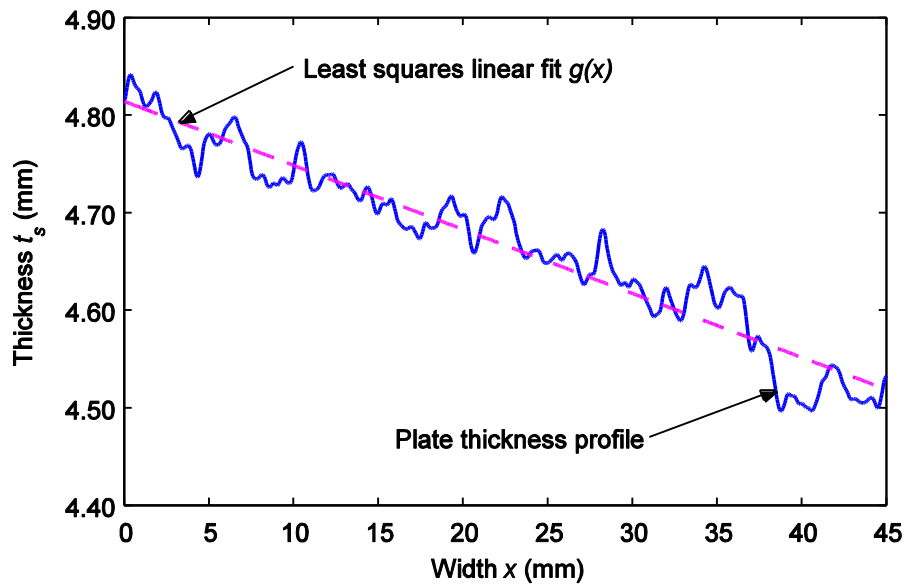
Figure 5-5. Profile of the plate thickness.

5.4 Modelling the ply thicknesses profile for use in a FE model

5.4.1 *Formulation of the mathematical law of the thickness profile*

We have to keep in mind that the measured ply variability is used to feed a finite element (FE) model to test different material configurations and loading scenarios by means of a Multi-Instrumented Technological Evaluator [12]. The FE model is required to be robust and light-weight, since the principle of modelling is based on Monte Carlo simulations (MCS). The intended FE program is SAMCEF® using two-dimensional Mindlin shell elements. This type of element is chosen since the ply thickness can be controlled locally for each element.

As explained, the ply thicknesses exhibit variability in the order of 5 to 15 % of their mean thicknesses. Likewise, the overall plate thickness has variations which are up to 2 % of the mean plate thickness. Therefore a special control of the coupling of the thicknesses at any given point in the plate must be followed in order to keep within this restriction. One solution to model the composite is to assign a random thickness to each element of the plate for each ply. However, to comply with the imposed restrictions it should be verified that the adjacent

elements thicknesses are maintained within certain limits. By randomly assigning the thickness to each element, the continuity of the ply is not completely assured. Also, to comply with these restrictions, computationally intensive algorithms are necessary.

To overcome this limitation, from Figure 1 and Figure 5-4, it is seen that the ply thickness profiles exhibit a wave shape with different frequencies. This signal can be decomposed into its basic frequencies and then reconstructed by the summation of sinusoids of different frequencies and amplitudes. Thus, a digital stratification can be generated by the use of a representative set of frequencies based on the measurements performed on the composite cross-section. The parameters of the digital lay-up can be adapted to reach values of ply variability similar to the real plies, while having a precise control on the shape of plate thickness. The proposed model is as follows:

$$t_k(x) = \bar{t}_k + \sum_{i=1}^{n} A_i \sin\left(2\pi \frac{x}{\lambda_i} + \phi_{k,i}\right) + \delta t_{plate}(x) \tag{5-1}$$

where $t_k(x)$ is the evolution of the thickness of the kth ply through x, $\bar{t}_k$ is the mean thickness of the kth ply, A_i is the amplitude of the corresponding wavelength λ_i (or the inverse of the frequency f_i^{-1}) of the ith peak, $\delta t_{plate}(x)$ is the contribution of the thickness variation of the plate on the ply mean thicknesses. In other words, $\delta t_{plate}(x)$ is the desired plate profile divided by the number of N plies (cf. Chapter 3, eq. 3-7 for a bidirectional representation).

To plate thickness profile is effectively controlled by the expression $\delta t_{plate}(x)$, it is necessary to assure the coupling of the variability of the different plies using a pseudo random phase shift $\phi_{k,i}$. The phase shift ranges from $-\pi$ to π for each ith sinusoid. To maintain a constant plate thickness profile, the sum of the kth ply phases must be equal for all the ith sinusoids:

$$\sum_{j=1}^{k} \phi_{j,1} = \sum_{j=1}^{k} \phi_{j,2} = \ldots = \sum_{j=1}^{k} \phi_{j,i} \tag{5-2}$$

To achieve this condition, the phase shift is obtained with:

$$\phi_{k,i} = \frac{2\pi}{k} \xi_{k,i} - \pi \tag{5-3}$$

where $\xi_{k,i}$ is a vector containing the kth ply numbers randomly shifted for each ith frequency peaks.

Indeed, the use of different phase shifts for each frequency peak assigned by equation 5-3 permits the generation of a broad number of stratifications maintaining the plate shape and, at the same time, the ply profiles will be different while maintaining similar levels of variability.

5.4.2 *Determination of the representative frequency peaks*

The inputs of the proposed model in equation 5-1 are the representative frequencies of the composite ply thickness profiles. To determine the ith frequency peaks representative of the measured composite plate, a discrete Fourier transform (DFT) is performed on the thickness profiles. In order to apply the DFT, it is necessary to keep the mean value of the thickness profile at 0 mm. In this step, the plate thickness contribution to the ply profile (cf. Figure 5-4) is taken into account to avoid spurious frequency peaks at the low frequencies of the spectrum. These values, represented by the function $\delta t_{plate}(x)$ will be restored when generating the digital stratification. The high frequencies in the spectrum are attributed mostly to the selection of points at the ply interfaces, indicated by the serrated shape of the thickness profile.
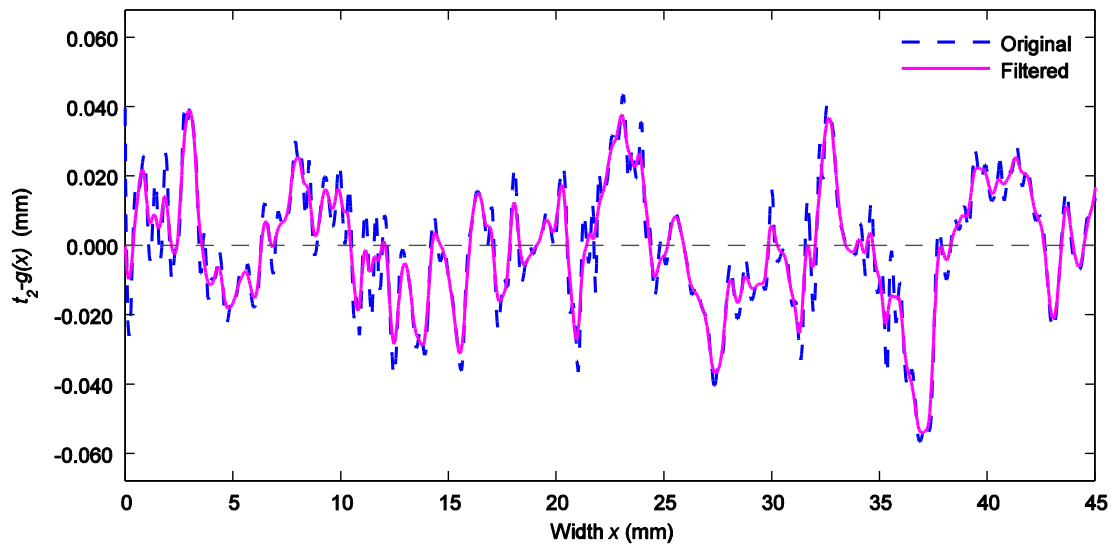
Figure 5-6. Zero mean thickness profile of the #2 ply before and after the application of a low pass filter with a cut-off frequency of 1 Hz.

A low pass Butterworth filter is used to remove the frequencies higher than 1 mm^{-1} present in the thickness profile (cf. Figure 5-6) since these frequencies are in the range of uncertainty of the point selection at the ply interface. The mean thickness values do not show any difference between the filtered and unfiltered data after the application of the low pass filter. However, the standard deviation of the thickness is reduced from 0.0191 mm to 0.0169 mm. This means that the CV of the filtered thickness shows an average reduction of 0.8 % compared to the original CV of 6.6 %. The same procedure is applied to the plate profile with no change of the mean and standard deviation of the plate thickness. The reduction of variability of the plies has little impact on the main properties since this value is still 2.5 to 4 times greater than the variability of the plate thickness.

Using the DFT spectrum of the ply thickness profile (cf. Figure 5-7), the representative frequency peaks for each ply are manually selected. The proposed element size of the FEA model is 1 mm. The element size is chosen as a compromise between the fineness of the mesh and the number of the elements in the model. Hence, the effect of the thickness variations of peaks having a wavelength lower than 2 mm, corresponding to frequencies higher than 0.5 mm^{-1}, are not considered. Likewise, the peaks that show amplitudes lower than

0.0035 mm are not taken into account in order to keep a consistent number of peaks through all the plies. This is also done to neglect the impact of the resolution of the image in the selection of the points and to distinguish between the main lobes and the side lobes in the DFT spectra.
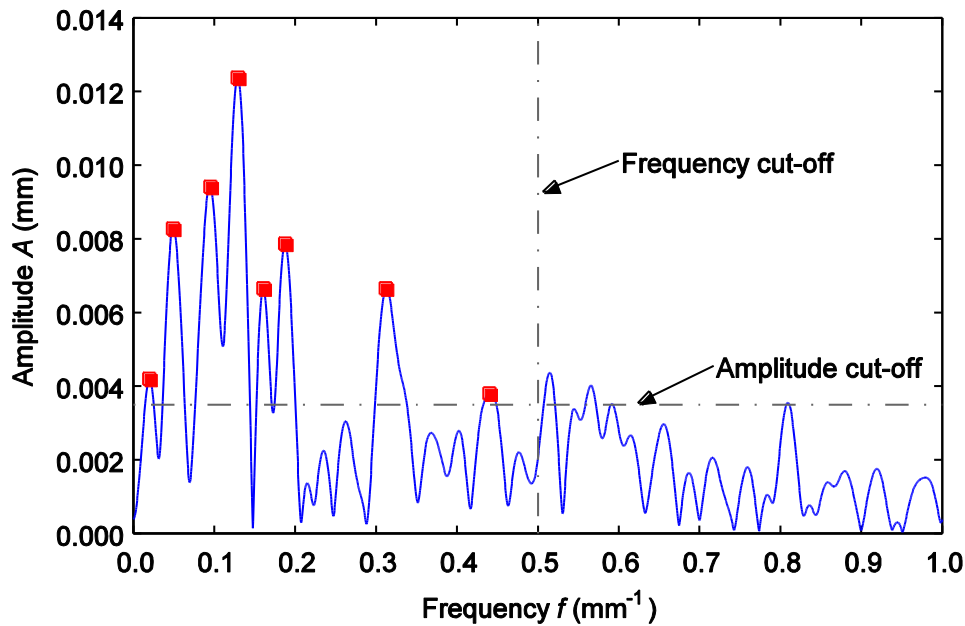
Figure 5-7. Amplitude spectrum of the thickness profile of #2 ply with selected frequency peaks.

The number of peak frequencies selected from the DFT spectra is different for each ply (cf. Figure 5-8) along with their pairing of frequencies and amplitudes. The relationship between the number of peaks, frequencies and amplitudes for each ply, as well as their position on the composite plate is not yet understood. The necessity to propose a solution that takes into consideration the number of variables involved is difficult as the relationship between the frequency and its associated amplitude does not generate any clear trend (cf. Figure 5-8).
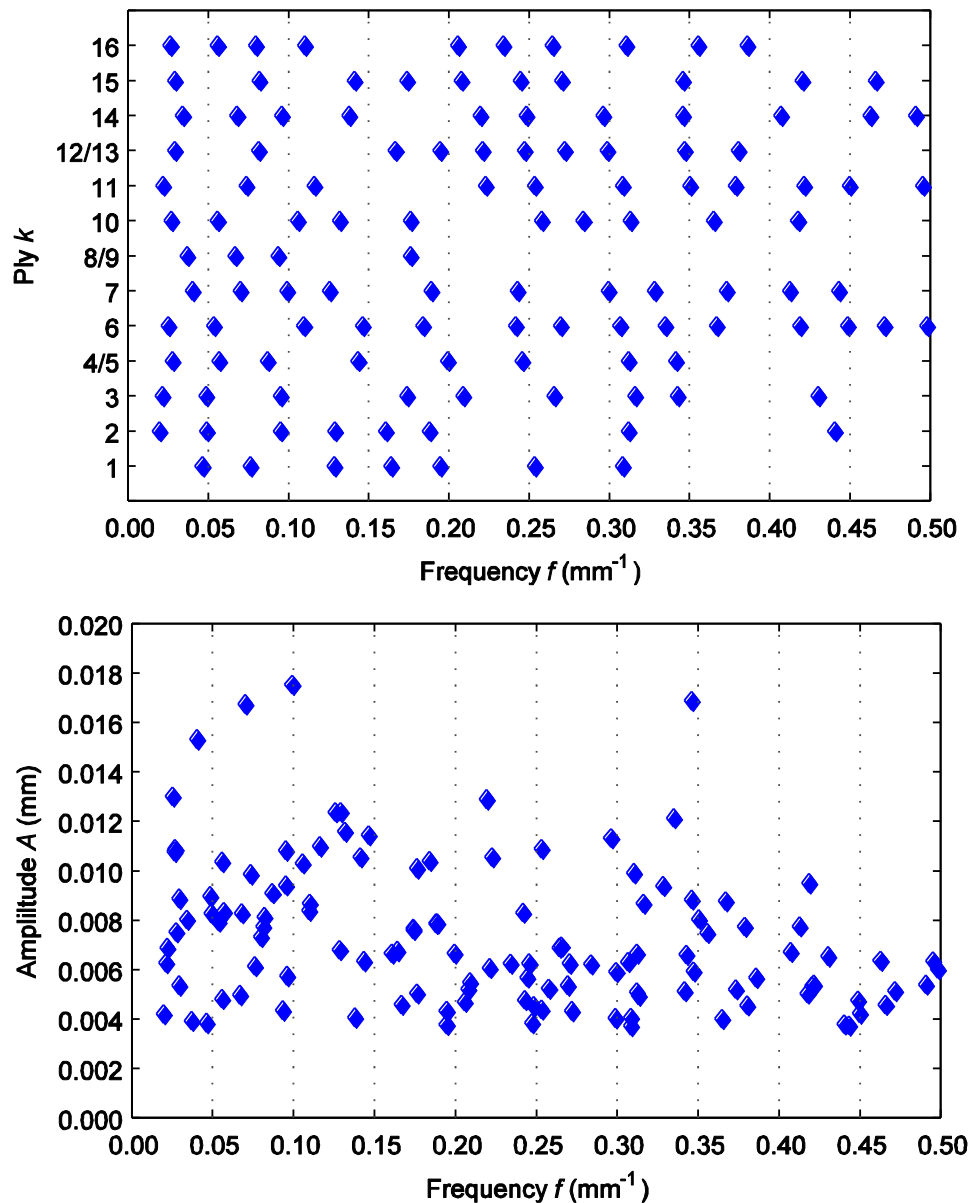
Figure 5-8. Distribution of the number of peaks per ply (top) and amplitude distribution in function of the frequency peaks (bottom) with the double plies 4/5, 8/9 and 12/13 considered as single plies.

To overcome this problem, a new set of frequency peaks can be generated using the acquired data as an input base for a pseudo random amplitude spectrum generator. The complete spectra are divided into ten frequency bands of 0.05 mm^{-1} each from 0 to 0.50 mm^{-1} (cf. Figure 5-8). A pair of values (frequency and amplitude) is selected within each frequency band. Table 5-2 shows the range of values of frequency and amplitude that are used to generate the digital stratification. Double plies 4/5, 8/9 and 12/13 are listed once since there is only

one profile for each pair of plies. To form the peaks that constitute the digital lay-up, the spectrum generator operates as follows:

1. a single peak is generated from each of the 10 frequency bands;

2. not all the plies have peaks contained within certain frequency bands. Only the first two frequency bands contain the spectral peaks for all the plies. The peaks in each band of frequency are generated according to their probability of appearance. The probability of appearance for the rest of the peaks goes from 30 to 90 %. More than one peak can appear within a frequency band, but at this time this effect is not considered in order to maintain a consistent number of peaks;

3. the correlation between the frequency and amplitude was not found, both magnitudes are generated independently;

4. to select the probability distribution to draw the frequency peaks, a goodness-of-fit test was applied to the set of points contained in each band. The tested distributions are the normal distribution and the uniform distribution. The Kolmogorov-Smirnov (KS) test confirms the null hypothesis that the values, from each frequency band, come from an either uniform or normal distributions (p-values>0.05). A uniform distribution is preferred for the frequency since the points seem to be continuously distributed without any noticeable agglomeration. For each frequency band, Table 5-2 shows the values of the lower bound a and upper bound b;

5. to ensure that the frequencies from adjacent bands are not superposed, a minimum distance between the peaks D= 0.023 mm^{-1} is introduced. This value represents the absolute minimum distance measured between the identified frequencies per ply;

6. The KS test is also applied to the amplitude values contained within each band for normal and uniform distributions. In this case, the null hypothesis that these values come from a uniform distribution is rejected (p-values<0.05). On the contrary, the null hypothesis for a normal

distribution is maintained. Table 5-2 shows the amplitude mean x^- and standard deviation s for each ith peak.

5.5 Generation of a digital stratification

5.5.1 Digital profile

The values expressed in Table 5-2 are used to generate a digital set of variables which will be used to reconstruct a lay-up with variable ply thicknesses using equation 1. Table 5-3 shows an example of the set of variables that can be generated. Note that according to their probability of appearance, there are no parameters contained within the 0.25-0.30 mm^{-1} and 0.40-0.45 mm^{-1} frequency bands. The generated thickness profile of the ply #2 is presented in Figure 5-9 together with the real ply profile.

Table 5-2. Parameters of the distribution for the Frequency (uniform) and Amplitude (normal) associated with the probability of appearance of the ith peak within a frequency band.

i^{th} peak No.	Frequency band limits (mm^{-1})	Probability of appearance (%)	Frequency (mm^{-1})		Amplitude (mm)	
			a	b	x^-	s
1	0.00 to 0.05	100	0.020	0.049	0.0081	0.0033
2	0.05 to 0.10	100	0.054	0.099	0.0088	0.0036
3	0.10 to 0.15	80	0.106	0.146	0.0095	0.0026
4	0.15 to 0.20	70	0.161	0.200	0.0069	0.0021
5	0.20 to 0.25	70	0.206	0.248	0.0065	0.0026
6	0.25 to 0.30	70	0.253	0.299	0.0065	0.0024
7	0.30 to 0.35	90	0.307	0.347	0.0076	0.0035
8	0.35 to 0.40	50	0.350	0.386	0.0064	0.0018
9	0.40 to 0.45	60	0.407	0.450	0.0057	0.0018
10	0.45 to 0.50	30	0.463	0.498	0.0056	0.0007
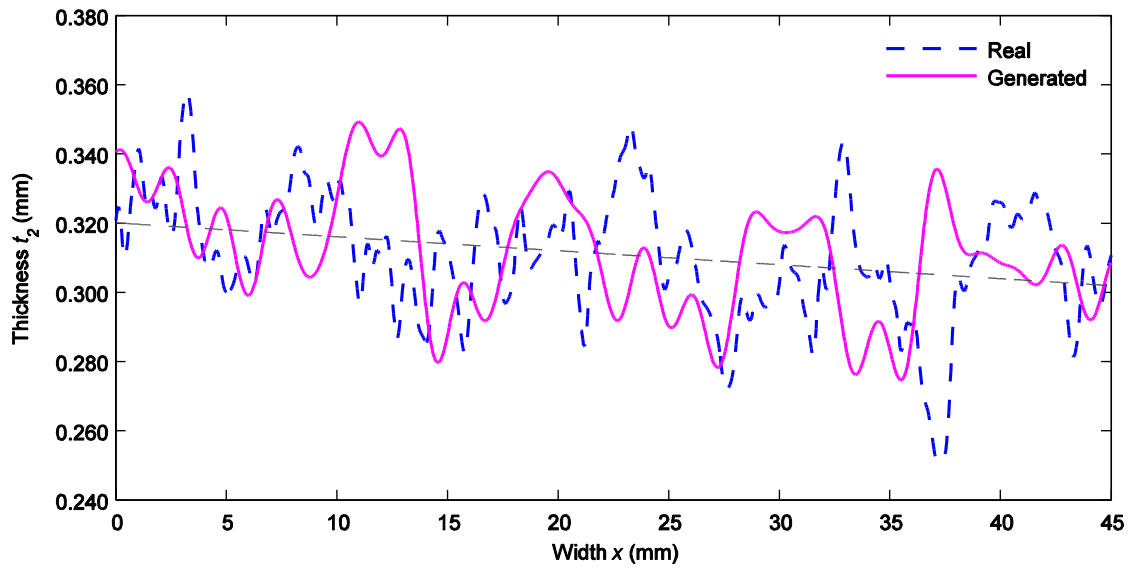
Figure 5-9. Digital profile generated by the model with equation 1 compared to the real profile of #2 ply.

Table 5-3. Frequencies and amplitudes of the thickness evolution for the digital stratification.

i^{th} peak (N°)	Frequency (mm^{-1})	Amplitude (mm)
1	0.027	0.0049
2	0.097	0.0065
3	0.110	0.0132
4	0.162	0.0110
5	0.235	0.0052
6	0.330	0.0035
7	0.374	0.0081
8	0.470	0.0047

As explained, the main goal is not to reproduce the exact form of the composite ply spread over the plate, but to generate a geometry having the same characteristics in terms of variability of the ply thickness profile. Consequently, the real and the generated profiles do not completely match since the form of the real profile is the product of a unique combination of number of frequencies, amplitudes, and phase shifts. However in terms of the statistical values, the mean and standard deviations of both profiles are very similar. The mean ply thickness

for both profiles is 0.291 mm, while the standard deviation is 0.018 mm for the original ply and 0.016 mm for the digital one. This comparison is valid for all the ply thicknesses, showing negligible differences in their mean values. The CV for the rest of the generated plies is within the values of the original measurements as illustrated in Figure 5-10.
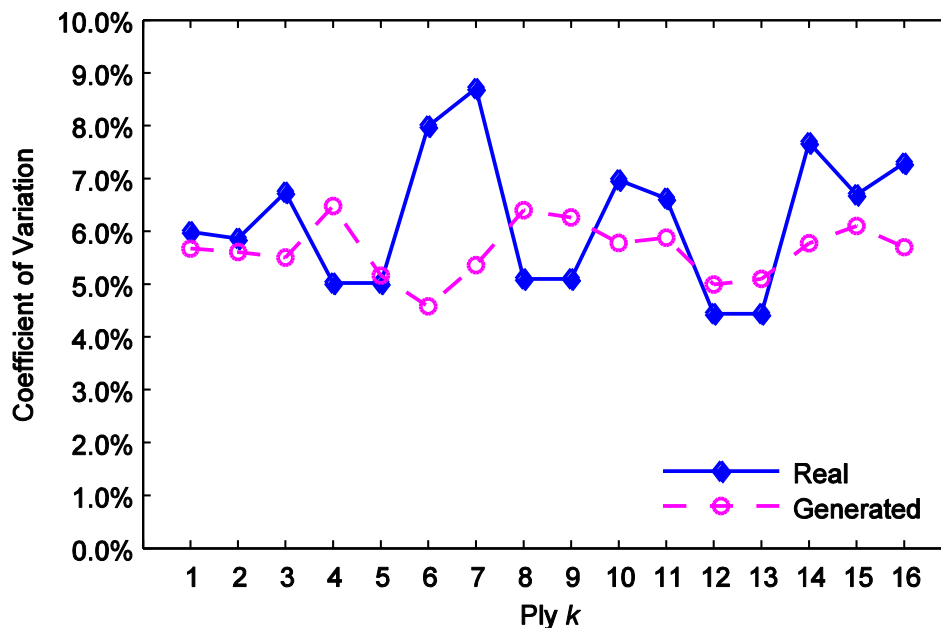
Figure 5-10. Comparison of the CV between the real plies (diamond markings) and the generated profiles (circle markings).

In comparison with the normal modelling of a composite stratification, where the thickness of the different lamina takes into account major changes in the plate thickness (cf. Figure 5-11a), a real stratification exhibits variations in the ply thickness which differs from half to one magnitude order of the variations in the thickness of the overall stratification (cf. Figure 5-11b). Any effort made in order to completely model the behaviour of the thickness variation will take considerable computing and analytical resources since there are four highly interdependent variables that give shape to the thickness profile. The model must account for the number of the different frequencies and the distance between each major peak, the associated amplitude for each frequency and the phase shifts. All these variables also depend on the ply position in the stratification. Different solutions to the

problem, such as using the frequency values "as is" from one single ply, or randomly selecting the frequencies and their associated amplitudes from all the identified peaks were discarded, since the selected points come from a very specific zone in the plate that may or may not describe completely the behaviour of the thickness variation along the full composite plate.

Indeed, the data collection cannot be performed in all types of composite structures and various composite plates due to its destructive nature, as well as the time and resources that this task demands. Therefore, simplifications must be made in order to obtain accurate data to be introduced into the model. The variability of the ply thickness, as well as the coupling between the different plies to obtain a constant plate thickness, can be controlled by using pseudo-random algorithms to vary the parameters involved in the thickness profile generation (cf. Figure 5-11c).

The proposed method, although it does not contain any of the actual peaks retrieved from the DFT spectra, generates a set of values that encompasses all the different frequencies and amplitudes found in these DFT spectra. This generator can then be used to produce a family of different laminates that observe similar levels of ply variability and it can be easily adapted into a finite element analysis model.
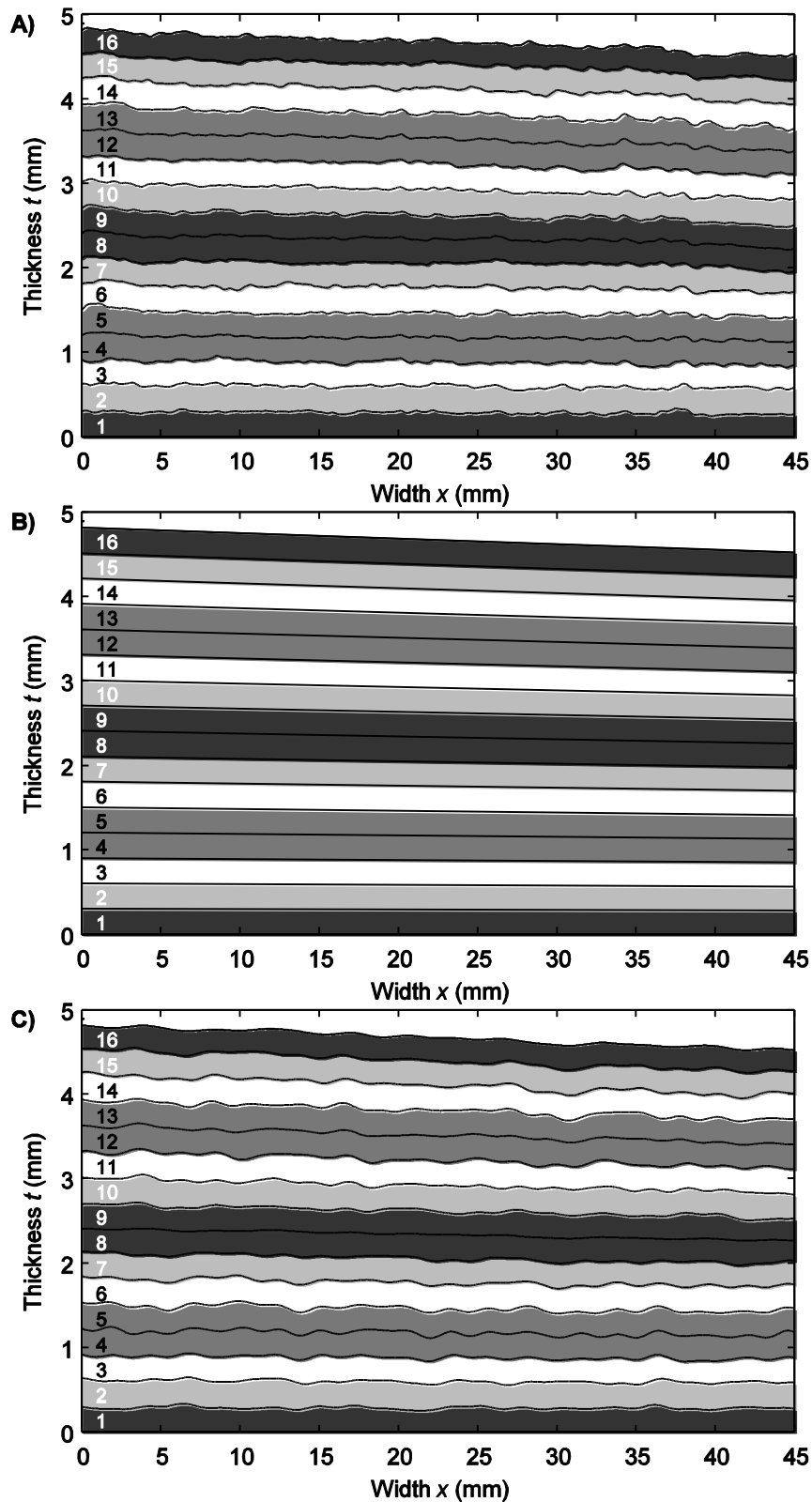
Figure 5-11. Representation of the cross section of the 16 ply stratification (plies 4/5, 8/9 and 12/13 shown as independent plies) with, a) reconstruction from the actual ply thickness profiles (after filtering), b) constant ply thickness accounting the contribution of the plate thickness variation in each ply and c) digital stratification generated by the proposed model.

5.5.2 FE model of the residual strains of a composite plate with variable thicknesses

To demonstrate that the variation of the ply thicknesses affects the mechanical properties of the composite part, a finite element model of a plate is subjected to a temperature change of $\Delta T = -120$ °C. This temperature change is applied in order to calculate the residual strains at the end of the cooling phase. The analysis is based on the assumption that the composite at cure temperature is stress free, and by inducing a temperature variation, due to the mismatch of the thermal properties of the constituent materials, residual strains and stresses are generated [13].

To illustrate the procedure, a section of the plate, having dimensions of 100×50 mm is analysed in SAMCEF® using a 2D Mindlin composite shell (element type T028/T029). The element size is set to be 1 mm per side in order to model the lower and upper peaks corresponding to a minimum wavelength of 2 mm of the amplitude spectra of the thickness.

Two cases are analysed, the first one considering constant plate and ply thicknesses, and the second one considering random laminate profiles generated by the algorithm explained in section 5.4. For the latter case, the mean of the plate and ply thicknesses are also considered as constant. The algorithm is performed three times to obtain different configurations. It is noteworthy that in this analysis the material properties are not dependent on the ply thickness. The homogenised coefficients of linear expansion of the principal axes of the lamina are $\alpha_1 = 0.54 \cdot 10^{-6}$ °C^{-1} and $\alpha_2 = 14.85 \cdot 10^{-6}$ °C^{-1}. The mean ply thickness for each plate is 0.302 mm, thus the plate thickness is 4.838 mm.

Figure 5-12 shows the strain field of the upper layer for both cases, constant and variable thickness. As expected, the plate with a constant thickness has a constant strain field equal to $-91 \cdot 10^{-6}$. Conversely, the plates with variable thicknesses exhibit strain fields with values ranging from -85 to $-95 \cdot 10^{-6}$ implying a variation up to 11 % of the residual strain spread over the composite plate. As shown in Figure 5-12, the three cases show different patterns.
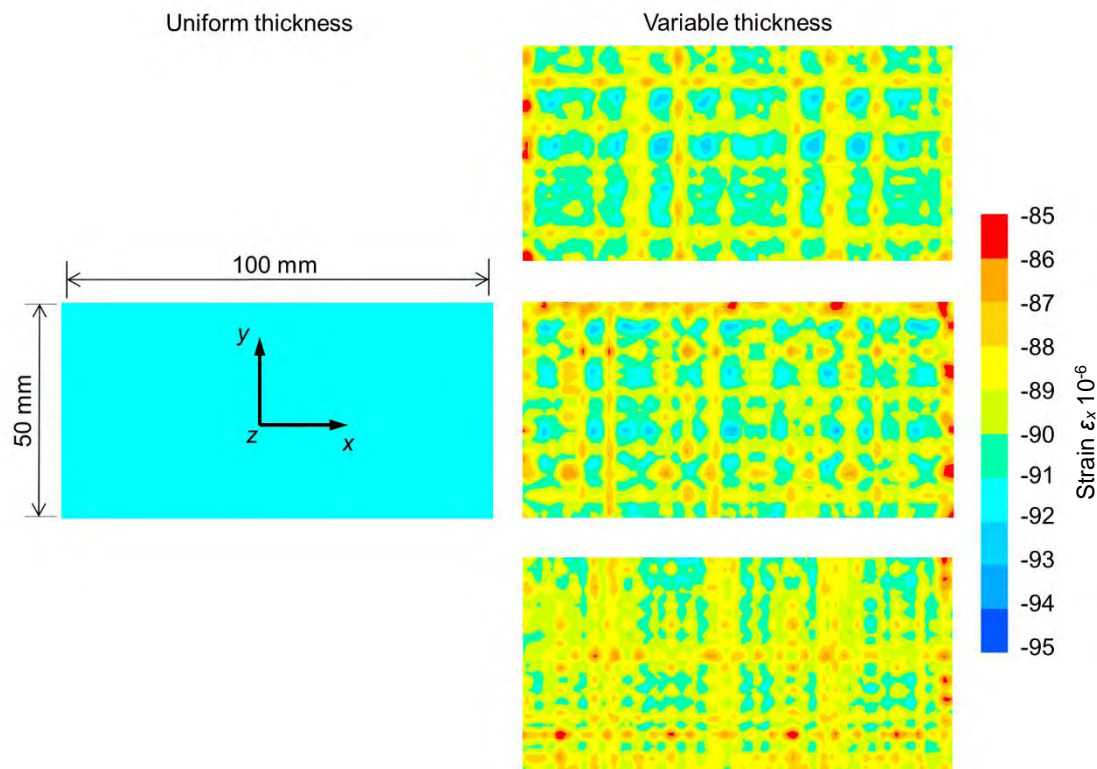
Figure 5-12. Strain field of the upper skin of a 16-ply composite plate subject to a thermal of -120 °C simulating the cooling process of a composite (on the left hand side) with constant thickness and (on the right hand side) with variable ply thickness.

5.6 Conclusions

The first input parameter towards the creation of a finite element model, affected by material variability, is the geometry variation of the ply thickness over the plate. Indeed, the geometry characteristics such as the ply thickness impact on the material properties such as the volume fractions of the elementary materials. An identification and correlation between the ply thickness and the material properties through the variation of the fibre volume fractions require a deeper study that is costly in both time and resources, since a simple correlation between the volume fractions and the thickness must be made by respecting the spatial continuity as defined in the proposed methodology. However, the variation of the thickness and, thus, its position in the stratification, impact also the structural

properties for bending and torsional loading cases, as well as the residual stresses/strains.

Variations up to 15 % of the mean ply thicknesses have been observed. The cross-section reveals a continuous variation in the ply thickness, and a non-linear coupling between the variations of the plate thickness and the variations of the ply thicknesses, that reflects the low variability of the plate thickness with a CV less than 2 %.

A mathematical model of the ply variability was proposed in order to generate a digital laminate that contains the same dispersion as the ply thickness under the condition of a controlled plate thickness. The values of frequency and amplitude used to generate the digital ply are the identified by a DFT of the real ply and plate thickness profiles. The thickness of the digital stratification that was generated by the proposed method shows coefficients of variation between 4.5 % and 6.5 %. These values are comparable to the real ply CV ranging from 4.5% to 9 %, while maintaining an overall plate variability of 2 %. This method produces relevant ply thickness variability through valuable frequencies and amplitudes in terms of number and magnitude. Thus, a different set of relevant parameters can be generated at each simulation. Although at this moment the set of parameters has been obtained from a single specimen (45 x 45 mm) studied in only one direction, the current data allows the generation of a complete dataset since the influence of the ply orientation, a priori, does not affect the behaviour of the thickness undulations since the stratification of the plates is both balanced and symmetrical.

5.7 References

[1] E. Barkanov, S. Gluhih, O. Ozolins, E. Eglitis, F. Almeida, M. C. Bowering, and G. Watson, "Optimal weight design of laminated composite panels with different stiffeners under buckling loads," in *27ᵗʰ International Congress of the Aeronautical Sciences*, 2010, pp. 1–9.

[2] Y. Li, M. Li, Y. Gu, and Z. Zhang, "Numerical and Experimental Study on the Effect of Lay-Up Type and Structural Elements on Thickness Uniformity of L-Shaped Laminates," *Appl. Compos. Mater.*, vol. 16, no. 2, pp. 101–115, Feb. 2009.

[3] J. Sun, Y. Gu, Y. Li, M. Li, and Z. Zhang, "Role of Tool-Part Interaction in Consolidation of L-Shaped Laminates during Autoclave Process," *Appl. Compos. Mater.*, vol. 19, no. 3–4, pp. 583–597, Oct. 2011.

[4] J. S. Lightfoot, M. R. Wisnom, and K. Potter, "A new mechanism for the formation of ply wrinkles due to shear between plies," *Compos. Part A Appl. Sci. Manuf.*, vol. 49, pp. 139–147, Jun. 2013.

[5] F. Collombet, M. Mulle, Y.-H. Grunevald, and R. Zitoune, "Contribution of Embedded Optical Fiber with Bragg Grating in Composite Structures for Tests-Simulations Dialogue," *Mech. Adv. Mater. Struct.*, vol. 13, no. 5, pp. 429–439, Aug. 2006.

[6] P. Olivier and M. Cavarero, "Comparison between longitudinal tensile characteristics of thin and thick thermoset composite laminates : influence of curing conditions," *Comput. Struct.*, vol. 76, pp. 125–137, 2000.

[7] Y. Li, M. Li, Y. Gu, and Z. Zhang, "Numerical and Experimental Study of the Bleeder Flow in Autoclave Process," *Appl. Compos. Mater.*, vol. 18, no. 4, pp. 327–336, Sep. 2010.

[8] H. M. Hsiao and I. M. Daniel, "Effect of fiber waviness on stiffness and strength reduction of unidirectional composites under compressive loading," *Compos. Sci. Technol.*, vol. 56, no. 5, pp. 581–593, Jan. 1996.

[9] H. Chun, J. Shin, and I. M. Daniel, "Effects of material and geometric nonlinearities on the tensile and compressive behavior of composite materials with fiber waviness," *Compos. Sci. Technol.*, vol. 61, pp. 125–134, 2001.

[10] M. C. W. Lee, R. M. Payne, D. W. Kelly, and R. S. Thomson, "Determination of robustness for a stiffened composite structure using stochastic analysis," *Compos. Struct.*, vol. 86, no. 1–3, pp. 78–84, Nov. 2008.

[11] M. C. W. Lee, Z. Mikulik, D. W. Kelly, R. S. Thomson, and R. Degenhardt, "Robust design – A concept for imperfection insensitive composite structures," *Compos. Struct.*, vol. 92, no. 6, pp. 1469–1477, May 2010.

[12]   F. Collombet, L. Crouzeix, Y. Davila, A. Cerisier, B. Douchin, and Y.-H. Grunevald, "Added value of technological evaluators for structural repair characterization: MITE Toolbox," in *Sampe Europe 34th International Conference & Forum*, 2013, pp. 179–186.

[13]   M. Mulle, F. Collombet, P. Olivier, R. Zitoune, C. Huchette, F. Laurin, and Y. Grunevald, "Assessment of cure-residual strains through the thickness of carbon–epoxy laminates using FBGs Part II: Technological specimen," *Compos. Part A Appl. Sci. Manuf.*, vol. 40, no. 10, pp. 1534–1544, Oct. 2009.

- 140 -

Chapter 6: Proposition of a finite element model for the introduction of local variabilities with controlled gradient

6.1 Introduction

This chapter deals with the convergence of the measured quantities and the proposed method to generate a finite element model taking into account the variabilities of composite material.

As explained in Chapter 1, the majority of studies that deal with stochastic analysis of composite materials, vary the material properties in all the structure at each simulation performed. Crouzeix [1] noted that a composite structure has local variations in the local elastic moduli that can be identified through an inverse method. Feraboli [2] introduced into a FE model elements with different elastic moduli identified from the strain field of a discontinuous composite material during a traction test. For continuous materials, Karami [3] presented a model that measures the impact on the elastic moduli of the fibre waviness out-of plane along a unitary cell. For direct formulations using true parameters, Spanos [4] proposed the calculation of the elastic modulus in different parts of a discontinuous nanocomposite using the local mass fractions of its elementary constituents.

In the present chapter, a direct formulation of the variability of the composite properties is proposed by means of the introduction of a variable morphology that includes the ply thicknesses, the plate thickness and the in-plate fibre misalignments, as well as a variable material parameter such as the porosity

volume fraction, in order to determine the elastic inputs in the FE model. Three different examples are proposed: the first is the calculation of the flexural modulus of a composite beam in a 4 points bending test, the second is a study on the residual thermal strains of a composite plate during the cooling phase after polymerisation, and the third example presented is the analysis of a technological evaluator in a flexion-compression test.

In these models, the input values are based on the gradients observed in a real composite plate in order to maintain a spatial continuity of the material property variation. However, the scope of this work is not to restore exactly the properties as they are obtained during the measurement of variability.

6.2 Description of the characteristics of the finite element model

The commercial software SAMCEF® is used to perform the different FE analyses, using a 2D Mindlin composite shell (T028/T029 element type). This type of element allows the modelling of the transverse displacement of the plate (see SAMCEF® library). With this type of element, the individual input material properties, thickness and orientation for each ply and each element can be considered. Thus, it is possible to introduce individual properties that change from one point to another in the analysed composite plate. The elastic quantities required for this element are shown in Table 6-1 for the fibre direction *1* and the transversal directions *2* and *3*. These quantities are derived from the volume fractions of constituent materials, such as the fibre, matrix and porosity (cf. Chapter 3), the material morphology, such as the orientation of the reinforcements (cf. Chapter 4) and the ply and the plate thicknesses (cf. Chapter 5). The calculations of these properties are done by means of the law of mixtures in taking into account the anisotropic nature of the carbon fibre. The constituent material properties are assumed as being deterministic (cf. Table 6-2). The elements used in the following analysis are linear elastic.

Table 6-1. Homogenized elastic constants necessary for the composite shell element according to the SAMCEF® software syntax.

"material_number"				Material number
YT	E_1	E_2	E_3	Young's moduli (MPa)
G	G_{12}	G_{23}	G_{13}	Shear moduli (MPa)
NT	ν_{12}	ν_{23}	ν_{13}	Poisson's ratios
A	a_{12}	a_{23}	a_{13}	Coefficients of linear thermal expansion (°C⁻¹)

The creation of the input file, including the geometry, the elastic properties calculation and their assignation to the elements for each FE model is written in MATLAB® software. This allows the capacity of generation multiple sets of input files with variable properties.

Table 6-2. Mechanical properties of the CHS reinforcement and M10.1 resin.

Property	Manufacturer Value
Young's modulus of the carbon fibre in the longitudinal direction E_{1f} (GPa)	230
Young's modulus of the carbon fibre in the transverse direction E_{2f} (GPa)	15
Shear modulus of the carbon fibre G_{12f} (GPa)	50
Poisson's ratio of the carbon fibre ν_{12f}	0.4
Density of the carbon fibre ρ_f (kg·m⁻³)	1800
Mass per unit area of the carbon fibre ρ_{Af} (kg·m⁻²)	0.305
Coefficient of linear thermal expansion of the carbon fibre a_{1f} (°C⁻¹)	$-1 \cdot 10^{-6}$
Young's modulus of the epoxy resin E_m (GPa)	3.6
Poisson's ratio of the epoxy resin ν_m	0.3
Density of the epoxy resin ρ_m (kg·m⁻³)	1200
Coefficient of linear thermal expansion of the epoxy resin a_m (°C⁻¹)	$25 \cdot 10^{-6}$

The elastic quantities E_1, E_2, E_3, G_{12}, G_{13}, G_{23}, ν_{12}, ν_{13} and ν_{23} must guarantee the following standard inequalities in order to correctly setting the Hooke matrix:

$$E_1, E_2, E_3, G_{12}, G_{13}, G_{23} > 0$$
$$(1 - v_{23}v_{32}), (1 - v_{13}v_{31}), (1 - v_{12}v_{21}) > 0 \tag{6-1}$$
$$1 - v_{12}v_{21} - v_{23}v_{32} - v_{13}v_{31} - 2v_{21}v_{32}v_{13} > 0$$

The basis of the modelling is the distribution of thicknesses of the ply t_k, which varies as a function of a mean thickness per ply $\bar{t}_k$. The change of the ply thickness, described in Chapter 5, is:

$$t_k(x, y) = \bar{t}_k + \xi t_k(x, y) + \delta t_{plate}(x, y) \tag{6-2}$$

where the periodic variation of the ply ξ_{tk} can be rewritten in 2-dimensions in assuming the same undulation repartition along the x and y axes because the composite stratification is quasi-isotropic, and therefore, the variation is of the same order of magnitude for both principal directions of the laminate:

$$\xi t_k(x, y) = \sum_{i=1}^{10} \frac{A_i}{4} \left[\sin\left(2\pi \frac{x}{\lambda_i} + \phi_{k,i} \right) + \sin\left(2\pi \frac{y}{\lambda_i} + \phi_{k,i} \right) \right] \tag{6-3}$$

with A_i and λ_i are the parameters of the ith frequency peak retrieved from the amplitude spectrum of the ply thickness. In order to obtain a coupling between the ply thickness and the plate thickness, a pseudo-random phase shift $\phi_{k,i}$ is introduced.

The contribution of the plate variation δt_{plate} to the ply thickness, based on the results of Chapter 3, is:

$$\delta t_{plate}(x, y) = \frac{1}{16} \left[\frac{A_{plate}}{4} \left[\cos\left(\frac{2\pi}{\lambda_{pla \cdot x}} (x + X_c) \right) + \cos\left(\frac{2\pi}{\lambda_{pla \cdot y}} (y + Y_c) \right) \right] \right] \tag{6-4}$$

It is noteworthy that, due to the previous remark, the values of the amplitude and the wavelength for each of the ith frequency peak of the ply thickness amplitude spectrum are the same for both x and y-directions. Thus, a very distinctive and regular pattern appears when mapping the ply thickness (cf. Figure 6-1).
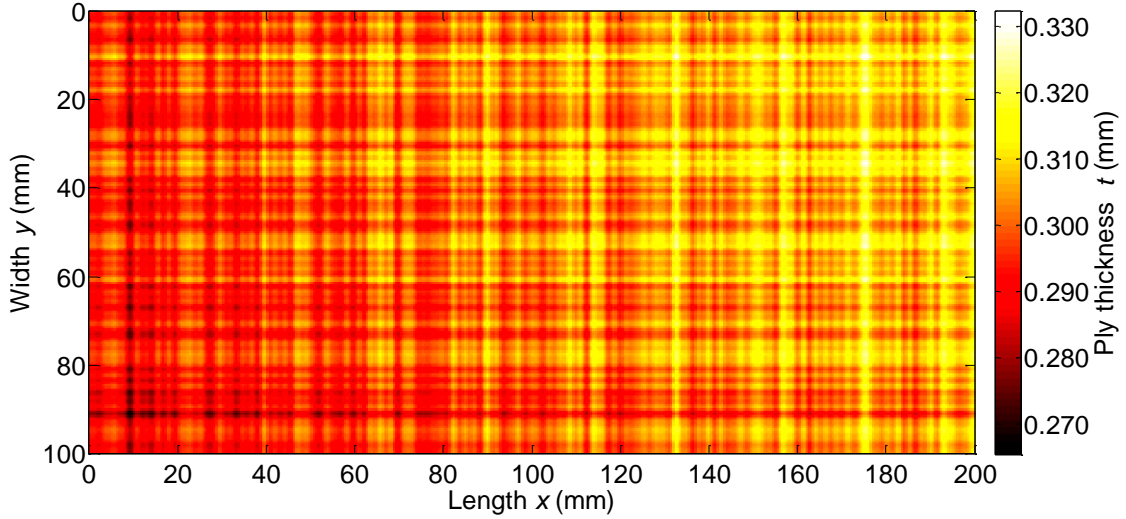
Figure 6-1. Map of the generated ply thickness in a ply of 200 x 100 mm dimensions.

Using the thickness of the ply t_k, the local changes in the porosity volume fraction V_{pk} are calculated from a random parameter ξ_k (cf. Chapter 3). This random parameter has a zero-mean.

$$V_{p \cdot k}(x, y) = f(t_k, x, y) + \xi_k(x, y) \tag{6-5}$$

At this point, the mass per unit area of the reinforcement ρ_{Af} is considered as constant over all the manufactured plates (i.e. for a given plate and from one plate to another). However, this value is calibrated from observations of the manufactured plates and is set, for the M10.1/CHS, to a value of 305 g·m⁻².

$$\rho_{Af} = \text{constant} \tag{6-6}$$

To obtain the local volume fractions of the fibre and the matrix, in a first step, an equivalent thickness of the reinforcement t_f is calculated. This parameter, which is constant through the plate, is obtained from the relationship of the mass per unit area of the reinforcement ρ_{Af} and the density of the reinforcement ρ_f:

$$t_f = \frac{\rho_{Af}}{\rho_f} \tag{6-7}$$

Therefore, the volume fractions of reinforcement $V_{fk}(x,y)$ and matrix $V_m(x,y)$ are obtained from:

$$V_{f\cdot k}(x, y) = \frac{t_f}{t_k(x, y)} \tag{6-8}$$

$$V_{m\cdot k}(x, y) = 1 - V_{f\cdot k}(x, y) - V_{p\cdot k}(x, y) \tag{6-9}$$

Afterwards by using the law of mixtures, the values of the volume fractions, the elastic quantities for each element (cf. Table 6-1) can be calculated using the properties of the constituent materials expressed in Table 6-2.

The local variations of the reinforcement directions θ_k are given by the sum of the theoretical orientation (according to the stratification) θ_{th}, the global ply misalignment $\delta\theta$, the local fibre undulations [5] θ_{wav} and the local perturbations that are due to the manipulation of the prepreg θ_{pert} as discussed in Chapter 4.

The local fibre waviness can be expressed as a function of the amplitude A_{wav} and the wavelength λ_{wav} of the undulations.

$$\theta_{wav}(\theta_{k\cdot th}) = \frac{A_{wav}}{2} \sin\left(\frac{2\pi x \cos\theta_{k\cdot th} + 2\pi x \sin\theta_{k\cdot th}}{\lambda_{wav}} \right) \tag{6-10}$$

Finally, the distribution of local perturbations is introduced by the sum of 12 pseudo-Gaussian surfaces as identified in Chapter 4, where its parameters B_i, α_i, β_i, X_i, and Y_i are chosen in accordance with the measurements and analysis done in the related Chapter.

$$\theta_{pert}(x, y) = \sum_{i=1}^{12} B_i e^{-\left(\left(\frac{x-X_i}{\alpha_i} \right)^2 + \left(\frac{x-Y_i}{\beta_i} \right)^2 \right)} \tag{6-11}$$

A theoretical example using (6-10) and 6-11) of the resulting map of the fibre orientation is shown in Figure 6-2, for a ply oriented at 45°. The visible lines are the periodic undulations of the fibre; they appear perpendicular to the fibre direction.
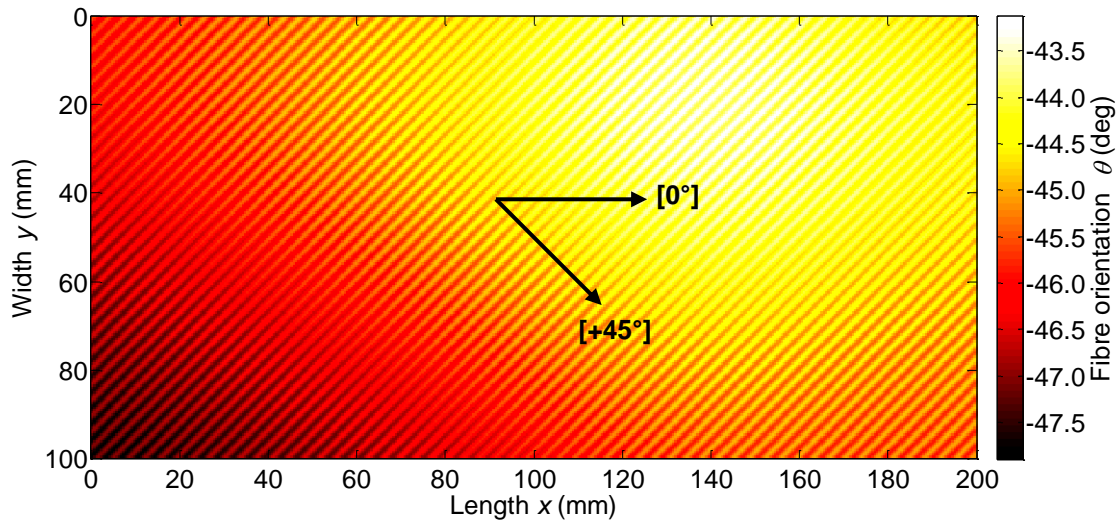
**Figure 6-2. Theoretical example of the reinforcement misalignment in a +45°
200 x 100 mm ply.**

To illustrate the effects of the continuous variability of an elastic quantity in a composite ply, Figure 6-1 through Figure 6-3 show the spatial evolution of the ply thickness, the fibre orientation and the Young's modulus in the x-direction of a single composite ply of dimensions 200 x 100 mm and oriented at 45°.

The law of mixtures is applied to obtain the lamina compliance matrix in the fibre direction $[S]_{lt}$. The compliance matrix is then transformed into the general laminate coordinates $[\overline{S}]_{xy}$. The Young's modulus E_x in the laminate direction xy for each element of the lamina is thus:

$$E_x = \frac{1}{\overline{\overline{S}}_{11}} \qquad (6\text{-}12)$$
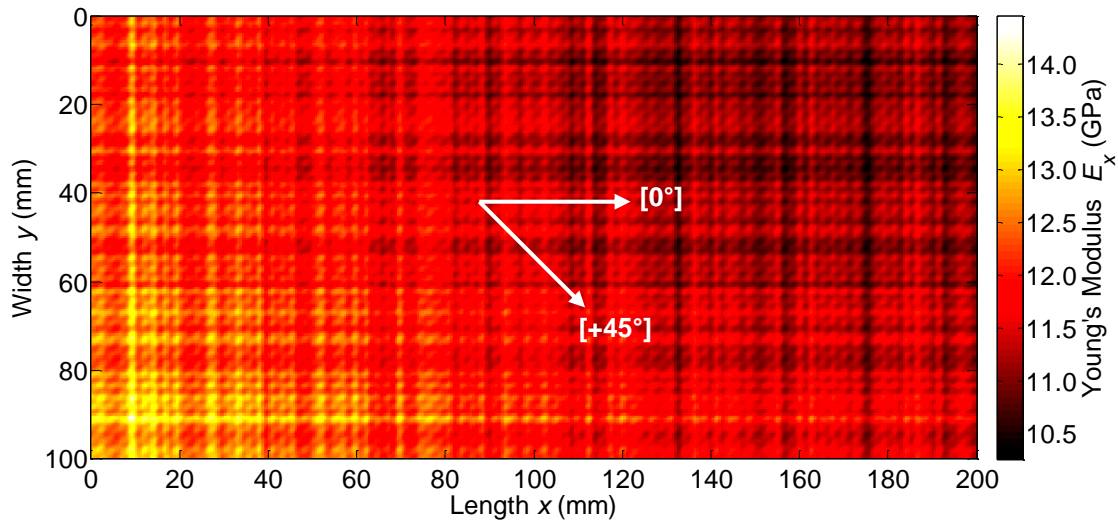
Figure 6-3. Theoretical example of a map of the Young's modulus E_x distribution in a 200 x 100 mm ply oriented at +45°.

The Young's modulus of the lamina depends on both the ply thickness and the fibre orientation and with variations up to 3 GPa from one point of the ply to another. In the case of a lamina oriented at ± 45°, the mechanical variations in the directions of the laminate coordinates xy depend on both the ply thickness and the fibre orientations (cf. Figure 6-3). For the 0° and 90° orientations, the mechanical properties in the laminate coordinates xy are more dependent on the ply thickness variations than the fibre orientation.

6.3 Four-point bending test

6.3.1 Introduction and experimental results

As a first example to test the feasibility of a finite element model with varying properties, a four-point bending test is performed on the composite material. At this stage, a comparison between the analytical analysis, numerical analysis and experimental data is performed. The test was initially chosen to determine the stress properties of the plates in pure bending, since one of the

objectives of this study is to test a technological evaluator in a flexion-compression loading.

The stratification employed for this test is still $[90/45/0/(-45)_2/0/45/90]_s$ as discussed previously. The specimens were cut such both the outer plies are oriented at 90°. The specimen dimensions are w = 15 mm and L_{spec} = 100 mm. A controlled displacement is applied through the loading noses. The span is L = 81 mm and between the loading noses L' = 27 mm (cf. Figure 6-4).
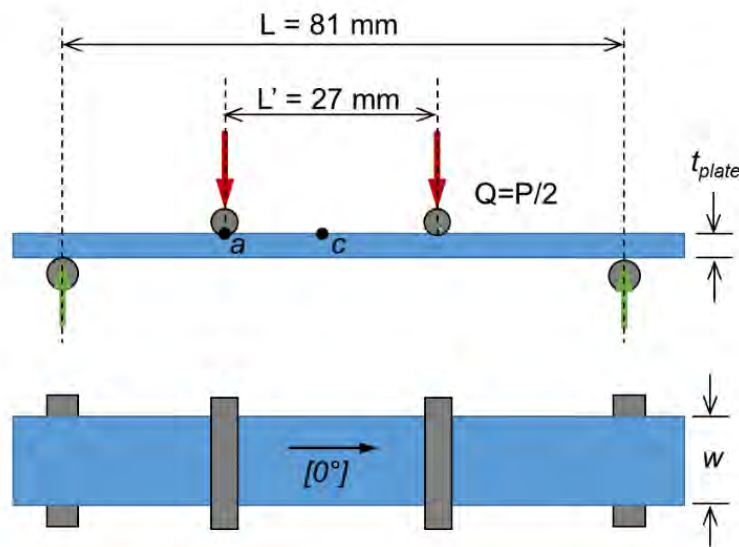
Figure 6-4. Schema of the 4-point bending test with front view (top) and top view (bottom).

During the tests, the obtained data is the load-displacement curve for each specimen. The flexural modulus is then computed using the following equation, in which ΔP is the variation of the load and Δs_c is the variation of the displacement between two points at the centre of the specimen.

$$E_{f \cdot x} = 0.213 \frac{L^3}{w \cdot t_{plate}^3} \left(\frac{\Delta P}{\Delta s_c} \right) \tag{6-13}$$

However, the obtained displacement is not measured at the mid-span of the specimen (cf. point c in Figure 6-4), but at the position of the loading nose Δs_a

(cf. point *a* in Figure 6-4), the formula is used for a loading span one third of the support span:

$$E_{f \cdot x} = 0.185 \frac{L^3}{w \cdot t_{plate}^{\ 3}} \left(\frac{\Delta P}{\Delta s_a} \right)$$

(6-14)

The specimens are obtained by water jet for cutting from the composite plates. Two composite plates from the autoclave batch *C* (cf. Chapter 3) have been employed. From the plate C-11, 7 specimens are obtained. Plate C-22 has been sectioned in 2 halves of dimensions 600 x 130 mm. Section C-22.1 is used to generate a technological evaluator in a compression-bending test. The other section, C-22.3 is used to obtain 8 additional specimens for the bending tests. The specimens are evenly spread over the plates.

The 15 specimens were tested in an Instron universal testing machine, in accordance with the standard test EN ISO 14125 [6] for a third of the support span *L*. Both the support noses and the loading noses in the testing fixture have lateral stops to guarantee that the positioning of the specimens is the same between the tests. The first two specimens C-11-1 and C-11-2 were tested using a 100 kN load cell which does not provide the required accuracy for the range of loading during the test (see in italics in table 6-3). The rest of the specimens were tested using a 10 kN load cell. Due to possible differences in the calibration of the two load cells, and to the dispersion linked to the demounting and mounting the test fixture to install the load cells, the results of the first two specimens are not taken into account with the rest of the samples. Notwithstanding the behaviour of the C-11-1 and C-11-2 is completely coherent with the rest of the specimens.

The slope of the load–displacement diagram m_{4p} is taken between a displacement of 1 and 3 mm (cf. Figure 6-5), with the exception of the specimen C23.2-6 which failed prematurely at 1.5 kN (cf. Figure 6-6). The strength of the composite plate is taken at the maximum load value recorded during the test. After the first ply failure, the composite can still carry some load, albeit with a significant loss of stiffness, until the ultimate failure of the composite structure. In

the present case, the interest is to study the elastic behaviour of the composite before the first failure.
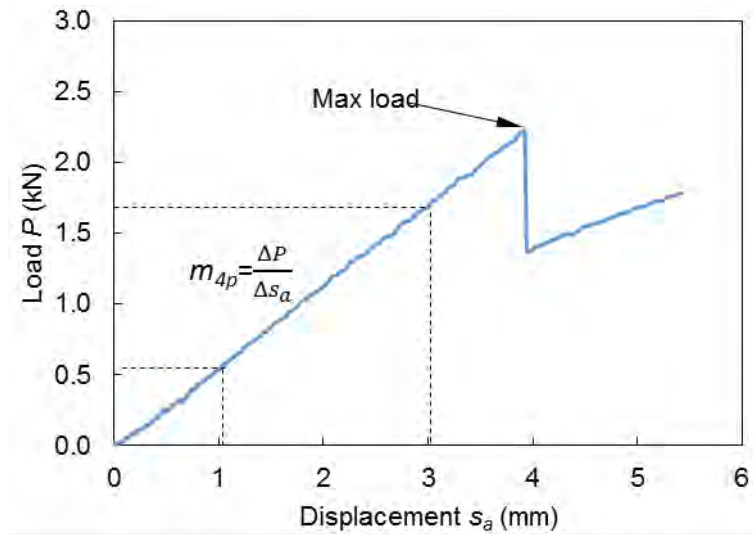
Figure 6-5. Load as function of the displacement in a 4-point bending test.

Table 6-3 summarises the geometrical and mechanical values obtained during the test for all the 15 specimens. All the specimens are taken from two different plates manufactured in autoclave batch C. To test whether the results obtained for the two different plates can be grouped as a single sample, an analysis of the variance (ANOVA) is performed. The null hypothesis is made that all the specimens are part of the same sample regardless the used plate. The ANOVA results show that there is no statistically significant difference between these two sub-samples for both specimen thicknesses and flexural modulus. Thus, the tested specimens can be considered as a single sample.

Figure 6-7 shows the two types of failure of the coupons during the bending tests. From the 15 tested specimens, 13 failed by compression of the 0° ply closer to the upper skin (ply #14) followed by the delamination and rupture of the second 0° ply in compression (ply #11). The remaining two specimens (C-23.2-6 and C-23.2-8) failed by delamination between the 7th and 8th plies. The delamination probably occurred at a surface defect generated by the water jet cutting procedure, possibly due to an irregular abrasive stream.

Table 6-3. Measurements and calculations coming from the 4-point bending test.

Specimen	Mean thickness (mm)	Mean width (mm)	m_{4p} (kN/mm)	E_{fx} (GPa)	P_f (kN)
C-11-1	4.788	14.932	0.613	34.116	2.350
C-11-2	4.776	14.814	0.617	34.859	2.213
C-11-3	4.844	14.804	0.571	30.965	2.404
C-11-4	4.855	14.826	0.573	30.805	2.228
C-11-5	4.899	14.853	0.607	31.713	2.230
C-11-6	4.840	14.820	0.572	31.050	2.180
C-11-7	4.812	14.818	0.573	31.638	2.116
C-23.2-1	4.774	14.834	0.573	32.372	2.370
C-23.2-2	4.867	14.897	0.591	31.416	2.309
C-23.2-3	4.820	14.850	0.567	31.107	2.347
C-23.2-4	4.818	14.829	0.564	30.995	2.299
C-23.2-5	4.833	14.837	0.581	31.656	2.151
C-23.2-6	4.899	14.831	0.594	31.049	1.323
C-23.2-7	4.875	14.854	0.586	31.050	2.220
C-23.2-8	4.872	14.832	0.573	30.479	2.276
Mean	**4.847**	**14.837**	**0.579**	**31.253**	**2.189**
Std. dev.	**0.036**	**0.023**	**0.012**	**0.491**	**0.274**
CV (%)	**0.7**	**0.2**	**2.1**	**1.6**	**12.5**
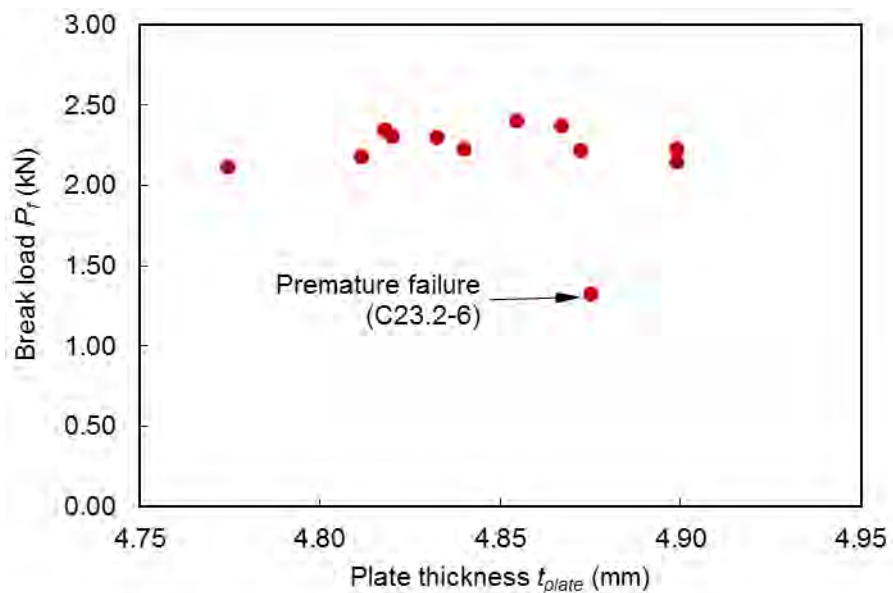
Figure 6-6. Flexural break load P_f of the tested specimens.
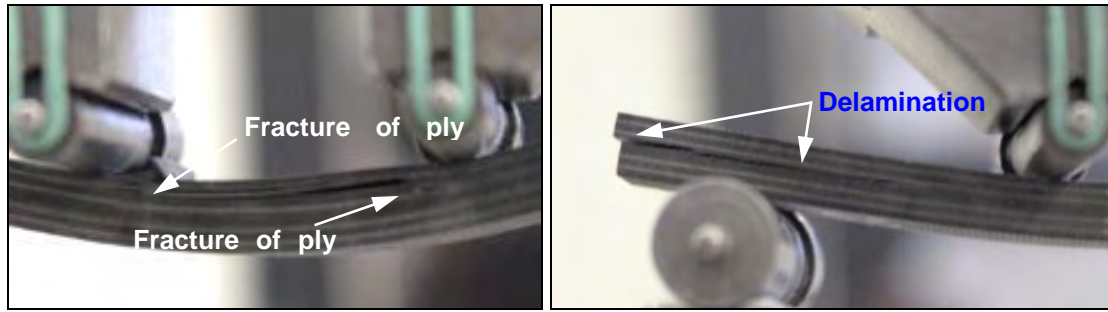
Figure 6-7. Composite failure in a 4 points bending test with (on the left hand side) the expected failure of the 0° oriented plies under compression, and (on the right hand side) delamination of the mid plane.

The calculated flexural modulus E_{fx} is shown in Figure 6-8. The variation exhibits a reduction of this modulus with the increase of the plate thickness. It also exhibits a scatter around the linear fit. The mean E_{fx} is 31.253 GPa with a coefficient of variation of 1.6 %.
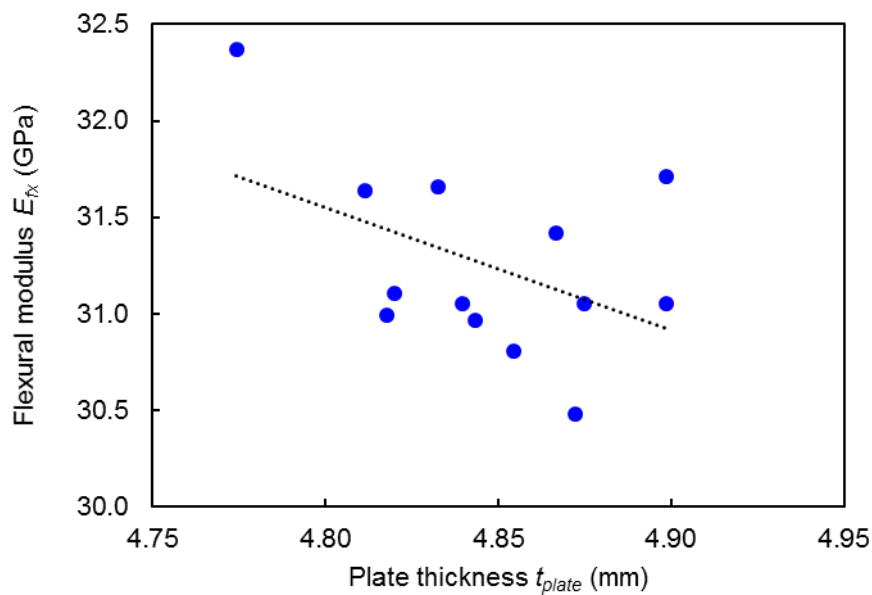
Figure 6-8. Flexural modulus E_{fx} of the tested specimens.

6.3.2 *Analytical simulations in bending*

An analytical calculation using the classical stratification theory is used to obtain the variations of the flexural modulus E_{fx}. This analysis considers that all the plies have the same property, without local variations from one point to

another, but with variation of thicknesses and orientation for each ply. This analysis can be considered as intermediate to determine the influence of the major morphological properties of the plate. First, a deterministic case is done using the classical stratification theory without any variations (case 1). Then four different cases are analysed. In the case 2, the ply thickness is obtained dividing the plate thickness by the number of plies with a variation of 1.11 % of the plate thickness. In the case 3, the ply thicknesses are assigned with a mean of 0.302 mm and coefficient of variation of 4.5 %. In the case 4, the orientation angle is variable assigning a variation on the overall misalignment of the ply of 0.33°. In the last case 5, both the ply thickness and the angle orientation are variables.

The variation of 1.11 % of the plate thickness, applied in case 2, has the same order of magnitude than the thickness variation observed in cases 3 and 5 (except case 4). The flexural modulus E_{fx} is obtained from the element D_{11} of the compliance matrix ABBD^{-1} of the laminate using the relationship:

$$E_{f \cdot x} = \frac{12}{D_{11} t_{plate}^{3}} \tag{6-15}$$

Figure 6-9 exhibits the results for cases between 2 and 5. Table 6-4 summarizes all cases. In the 2nd case when the variation of the plate thickness is proportional to the variation of the ply thickness, the evolution of E_{fx} is linear without scatter, since all the plies carry the same load.

When varying the ply thickness (case 3), a linear variation is no longer possible, and a significant scatter is observed, which for a given plate thickness this variation is up to ± 3 GPa (± 3.3 %) on the mean E_{fx} for such plate thickness. In the 4th case, the ply thickness is maintained constant and the ply orientation is affected by a general misalignment. The variation created for the ply misalignments accounts for approximately ± 1 GPa (0.27 %) of the mean flexural modulus. In the case 5 where the structure has both the fibre orientation and the ply thickness variable, the change in the CV is due to the combination of the effects in ply thickness and fibre orientations.

The shape of the E_{fx} distributions is very similar for all cases, with the distribution of the case 3 slightly flatter. As expected, the variations in the ply thickness have a greater effect on the composite laminate in flexion.
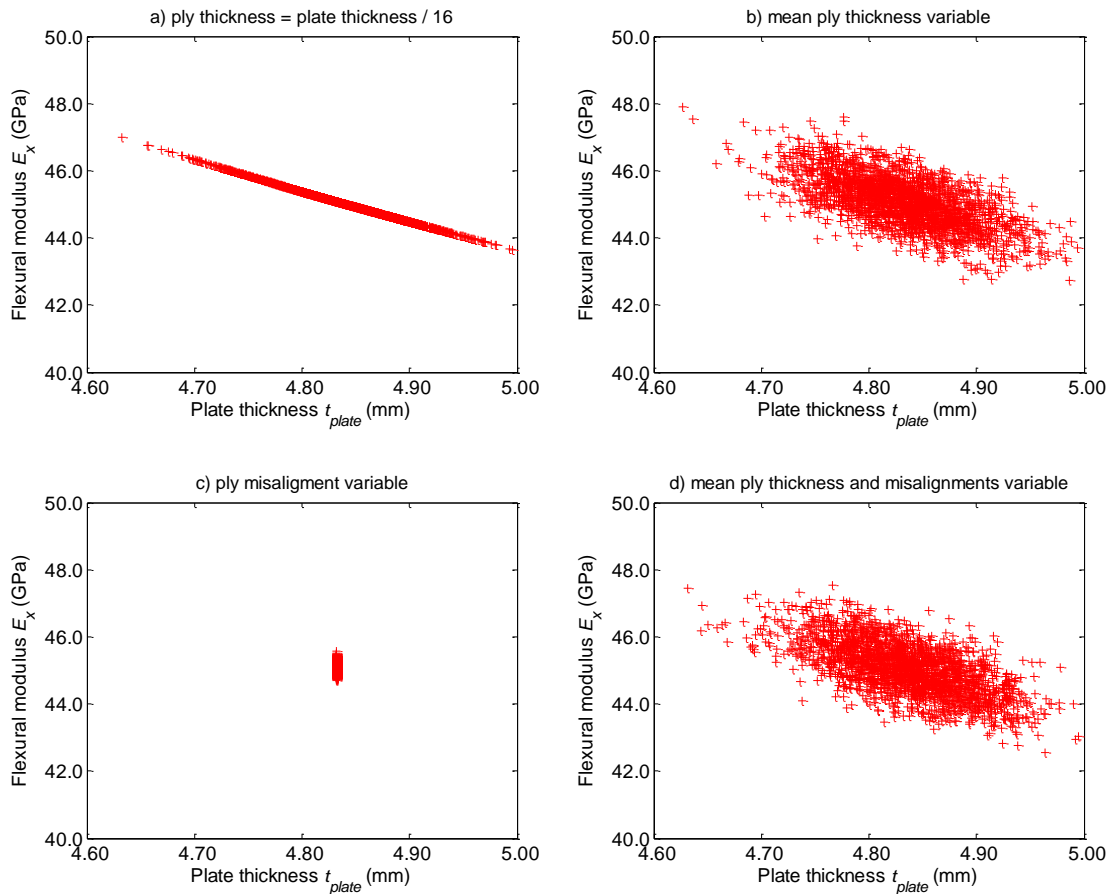
Figure 6-9. Distribution of the flexural modulus E_{fx} for a 16-ply laminate for a mean ply thickness of 0.302 mm and standard deviation of 0.014 mm with (a) the plate thickness with the values x 16 (case 2); (b) each ply thickness different (case 3); (c) the ply thickness constant with ply misalignments (case 4) and (d) both the ply thicknesses and misalignments variables (case 5).

Table 6-4. Statistical values of the plate thickness and flexural modulus E_{fx}.

Cases	Plate thickness		Flexural modulus E_{fx}	
	Mean (mm)	CV (%)	Mean (GPa)	CV (%)
Deterministic	4.832	0	45.092	0
Case 2	4.834	1.11	45.084	1.08
Case 3	4.832	1.10	45.125	1.68
Case 4	4.832	0	45.092	0.27
Case 5	4.832	1.12	45.110	1.71

6.3.3   FE model of the four points bending test

The element size is 1 x 1 m in agreement with the minimum wavelength of the ply thickness variation set to 2 mm (cf. Chapter 5). For simplification of the calculations and reduction of the input file, the range of the ply thickness is discretised in 29 sections starting from 0.230 mm to 0.370 mm (for a median ply thickness equal to 0.300 mm) with a step of 0.050 mm. The elastic quantities are calculated for each of these discretised thicknesses and then assigned individually to each element according to its ply thickness. In Table 6-5, the median value of the elastic quantities is shown for the two principal lamina directions *1* (fibre direction) and *2* (transversal direction). The median is used instead the mean in order to give an estimation of the order of magnitude of the elastic quantities which depend on the ply thickness, which can exhibit different mean values across the Monte Carlo simulations.

Table 6-5. Elastic quantities for the principal directions 1 and 2 calculated for the median ply thickness of 0.300 mm.

Elastic property	*Direction 1 (or 12)*	*Direction 2 (or 21)*
Young's moduli (GPa)	131.44	9.71
Shear moduli (GPa)	4.26	4.20
Poisson's ratios	0.332	0.025
Coefficients of thermal expansion (°C^{-1})	$-0.56 \cdot 10^{-6}$	$14.34 \cdot 10^{-6}$

The composite plate model considers the dimensions of the test specimen with length L_{spec} = 100 mm and width w = 15 mm. The length between the support noses is L = 81 mm and the distance between the loading nose is L' = 27 mm (same as in tests). The number of elements is 1 500 elements per 16 plies corresponding to 9 661 degrees of freedom (DOF). The boundary conditions are applied in accordance to the real test, in which the nodes sitting over the support noses have their displacement along the *z*-axis is inhibited, and the nodes along the loading noses are imposed a displacement in the *z*-axis of -3 mm. Figure 6-10 shows the

deformed shape and the strain field along the *x*-axis of the upper skin of one of the numerical 4-point bending test.
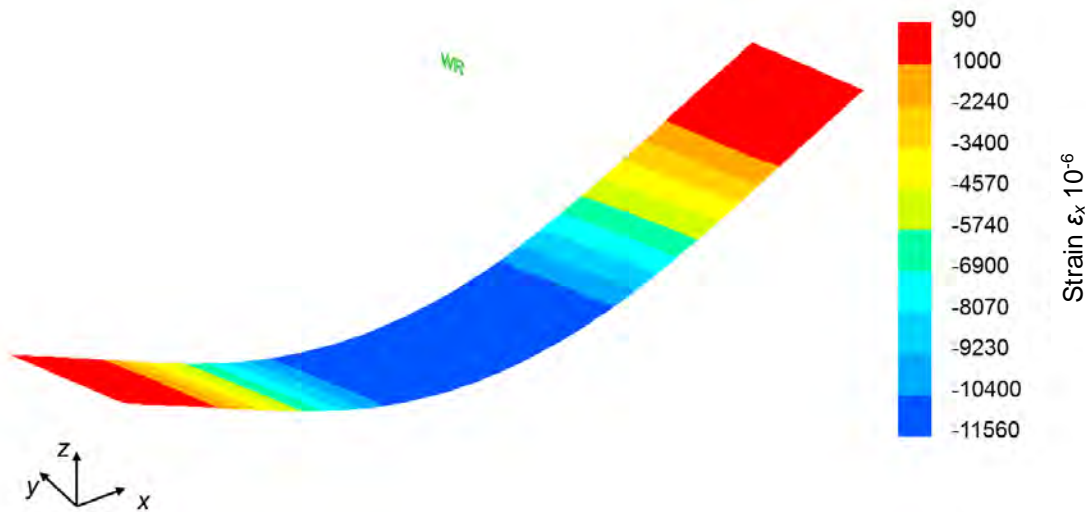
Figure 6-10. Strain field of the upper skin along the *x*-axis ε_x in a 4-point bending test for Δs_a = 3 mm (nose displacement).

In a first experience, both the plate and the ply mean thicknesses have been maintained as constants in order to determine the sole contribution of the ply waviness to the flexural modulus E_{fx}. It is important to determine whether the material properties have a significant impact on the calculated material properties, or not. In first place, a deterministic model without any property nor geometrical variations is used as a comparison point (case 1). Case 2 refers to a variation of the thicknesses profile while maintaining constant material properties given by the mean ply thickness. And case 3 refers to a variation in the ply thicknesses profiles, and the material properties are calculated for each element in accordance with the local ply thickness. 20 Monte Carlo simulations are performed for cases 2 and 3.

Erreur ! Source du renvoi introuvable. shows the mean values for the flexural modulus and coefficient of variations for the three different cases. For the variation of the ply thickness, both stochastic solutions show an increase of the flexural modulus by 180 MPa.

Table 6-6. FE model results for a digital 4-point bending test with constant plate thickness.

Type	Plate thickness (mm)	Flexural modulus E_{fx}		
		Mean (GPa)	CV (%)	Dif. max min (%)
Case 1: Deterministic	4.838	40.881	0	0
Case 2: Constant material	4.838	41.047	0.11	0.47
Case 3: Material variation	4.838	41.062	0.10	0.37

It is noteworthy that all the simulations with variable ply thickness exhibit a flexural modulus higher than that from the deterministic solution. The coefficients of variation (CV) for both cases are very close with a difference that is not statistically significant. Even though, by observing the cumulative distribution of E_{fx}, for the simulations with constant material properties, the slope of the distribution is steeper than the case with material variation, regardless of the increased CV and maximum difference between extreme values (cf. Figure 6-11). This can lead to the conclusion that the impact of using constant material properties is the same as if variable properties would be used. However, the extreme values are responsible for the increased variability, while the core of the distribution that the flexural modulus with a constant material is less sensitive the in majority of the cases and much more sensitive towards the tail of the distribution.

By introducing a variable geometry in the composite ply, the plate gains in rigidity. In this case, the variabilities in the flexural modulus are purely function of the local thickness undulations, since the cross-section of the composite beam is the same for all cases. In any case, by only varying the local values of ply thicknesses without affecting the mean value, only accounts for 0.1 % of the variation in the properties. This however can may be impact on the calculations of safety margins when adding more features to the analysed system.
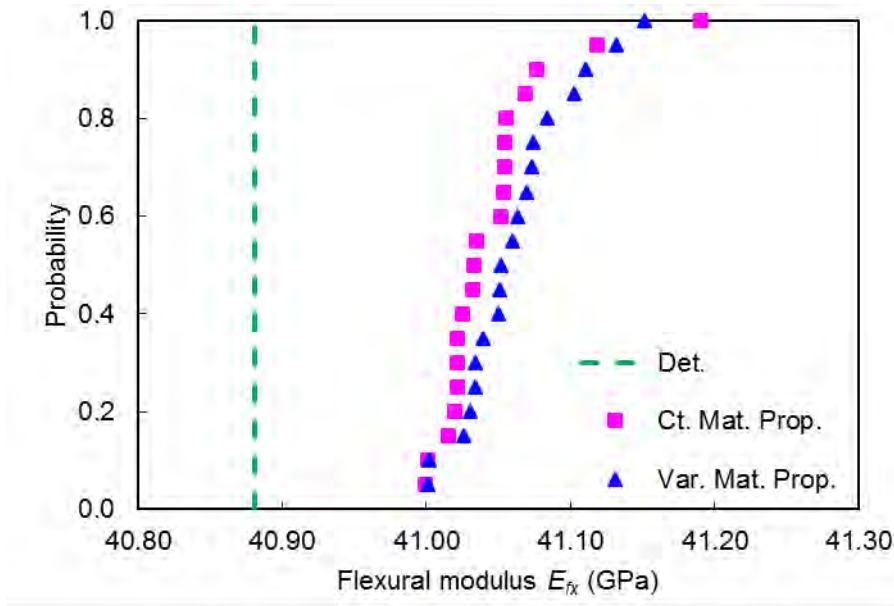
Figure 6-11. Cumulative distributions for the flexural modulus of the 4-point bending test FE model for the deterministic case (dashed line), constant material properties (square markings) and material properties varying according to the local ply thickness (triangle markings).

Unfortunately, the chosen element type, a 2D Mindlin composite shell, overestimates the flexural modulus by 30 %. Since the interest of this exercise is to study the variability around the mean values, a normalised flexural modulus NE_{fx} is used to compare the numerical data against the experimental data. The normalised modulus is:

$$NE_{f \cdot x} = \frac{E_{f \cdot x}}{\overline{E_{f \cdot x}}} \qquad (6\text{-}16)$$

The results comparison between the model without any variations other than the plate along with the full stochastic model and the experimental data is shown in Figure 6-12. As expected, the model with constant properties, in which the ply thicknesses are obtained by dividing the thickness of the plate by the number of plies, the flexural modulus E_{fx} of the laminate are aligned to the theoretical curve as a function of the plate thickness. On the contrary, the model with all the variabilities exhibits a significant scatter from the expected value (constant thickness) and it is within the same order of magnitude as the

experimental data. These results effectively prove that the variability in the macroscopic property such as the flexural modulus can be recreated by the proposed modelling strategy.
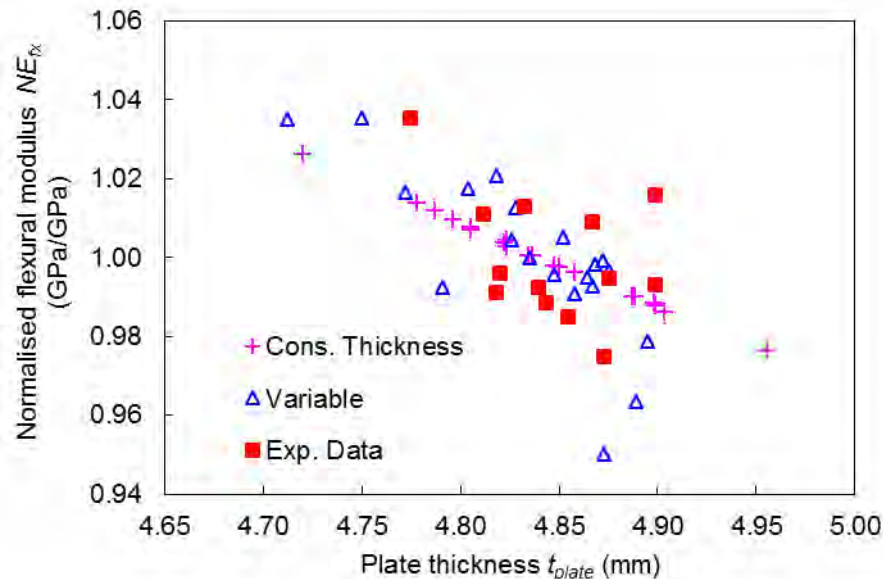
Figure 6-12. Comparison of the normalised flexural moduli as function of the plate thickness for 3 cases with constant thickness with ply thickness divided by 16 (cross markings), all parameters variable (triangle markings) and experimental (square markings).

6.4 Residual strains of a cured plate subject to cooling

Another application of the proposed model concerns the residual deformation of the composite plate subject to cooling at the end of the cure dwell. It is assumed that at this point the composite material is already consolidated and in a zero-residual strains/stress state [7]. Thus, due to a mismatch between the coefficients of thermal expansion of the fibre and the matrix, residual stresses and strains can be generated by the uneven deformation of these two materials. In this test, only the thermal properties of the element obtained by the law of mixtures are considered, as the micromechanical interactions between the fibre and matrix are beyond the scope of this work. Likewise, the interaction between the piece and the tool are not considered in this exercise [8].

The FE model considered the whole composite plate of dimensions 300 x 600 mm, subjected to a temperature change of $\Delta T = -120$ °C. The total number of elements for this simulation is 180 000 and 16 plies per element, for a total of 1 085 400 DOF.

Figure 6-13 shows the plate profile and Figure 6-14 shows the shape of a randomly chosen ply (ply #7). It must be noticed the piece does not have a uniform thickness, but it exhibits a thicker zone at the centre of the plate, as the measurements of the composite plates has shown (cf. Chapter 3). Similarly, the ply thickness accounts for the variations of the plate. The composite ply also presents local variations due to the local undulations.
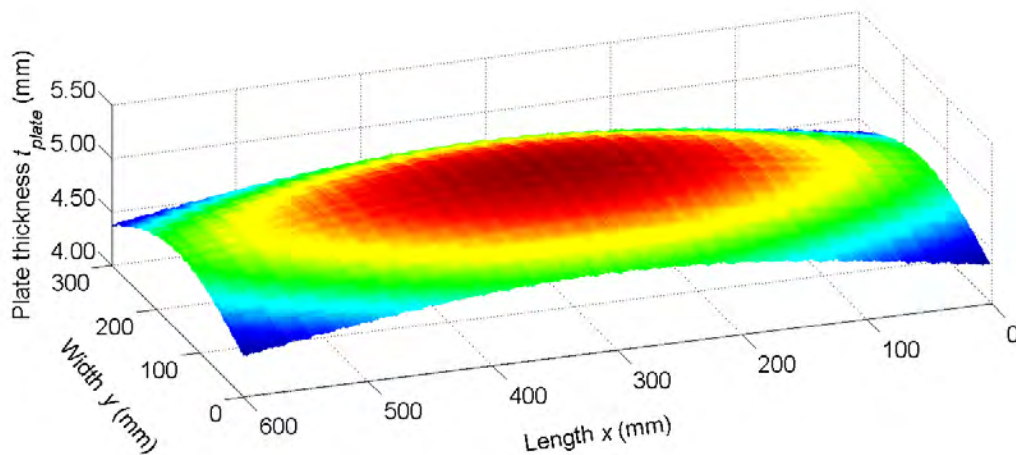
Figure 6-13. Thickness variation of the composite plate.
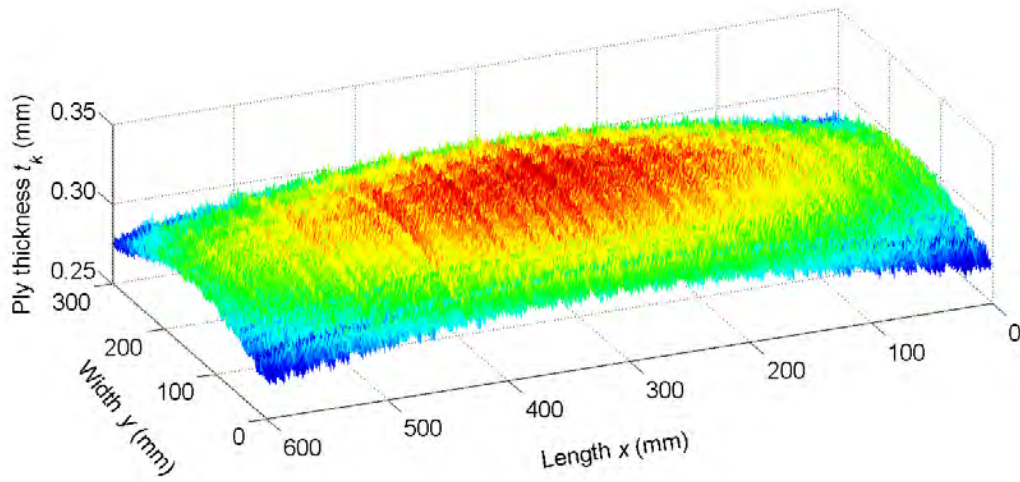
Figure 6-14. Thickness variation of ply #7.

Figure 6-15 shows the fibre orientation, accounting for the general misalignment of the ply, the local perturbations created by the manipulation of the ply and the continuous waviness of a randomly chosen ply. In this case the ply #4 ply oriented at +45°.
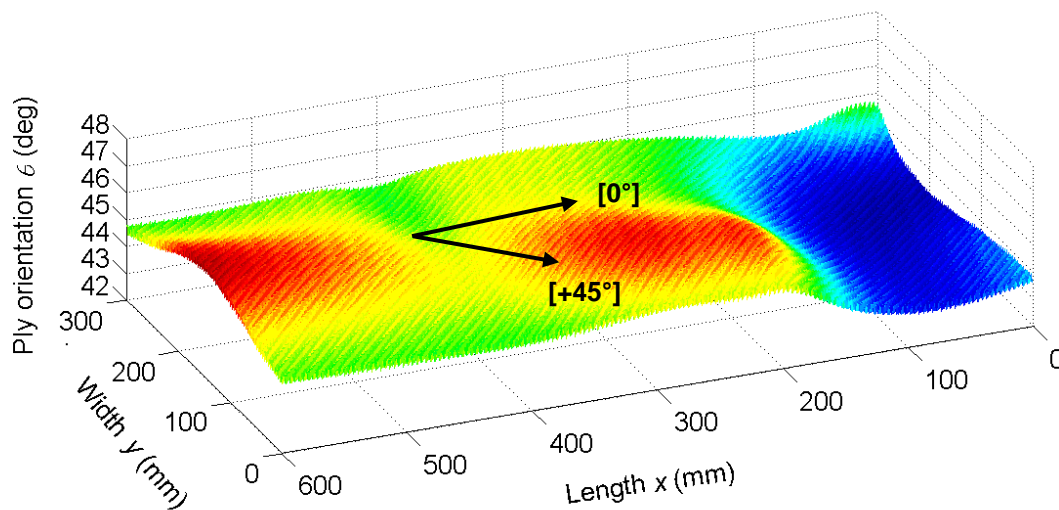
Figure 6-15. Variation of the fibre misalignment in a ply (ply #4) with a theoretical orientation (at +45°).

The nodal displacements w of the composite plate along the z-axis are shown in Figure 6-16. The plate was supported at 3 corners, points A, B and C, in

the z-direction and points B and C, the movements are blocked in the x-direction and the A point in the y-direction. The plate exhibits a significant deflection of 0.5 mm in the edge near the free corner. The deformation of the plate is only due to the morphological variabilities present in the model. In comparison, a model without the inclusion of variabilities, the nodal displacements w will be equal to zero. Also in the manufactured plates, a similar deformed shape was observed, albeit with less significant warping.
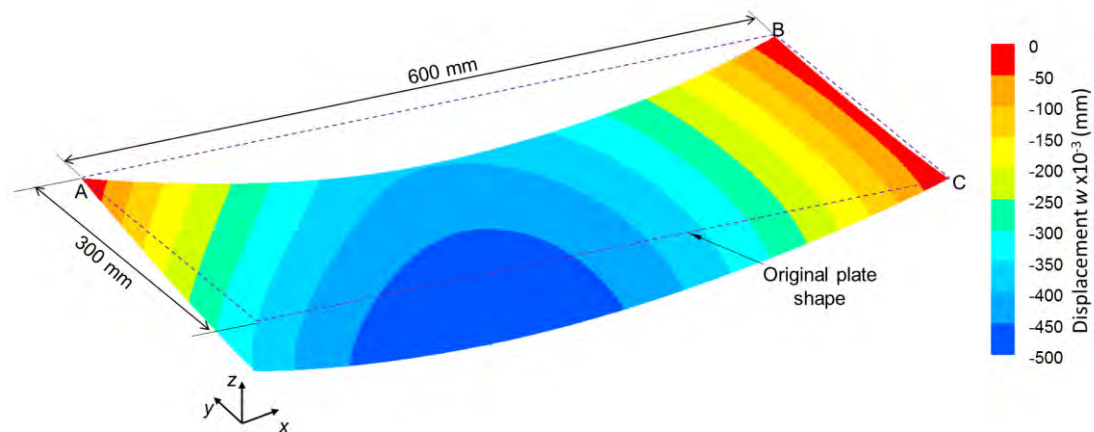
Figure 6-16. Nodal displacements w along the z-axis.

Finally in Figure 6-17, the strain fields in the x-direction ε_x for the upper and lower skins of the composite plate are shown. There are some differences in the strain field due to the different shapes of the upper and lower skins of the composite, where all the plate is under compression along the x-axis. There is a difference of $40 \cdot 10^{-6}$ between the values from the upper and lower skins, being the lower skins that exhibit a lower deformation than the upper one. These values are in agreement with the deformed shape of the plate. It is also noteworthy that there is a difference of $70 \cdot 10^{-6}$ between the extreme values in both skins. This difference is mainly due to the difference in thickness at the centre of the plate and its corners.
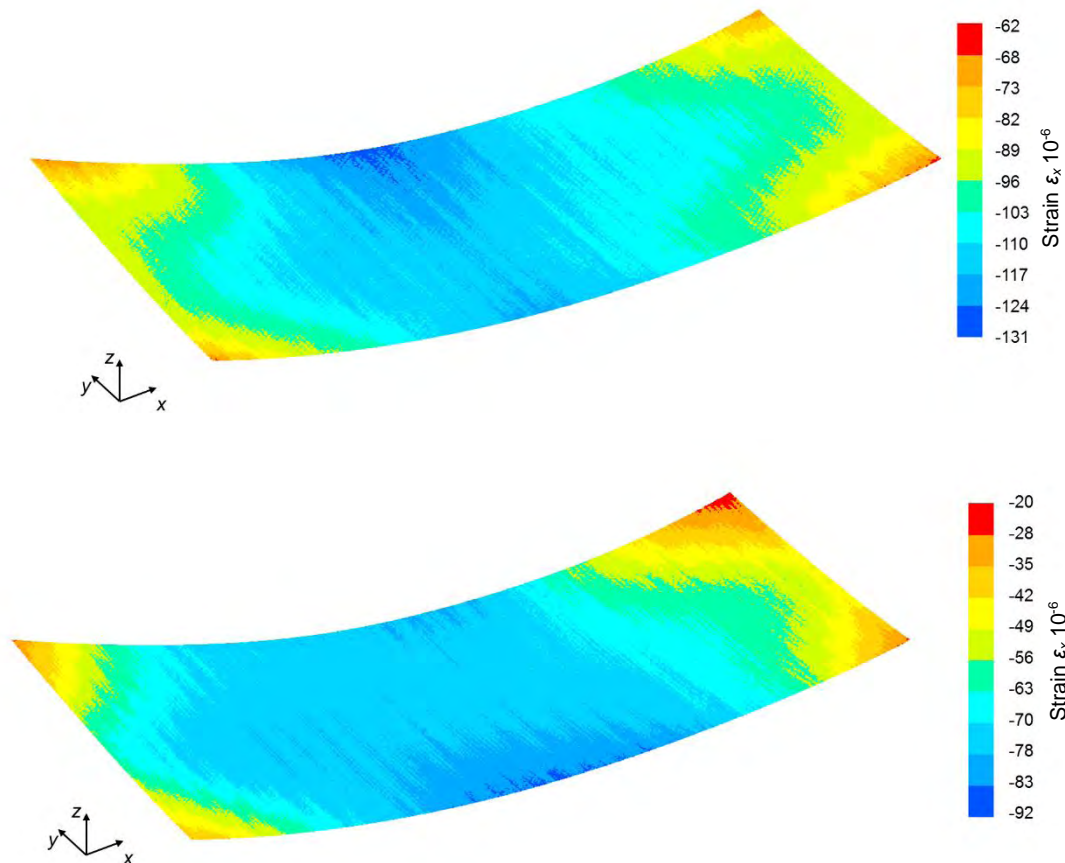
Figure 6-17. Strain field along the *x*-axis ε_{xx} for the upper skin ply#16 (top) and the lower skin ply #1 (bottom).

6.5 Technological evaluator under flexion-compression loading

6.5.1 *Presentation of the 'toolbox': Multi-instrumented Technological Evaluator*

The Multi-instrumented Technological Evaluator *toolbox* (MITE toolbox) [9] is designed to study composite structures developed at the Clément Ader Institute. One of the components of the MITE toolbox is the experimental equipment composed by an original multi-axial testing machine, which is used to apply combined loads to a predefined composite structure. The ability to applying complex loading scenarios is coupled with the possibility to use various

instrumentation methods. The experimental setup is also combined by the numerical models to design and analyse the defined tests in a loop of optimization [10,11].

The multi-axial testing machine (cf. Figure 6-18) consists of 4 electro-mechanical actuators with hinged attachments to the frame-side end. In their other end, these actuators are attached to a steel quadrangle. This quadrangle transmits the load to one end of the composite evaluator. The independent movements of the four actuators permit to obtain four elementary displacements and loadings: tension/compression along the x-axis, and three bending moments around the x, y and z-axes (cf. Figure 6-19). An articulated arm attached to the steel rectangle is to prevent its displacement along the y and z-axes. This offers the possibility to place composite evaluators in a multi-axial state of stresses, which could be representative of stresses chosen and/or encountered during the service life of a structural part.
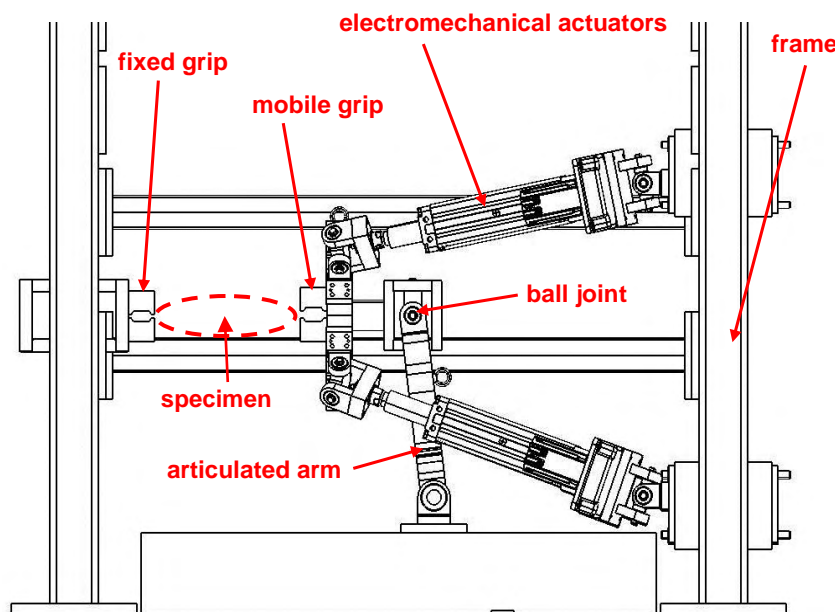
Figure 6-18. Side view of the multi-axial testing machine.

The evaluators are fixed between the frame and the mobile rectangle. In the current configuration of the modular testing machine, the maximal dimensions of the test coupons are 600 mm long and 300 mm wide. The maximum loads are

approximately 140 kN in traction and compression, 8 kN·m of bending moment around x, 30 kN·m of bending moment around y, and 40 kN·m of bending moment around the z-axis.
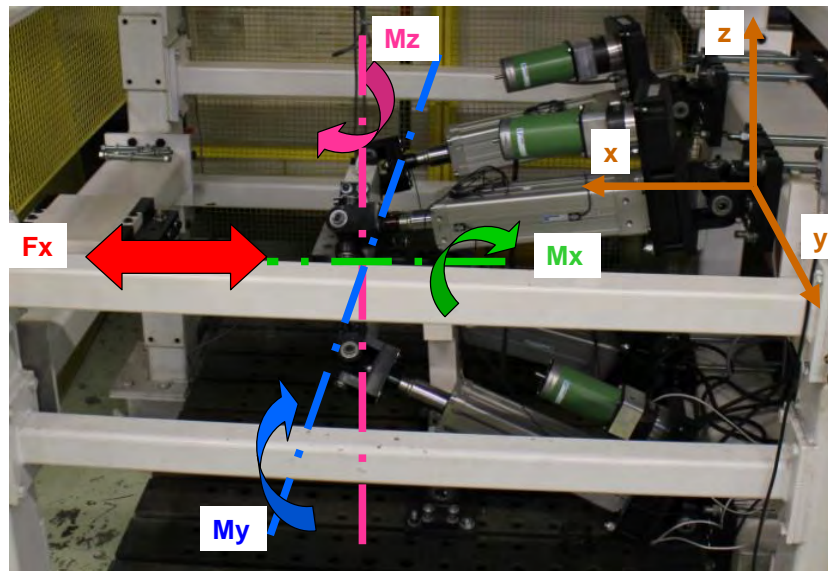
Figure 6-19. Different loading scenarios possible with the actual configuration of the multi-axial testing machine.

To ensure a correct load transfer from the testing machine, at the place of the attachment, composite tabs are bonded to the composite using an epoxy adhesive. These tabs are designed to transfer the loads to the coupon, particularly to bending and flexural moments, and they have a variable thickness to avoid stress concentrations. They are designed to be easily moulded using the HexTOOL® M61, whose stiffness is chosen to be similar to that of the testing coupon.

The tested structure is shown in Figure 6-20. It consists of a composite plate of 600 x 130 mm, with a stratification of $[90/-45/0/(45)_2/0/-45/90]_s$ obtained from the composite plates fabricated in Chapter 3. The composite is prepared with a black and white pattern to be tested using a digital image correlation (DIC). In conjunction with the DIC, the composite evaluators are instrumented by strain gages to assess the strain variation at different zones of interest.
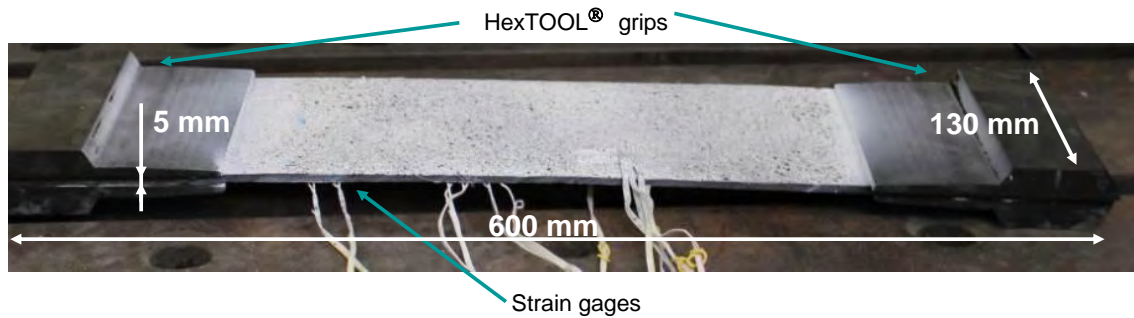
Figure 6-20. Composite evaluator to be tested in the multi-axial testing machine.

The loading case is imposed to the evaluator by the movement of the steel rectangle. The displacement of the point between the clamps follows a rotation along the y-axis of -5°. The eccentricity between this point and the attachment to the swinging arm creates a displacement of this point along the z-axis. After the angle of the rectangle reaches its intended rotation, the actuators push the rectangle in the x-direction, effectively compressing the composite plate. The angle of the rectangle is maintained at -5° for the rest of the test. The first phase of the test lasts 4 minutes and while the second lasts at least 6 minutes (cf. Figure 6-21).
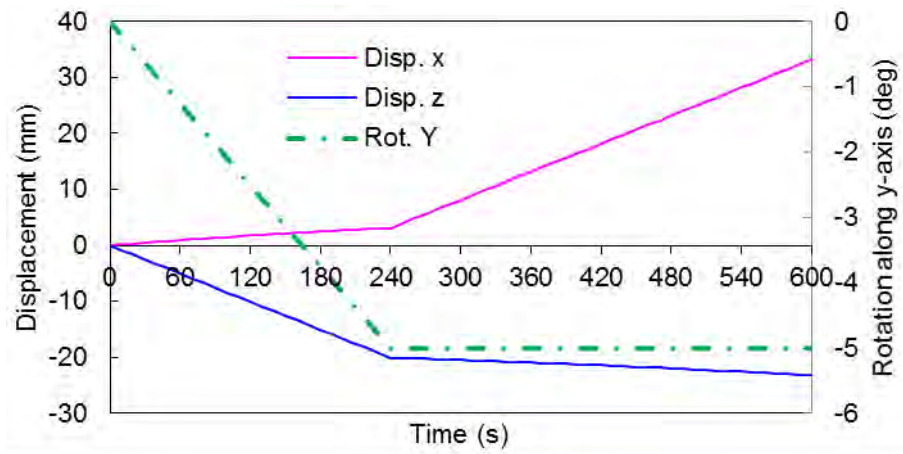
Figure 6-21. Boundary conditions in displacements imposed to the composite evaluator by mobile clamp.

The loading imposed by the displacements effectively sets the composite plate in bending and afterwards in buckling. The ultimate failure of the composite plate was near the fixed clamps, at the frame end (cf. Figure 6-22). The ply #5

oriented at 0° failed by compression near the clamp area. The fracture of ply# 5 propagates delamination in the surrounding area generating the rupture of the first 5 plies.
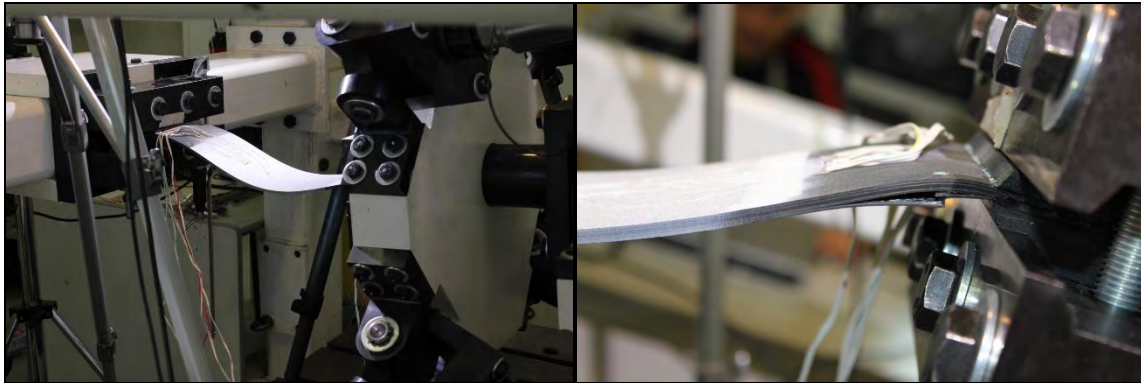
Figure 6-22. Composite evaluator during the testing, (right hand side) deformation of the plate in bucking moments before failure, (left hand side) failure of the composite, fracture of the outermost 0° ply subjected to compression near the clamp area.

6.5.2 FE model of the technological evaluator under a flexion-compression loading case

The initial results of the model are shown as the analysis is currently under development. The analysis is done using the non-linear solver to perform an iterative simulation, since the objective over time is the study of the buckling behaviour of the technological evaluator. The properties of the elements are maintained as linear elastic (cf. Table 6-5). The model was generated for the effective length of the evaluator of 440 mm. The first rows of elements were clamped at each end of the digital evaluator (cf. Figure 6-23). The size of the element is retained at 1 x 1 mm.

The testing kinematics is applied to a master node placed at the theoretical coordinates of the centre of the ball joint (cf. Figure 6-18). The load is then transferred to the composite plate through rigid elements between the master node and the first two rows of elements at the loading end of the composite evaluator. To evaluate the large displacement of the loading end, 20 increments

are applied between the initial and final position of the mobile clamps as shown in Figure 6-21.
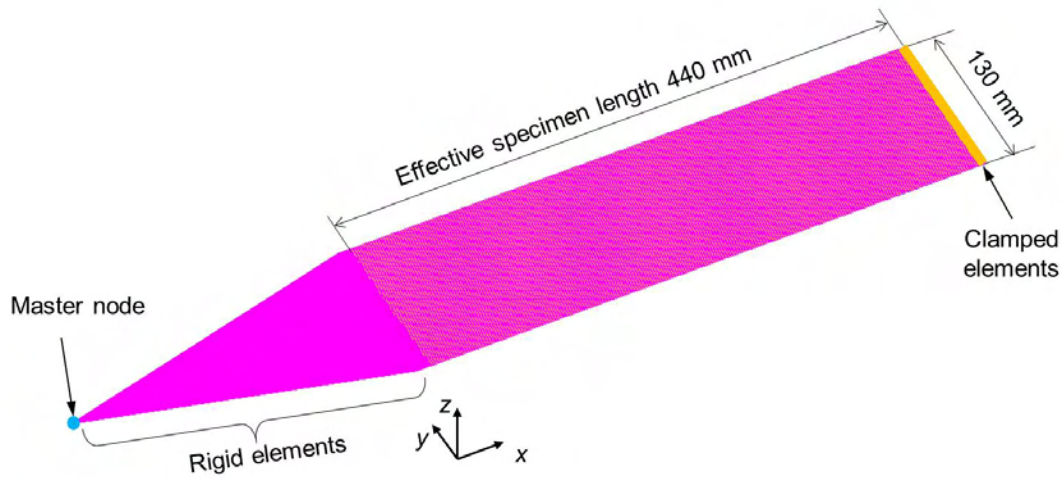
Figure 6-23. Numerical representation by composite shell elements of the composite evaluator tested in a flexion-compression test.

The strain field ε_x for the lower skin of the technological evaluator subject to flexion-compression loading is shown for a homogenous model without variabilities in Figure 6-24 and for the model including all variabilities (ply and plate thickness, and fibre misalignments) in Figure 6-25. Both figures illustrate the strain field at the last incremental step.

In the classical analysis the strain field, shown in Figure 6-24, is mostly symmetric with exception of the corners of the plate. This dissymmetry, however, is mostly due to the effect of a ply oriented at +45 near the exterior skins of the composite plate (plies # 2 and # 15). It is noteworthy that the strain bands are well defined, and run almost straight from one side of the plate to the other side. By comparing the classical homogeneous model to the model with variabilities (cf. Figure 6-25) it is evident that the strain field of the latter is not symmetric along the x-axis. This dissymmetry is most notably in the zone near the clamped end. In this area, a difference of $3\,300 \cdot 10^{-6}$ between the right hand side and the left hand side of the evaluator is observed. Also at the mid part of the evaluator, the edges present a larger deformation than the centre ($3\,300 \cdot 10^{-6}$). In comparison the

model without variabilities shows a homogeneous strain field from the right hand side to the left hand side of the evaluator.
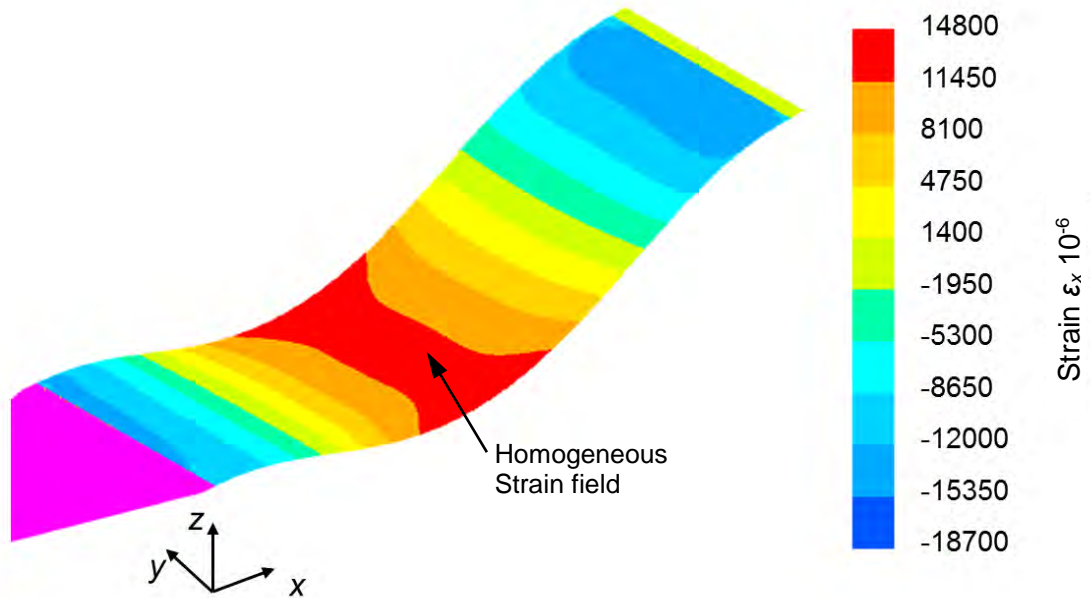
Figure 6-24. Strain field along the x-axis ε_x for the lower skin of a technological evaluator in a flexion-compression test with a homogenous material.
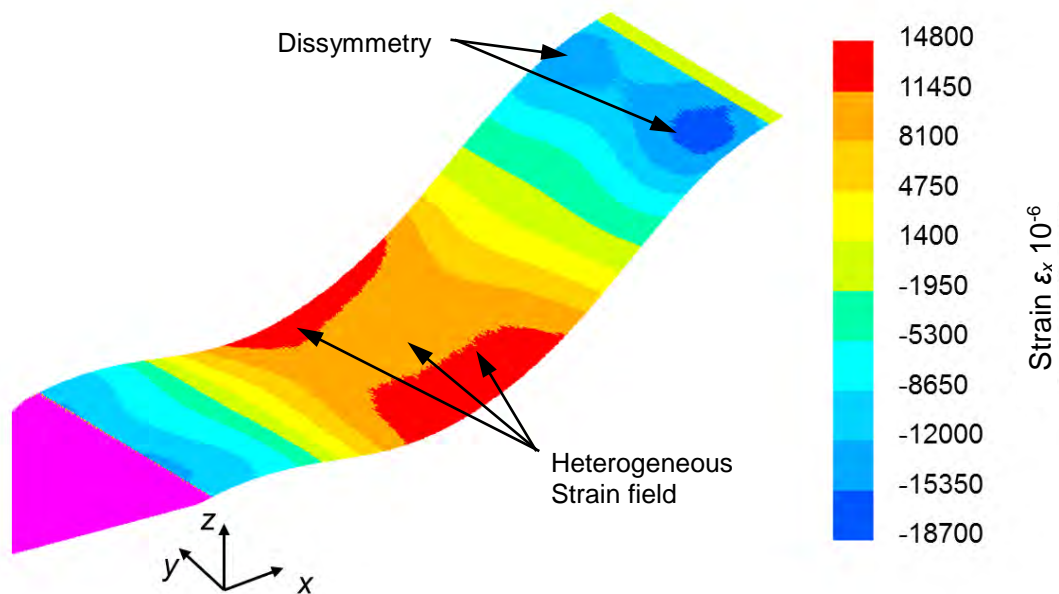
Figure 6-25. Strain field along the x-axis ε_x for the lower skin of a technological evaluator in a flexion-compression test with material variabilities.

This difference in the symmetry of the strain field is due to the local variabilities introduced to the model, most notably the plate thickness and ply misalignments. As can be seen in the homogenous analysis (cf. Figure 6-24), the difference between the absolute maximum and minimum strain values is roughly $500 \cdot 10^{-6}$. In this case, a fracture could be produced near the clamping end or the mid part of the evaluator. For the model including variabilities (cf. Figure 6-25), this difference is almost $4\,000 \cdot 10^{-6}$. This means that there is a higher probability of failure near the clamping area than the mid part of the evaluator. These results show that the proposed approach restores local phenomena not present in the analysis of homogenous materials. These heterogeneities in the strain field maybe indicate a possible failure initiation zones with more precision than classical FE models without material variability.

6.6 Conclusions

This chapter describes the application of the FE model with use of variability. The material elastic quantities are derived from the volume fractions of the constituent materials of the composite that depend on the local ply thickness and volume content of the porosity. To obtain the fibre and resin ratios, it is assumed that the mass per unit area ρ_{Af} is constant for all the points of the plate. From the calculated volume fractions, the elastic quantities of the element for the fibre direction *1* and both transverse directions *2* and *3* are obtained by the law of mixtures.

The geometrical parameters, ply thickness and ply orientation, as well as the elastic constants, are assigned directly to each finite element in the FE input file. This FE input file is generated using the mathematical laws and parameter databases identified in Chapters 3 through 5, as well as the material property database described in this Chapter 6.

It is noteworthy that the selection of the finite element size, and thus the number of elements in the analysis, as well as the method to assign the material to each element must be performed at the discretion of the designer in a case by case scenario. Although, the method is not dependent on a fixed mesh size, the amplitude of the perturbations and their physical dimensions must be taken into account when defining the element size.

Three different cases were presented as examples of the use of the proposed methodology in a FE analysis:

1. the first case deals with a 4-point bending test, in which the results of experimental test were compared to the FE analysis, for the flexural modulus of a composite beam of 100 x 15 mm dimensions. The results show a good agreement between the experimental data and the FE simulations in terms of variability of the flexural modulus;

2. the second case deals with the cooling phase after the curing dwell of a composite plate of 600 x 300 mm dimensions . The out-of-plane deflection and the upper and lower skin strain field show that both the geometry of the piece and the material properties have an important role in the cured state of the composite plate. This state would be otherwise overlooked in a test with constant geometry and material properties;

3. the third case deals with the technological evaluator, an experimental and numerical set-up in accordance with the proposed multi-instrumented technological evaluators approach.

The input files are generated in Matlab® in order to perform a large number of simulations required for a complete probabilistic analysis. The Matlab® scripts can generate from one to many thousands different input files for Monte Carlo simulations. However, mainly due to time constraints and a complex results post-treatment, only the feasibility of the method is presented for a limited number simulations in each case. For the 4-point bending tests, "only" 20 different simulations were performed for each of the FE analysis cases. For the both the analysis of the residual strains under cooling of the composite plate and the

technological evaluator, "only" one simulation was performed in each case due to the technical complexity of the complete analysis.

The principal issue with the actual programming is that the input files are not optimised for a rapid reading by the FE code due to the size of the generated input and output files, the latter being approximately at least 5 times the size of the input file. This constraint creates 2 major problems with the analysis and post-treatment of the results. The first problem deals with the loading time of the input file and the writing time of the output database. The second problem is related to managing both available RAM and disk storage memory during the analysis. These problems can be solved by the optimisation of the input file and proper memory management server side. Indeed, the CPU power and thus the calculation time are however not limiting factors for the different analysis hereby presented.

The present analysis demonstrates the feasibility of a FE model including material and geometrical variabilities with controlled gradients in both within a plate and from one composite plate to another. The next natural step is the optimisation of the FE models for their introduction in larger Monte Carlo simulations for a complete probabilistic assessment of the composite structure.

6.7 References

[1] L. Crouzeix, J. N. Périé, F. Collombet, and B. Douchin, "An orthotropic variant of the equilibrium gap method applied to the analysis of a biaxial test on a composite material," *Compos. Part A Appl. Sci. Manuf.*, vol. 40, no. 11, pp. 1732–1740, Nov. 2009.

[2] P. Feraboli, T. Cleveland, P. Stickler, and J. Halpin, "Stochastic laminate analogy for simulating the variability in modulus of discontinuous composite materials," *Compos. Part A Appl. Sci. Manuf.*, vol. 41, no. 4, pp. 557–570, Apr. 2010.

[3] G. Karami and M. Garnich, "Effective moduli and failure considerations for composites with periodic fiber waviness," *Compos. Struct.*, vol. 67, no. 4, pp. 461–475, Mar. 2005.

[4] P. D. Spanos and a. Kontsos, "A multiscale Monte Carlo finite element method for determining mechanical properties of polymer nanocomposites," *Probabilistic Eng. Mech.*, vol. 23, no. 4, pp. 456–470, Oct. 2008.

[5] K. D. Potter, B. Khan, M. R. Wisnom, T. Bell, and J. Stevens, "Variability, fibre waviness and misalignment in the determination of the properties of composite materials and structures," *Compos. Part A Appl. Sci. Manuf.*, vol. 39, no. 9, pp. 1343–1354, Sep. 2008.

[6] AFNOR, "NF EN ISO 14125: Composites plastiques renforcés de fibres - Détermination des propriétés de flexion," 1998.

[7] M. Mulle, F. Collombet, P. Olivier, R. Zitoune, C. Huchette, F. Laurin, and Y. Grunevald, "Assessment of cure-residual strains through the thickness of carbon–epoxy laminates using FBGs Part II: Technological specimen," *Compos. Part A Appl. Sci. Manuf.*, vol. 40, no. 10, pp. 1534–1544, Oct. 2009.

[8] D. Stefaniak, E. Kappel, T. Spröwitz, and C. Hühne, "Experimental identification of process parameters inducing warpage of autoclave-processed CFRP parts," *Compos. Part A Appl. Sci. Manuf.*, vol. 43, no. 7, pp. 1081–1091, Jul. 2012.

[9] F. Collombet and Y.-H. Grunevald, "Apport économique des évaluateurs technologiques multi-instrumentés sur l'ensemble du cycle de développement d'un avion commercial multi-matériaux à base composite," in *JNC 16*, 2009.

[10] L. Crouzeix, Y. Davila, F. Collombet, B. Douchin, Y. Grunevald, and R. Zitoune, "Study of double step lap composite repairs on CFRP evaluators," in *ECCM 15*, 2012.

[11]   F. Collombet, L. Crouzeix, Y. Grunevald, H. Zeng, Y. Davila, B. Douchin, and A. Gillet, "Primary principal composite structure repair with multi-instrumented technological evaluator tool box," in *ECCM 15*, 2012.

General conclusions and future work

The main goal of this dissertation is the study of morphological variations in a composite structure in order to enrich its performance analysis. The main motivation of this work is to introduce into finite element models the local variations of geometry and material properties. What distinguishes this dissertation from the works found in the literature is the demonstration that the material and geometry variations are not randomly assigned to each element into the FE model, but they are controlled by laws of spatial evolution to manage the gradient of properties between two different points within a single structure, in agreement with the reality of the material. The introduction of laws for managing spatial evolution is the main driver of the analysis, identification, and quantification at the core of this work. Additionally, one of the objectives is not to recreate an exact representation of a unique composite structure by employing fixed laws of evolution, but to propose a modelling strategy that respects the reality of the material. It deals with including physical quantities that are determined from mathematical laws that represent the dispersion of properties with a random generation of the parameters of these laws.

The literature review, presented in Chapter 1, demonstrates that there is no common framework for the study of variabilities in composite structures regardless of the evidence that composite materials exhibit, indeed, a dispersion in their properties. Usually during research, the variability in composite structures is considered either as local defects or as uncertainties in stochastic analysis. For the former consideration, dedicated models are created in order to study the effects of that particular localised defect on the composite structure. For the latter, a broader set of general approaches is employed such as probabilistic studies, reliability

based approaches and stochastic finite element methods. The Monte Carlo simulation is still the most common solution method due to the simplicity of its formulation. The model variables include the material properties which are obtained from probability density functions. Such material properties are varied through the composite structure at each simulation regardless of the method for the solution of the problem.

Based on the conclusions of the literature review, a methodology to introduce material variability into a FE model to study the behaviour of composite structures is presented in Chapter 2. The originality of the proposed methodology is the inclusion of mathematical laws to introduce and control the gradient of local property variations from one point of the structure to another. These laws do not only introduce a controlled and continuous variation of the properties, but they are based on the observation of a real composite structure. The material properties are introduced element per element in the FE model. These properties are thus derived from morphological and material properties such as the reinforcement angle, the geometry of the structure (plate and ply thicknesses), and porosity volume fractions.

To ensure that the laws of spatial evolution and the probability distributions of their associated variables are in agreement with the reality of the material, the identification and quantification are performed through the life cycle of composite plates fabricated with the carbon/epoxy unidirectional prepreg HexPly® M10.1/38%/UD300/CHS. The composite plates have 16 plies quasi-isotropic stratification and are cured in an autoclave. The identification and quantification of the variables are presented following the chronological order of the fabrication of the composite plates in Chapter 3, with the exception of the determination of the local fibre angles, which are measured during the lay-up phase, and the ply thickness variations, that are measured from the cured plates. These variables require a more in-depth analysis presented in Chapters 4 and 5 respectively.

In Chapter 3, the first parameter that has been studied is the variation of the mass per unit area of the prepreg plies. Two different methods have been used for the measurement of this quantity. The first method measured all the prepreg plies that were used by the fabrication of different composite plates. The second method, inspired from the standard NF ISO 10352, is used to obtain more precise measurements. The difference between the proposed method and the standard is the digitalisation of the specimen in order to determine its surface regardless the geometrical irregularities near the edge of the specimen. Nevertheless, the differences between the method 1 and method 2 are not statistically significant since the variability of the prepreg is greater than the uncertainty of the measurements. The method 2 is thus the preferred method to measure this quantity since it can be used to obtain trends through the prepreg roll. Regarding the prepreg material, a dispersion of the mass per unit area less than to 2 % was determined for each of the two prepreg lots that were studied. In contrast, a significant variation is shown between the two different rolls. It is difficult, at this stage, to assess the effects of the variability of the mass per unit area of the prepreg on the cured properties of the composite, notably the volume fractions of the constituents. Notwithstanding, it is proposed as a strong hypothesis that the fibre quantity, and thus its mass per unit area, is constant. This hypothesis is used to calculate the volume fractions of the constituent materials that are, in turn, used for the calculation of the elastic quantities of the element. This hypothesis must be confirmed in due course through more measurements.

During the curing stage of the composite plates, it is shown that the configuration of the vacuum products affects the characteristics of the final composite plates. In the first autoclave batch A, the resin impregnated the breather mat resulting in an average resin mass flow of 12 % of the uncured plate weight. When changing the vacuum products configuration for the second batch B, an average resin flow of 6 % was determined. The plates from the third autoclave batch C, that were fabricated using the same vacuum products sequence as batch B but using a different material lot, exhibit a resin flow of the same order of magnitude as batch B. After polymerisation, the composite plates of batches A

and *B* were measured in a coordinate-measuring machine to determine the distribution of thickness of the plates. This measurement has not only confirmed a difference in the average thickness between batches *A* and *B*, but has shown that there is a significant variation on the thickness within a single composite plate. The amplitude of these differences, most notably between the centre and the corners of the plate, is larger than the thickness of a ply. This difference in thickness is a major factor in the evolution of the mechanical properties at the scale of the composite plate. Likewise, it is assumed that this thickness variation is distributed evenly in the 16 plies forming the composite plate. A mathematical law is thus generated to introduce this variation in the models of variation of the ply thickness.

The last study presented in this Chapter 3, is a thermo-chemical analysis performed on the cured plates in order to determine the volume fractions of the constituents, especially the porosity content. This analysis, performed at the scale of the polymerised plate, showed that the porosity appears to linearly increase with the thickness. A mathematical law was thus proposed to link the plate thickness with the porosity content, though limited to have zero porosity under a certain thickness. The values of porosity were found less than 2 %. The low porosity content is linked to the non-controlled flow nature of the M10.1 resin that permits the evacuation of volatiles and entrapped air.

For the determination of the actual fibre orientation, presented in Chapter 4, an optical system is employed to obtain a single digital image of the complete prepreg ply during the lay-up sequence. By means of the development of a script based on the Hough transform, the fibre orientations have been determined. In the first place, the mean ply misalignment was determined, with a value less than 2°. This error appears to be more dependent on the ability (and fatigue) of the operator than the theoretical orientation of the ply. Due to the quality of the images and the resolution of the digital camera employed, the procedure has not permitted to obtain the misalignments up to the scale of the fibre mesh, and thus the periodic undulations created by the storage of the prepreg in rolls.

Nevertheless, this procedure was enough to identify local evolutions of fibre orientations that do not exhibit a periodic behaviour. These perturbations, covering several cm² exhibit completely random characteristics such as sizes, origins and magnitudes. Through the magnitude of these perturbations does not exceed ± 1°. To model the behaviour of the ply orientation, three scales have been proposed. The first is a mean ply misalignment. The second is the effect produced by the periodic undulations of the fibre, in which a value obtained from the literature is employed. And third, the local perturbation of the fibre orientation, modelled by the sum of Gaussian surfaces. The parameters of these surfaces were obtained from the image analysis.

It is very important to keep in mind that, although the images are taken from the prepreg plies, it is assumed that the fibres do not move considerably during the curing phase. This consideration must be made since it is the only manner to obtain a complete field of fibre misalignments in a composite ply, which in turn will be used to determine a law for the continuous variation of this quantity.

The last variability source is presented in Chapter 5. It is the evolution of the ply thickness profiles in the cured composite plate. It is shown that the thickness within the same ply can exhibit variations up to 20 % of its mean ply thickness. It is also shown the mean of the ply thicknesses within a composite stratification are different, with a coefficient of variation (the ratio between the standard deviation and the mean) of 4.5 %. These two results cast doubt on the classical geometry modelling of composite structures, where the ply thickness is considered as constant and is obtained by dividing the thickness of the structure by the number of plies.

The analysis of the ply thickness was performed by optical analysis of images acquired from the cross-section of the cured plate. The profiles of the ply thicknesses appear to have some regularity with periodic wavelengths. This hypothesis was confronted by a frequency analysis using a discrete Fourier transform of the ply thickness variations on a given direction. This analysis

showed that the undulations of each ply can be described by the sum of sinusoids, and that can be transcribed by the use of 10 frequency peaks from the amplitude spectrum of each profile. Although the analysis of the numerous plies (here 16) seemed to be difficult due to, on one hand, the interdependency of the number of wavelengths, their amplitude and phase shifts for each spectrum, and on other hand, the apparent randomness with which these 3 parameters appear for each ply. Regardless, by the use of a phase shift coupled to the ply position, it is possible to generate a digitally modelled plate with variations of ply thickness comparable to the real values and respecting a variation of the overall plate thickness, which is controlled by the spatial law established in Chapter 3.

Finally, Chapter 6 presents of the whole of mathematical models that are proposed for a control of the spatial properties evolution in a composite plate. It is employed in the creation of FE models with local material variations. The proposed FE modelling is based on the use of 2D Mindlin composite shell type elements. This is done in order to perform a significant number of simulations by changing the variable parameters in the proposed mathematical laws. In this modelling proposal, all the material and geometrical parameters change, not only from one element to another, but within the same composite shell elements, among the 16 different plies that constitute the composite shell element. It is very important to note that the material properties not only vary for one unique analysis, but for a set of different FE models that allow the generation of sets of different properties for the composite plate.

The elastic quantities of the element are derived from the geometrical variations of the ply thickness and from the volume fraction of the porosity. By maintaining the hypothesis that the mass per unit area of the fibre is constant, the volume fractions of the constituent materials (fibre and matrix) are calculated. Then, the geometrical parameters, ply thickness and fibre orientation are introduced element by element into the FE model.

The usability of this proposal is shown by the modelling of three different cases. First, in order to compare the FE model to experimental data, a 4-point

bending test of specimens with dimensions 100 mm x 15 mm was performed. In this test, the FE model is performed by varying all the material and geometrical properties at each performed simulation. In this study, the impact of the influence of variabilities is limited to the production parameters described for 2 "parent" plates. The realisation of this test, allowed to obtain variations of the flexural elastic modulus that are coherent with the variations of the experimental data, irrespective to significant error in the mean value, that is probably due to the modelling strategy rather than the strategy of introduction of variabilities. In a second case, to show the feasibility of the proposed strategy in the analysis of composite pieces of larger dimensions, an analysis of the residual strains was performed on the whole composite plate of 600 mm x 300 mm. The performed calculation has shown that, at this scale, the strain variability is significant ($\Delta\varepsilon_x = 100 \cdot 10^{-6}$) within a single plate. Finally in the third case the modelling strategy has been employed for the analysis of a complex multi-axial test of a technological evaluator of dimensions of 600 mm x 130 mm. The FE analysis demands incremental simulations in order to simulate the buckling of the structure when applying a combined flexion-compression load. The first application of the proposed modelling makes appear a dissymmetry in the strain field ($\Delta\varepsilon_x = 3\,300 \cdot 10^{-6}$) that is due to the material and geometrical variability of the composite material. The effects of introducing of variable material and geometrical variabilities could be used to reveal unexpected risk zones that would otherwise be overlooked by classical FE analysis.

The whole of the studies described in this dissertation illustrates the existence of variabilities present in composite structures, an occurrence that is widely recognized but that is not properly taken into consideration when designing composite structures. An innovative methodology is proposed to take into account such variabilities in finite element models based on the observation of the material through the composite part.

Future work

During the preparation of this dissertation, the case of a theoretically homogenous composite plate is presented with the finality of showing the feasibility of the studied approach and associated models. A unique stratification and a unique material have been employed during this study. Indeed, the proposed methodology can be applied to a broad number of composite applications.

Thus, the first action is to apply the proposed methodology to different stratifications and other material systems, in order to create a database to further enrich the FE models that are already in place. This is not a small task, since the number of data points is considerable, as equally are the resources and time needed to perform these tasks. To illustrate the size of the tasks involved, the orders of magnitude of obtained data points are: 600 points per each 10 mm for the ply thickness study (comprising the 16 plies); one point per 100 mm² for the plate thickness study; and 5 points per 100 mm² for the ply orientation study. This leads to a rough estimation of 7 000 data points presented on Chapters 3 to 5. Alas, the identification and quantification methodologies must be performed continuously to gather as much data as possible over time. There is no shortcut in the study of variability due of the interdependencies of the actors and parameters that are involved from design to service of the composite structure.

Regarding the characterisation of the volume fractions of the constituent materials in all the stages of the fabrication of a composite part, it is necessary to confirm the assumptions that the mass per unit area of the fibre is constant within the composite part. Likewise, the link between the ply thickness and the fibre volume fraction must be assessed in order to confirm the hypothesis that the variation of the ply thickness does not impact the repartition of the reinforcements along the plies. For the ply thickness, at the moment only one direction was considered, assuming the same behaviour for the transverse direction of the plate. This gives as a result a very distinctive straight pattern in the two principal directions of the composite plate. This pattern however is not likely to be present

in the actual structure. Therefore, further studies must be conducted on the transversal direction of the composite plate applying the same method as explained in Chapter 5. This study will lead to further developments of the mathematical laws describing the two dimension evolution of the ply thickness.

Additional developments on the algorithms for the image analysis are required in order to increase the measurements precision, of both fibre orientation and ply thickness. In the case of the ply thickness, it would be necessary to automate the procedure to reduce the uncertainties that are due to the manual selection of points along the ply interfaces. This action will also increase the number of points measured along the ply interfaces allowing a better distinction between the noise and the physical information obtained by the discrete Fourier transform.

It was demonstrated that with the proposed finite element model, we are capable to highlight the influence of variabilities on the mechanical responses of a composite structure. However, the FE model continues to be a work in progress, hence, efforts leading to its constant development must be made.

The technical aspects of the FE model that should be addressed on the short term deal with the automation of the input files generation, analysis and post-processing. This step is mandatory in order to be able to evaluate the very large number of simulations needed for the probabilistic analysis of composite structures. An optimisation of the input files is necessary to reduce their size and computing time (loading, calculation and writing). It is also necessary to improve the management for both, the memory needed by the FE code solver and the disk memory used to store the model output files. The inclusion of damage analysis of the composite structure could be envisaged using current criteria. To properly asses this condition, failure criteria need to be updated in function of variations of geometry and fibre and matrix volume fractions, thus, leading to an iterative calculation per finite element.

An assessment on mesh size must be performed in order to determine influence of each studied variable on behavior at different scales and sizes.

Compromises must be done when choosing between the number of elements, the size of the composite structure and the scale at which the studied variables is performed.

It is important to underline that this work follows previous developments on the framework Multi Instrumented Technological Evaluators (MITE) made by ICA and Composites, Expertise & Solutions (CES) during the last 15 years. One of the goals of the MITE framework, in its digital component (FE models), is to establish efficient links between "refined" models and simulations adequate to structural scale (e.g. the upper part of the test pyramid like a curved panel or even the complete aircraft). One way to reach these goals is to implement "digital markers" which benefit from results obtained from "refined" models that can deliver reliable information at a structural level. In our case, the first level of such markers is to consider material properties that are either the most representative or the minimum based on one or several elements of the structure model. A priori, the proposed approach interests to both researchers and industrials and begins to be operational.

Finally, although the proposed approach seems to yield adequate results, it is indispensable to compare the proposed calculation methodology versus a purely stochastic approach, such as the one proposed by prof. A. Chateauneuf.

Doctorat de l'Université de Toulouse

Délivré par : l'Université de Toulouse 3 - Paul Sabatier
Ecole doctorale : MEGeP : Génie mécanique, mécanique des matériaux
Date de soutenance : le 27 janvier 2015 à Toulouse
Nom du candidat : Yves Angel DAVILA MONTAÑO

Titre : Etude multi-échelle du couplage matériau-procédé pour l'identification et la modélisation des variabilités au sein d'une structure composite.

Résumé: Une des problématiques liées à l'utilisation des matériaux composites dans les structures tient à la difficulté de prévoir l'effet des variabilités inhérentes à ce type de matériau sur le comportement mécanique. Les propriétés d'une structure composite dépendent non seulement du procédé, mais aussi des matières premières et des choix de conception. Dans le but d'introduire des variabilités géométriques dans le calcul numérique des pièces composites, on part dans ce travail de l'hypothèse que les variations des grandeurs géométriques ne sont pas distribuées totalement aléatoirement, mais que celles-ci suivent des évolutions spatiales continues. Pour que les valeurs d'entrée qui nourrissent le modèle numérique soient basées sur la réalité du matériau, l'identification et la quantification des plages de variabilités et de leurs évolutions sont réalisées sur la période de la fabrication de plaques composites CFRP comptant ici 16 plis avec une stratification quasi-isotrope et polymérisées en autoclave. Parmi les sources de variabilité identifiées et quantifiées, l'étude de la répartition des désalignements des fibres dans le plan et de l'évolution des variations des épaisseurs des plis a mené à la proposition de lois mathématiques d'évolution spatiale basées sur la réalité du matériau dans la pièce. Ces lois mathématiques sont ensuite utilisées pour récréer numériquement plusieurs structures composites différentes de la structure observée mais qui possèdent des valeurs de dispersions des propriétés similaires aux plaques réelles. Enfin, les structures numériques sont analysées dans un modèle éléments finis pour évaluer l'impact des dites variabilités géométriques et matériaux sur les propriétés mécaniques de la structure finale au travers de plusieurs études de cas.

Mots-Clés : Matériaux composites, variabilité, procédés, modélisation, autoclave

Title: Multi-scale study of the material-processing coupling for the identification and modelling of variabilities in a composite structure.

Abstract: One of the major challenges related to the use of composite materials in structural applications is the difficulty to predict the effect of their inherent variabilities on the mechanical behaviour for such materials. The structural properties do not only depend on the fabrication process, but also depend on the raw materials and design considerations. The major goal of this thesis is the introduction of geometrical variabilities into a finite element (FE) model starting from the hypothesis that geometrical variations are not completely randomly distributed, but they maintain a spatial continuous evolution. To guarantee that the input parameters of the FE model are based on the reality of the material, the identification and quantification of the variability distributions together with their spatial evolutions are performed during the fabrication of CFRP composite plates. These plates have a 16 ply quasi-isotropic stratification and are cured in autoclave. Among the identified and quantified variability sources, the study of the in plane fibre misalignments and the evolution of the ply thickness variations has conducted to the proposition of mathematical representations of the spatial evolution of these variables based on the material reality. These mathematical representations are used to recreate different sets of virtual composites structures maintaining dispersion values similar to the real plates. Finally, the virtual structures are analysed in the FE model to evaluate the impact of such geometrical and material variabilities on the mechanical properties of the final structure.

Keywords: Composite materials, variability, manufacturing, modelling, autoclave.